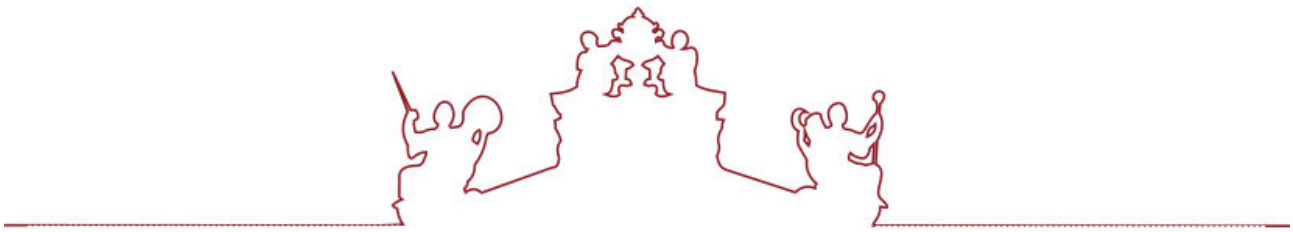

Universidade de Évora - Instituto de Investigação e Formação Avançada
Università degli Studi di Roma "La Sapienza" Aristotle University of Thessaloniki

Mestrado em Ciência dos Materiais Arqueológicos (ARCHMAT)

Dissertação

Nanomaterials for the conservation of iron gall ink-induced corrosion on paper

Ehsan Rahmath Ilahi

Orientador(es) | Penka I. Girginova
Cristina Galacho
Teresa; T.A.S. Ferreira Teresa Ferreira; T. Ferreira; Ferreira

Évora 2022

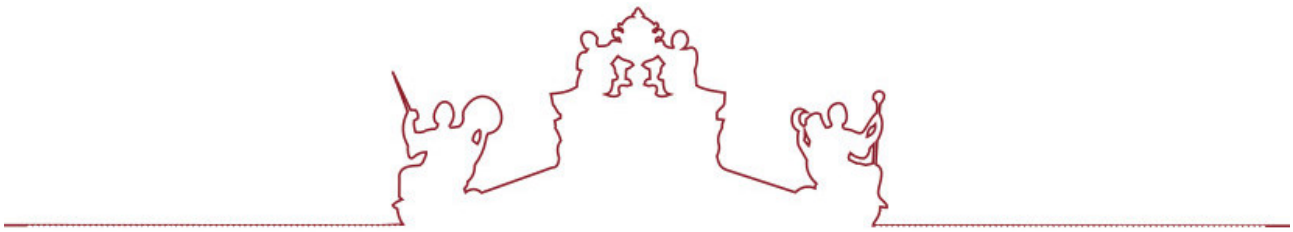

Universidade de Évora - Instituto de Investigação e Formação Avançada
Università degli Studi di Roma "La Sapienza" Aristotle University of Thessaloniki

Mestrado em Ciência dos Materiais Arqueológicos (ARCHMAT)

Dissertação

Nanomaterials for the conservation of iron gall ink-induced corrosion on paper

Ehsan Rahmath Ilahi

Orientador(es) | Penka I. Girginova
Cristina Galacho
Teresa; T.A.S. Ferreira Teresa Ferreira; T. Ferreira; Ferreira

Évora 2022

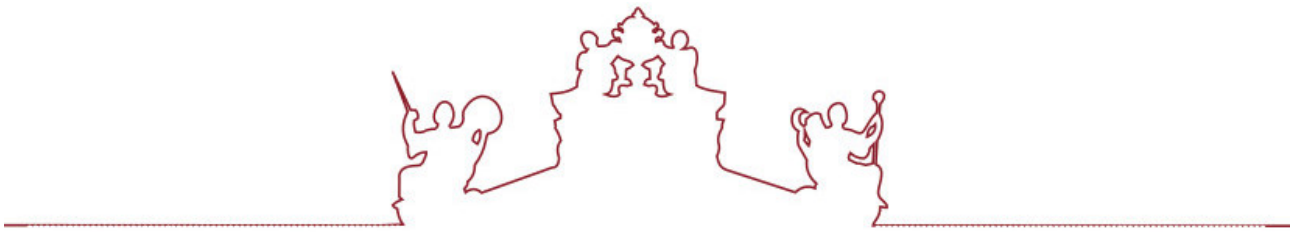

A dissertação foi objeto de apreciação e discussão pública pelo seguinte júri nomeado pelo Diretor do Instituto de Investigação e Formação Avançada:

Presidente	|	Nicola Schiavon (Universidade de Évora)
Vogais	|	Catarina Miguel (Universidade de Évora) (Arguente) Cristina Galacho () Donatella Magri (Università degli Studi di Roma "La Sapienza") Federico di Rita (Università degli Studi di Roma "La Sapienza") Panagiotis Spathis (Aristotle University of Thessaloniki)

Évora 2022

Co-funded by the
Erasmus+ Programme
of the European Union

UNIVERSITY OF ÉVORA

ARCHMAT

ERASMUS MUNDUS MASTER IN ARCHaeological MATerials Science

Nanomaterials for the conservation of iron gall ink-induced corrosion on paper

Ehsan Rahmath Ilahi

m47365

Supervisors | Penka I. Girginova

Cristina Galacho

Teresa Ferreira

Évora, Portugal, December 2022

ARISTOTLE UNIVERSITY OF THESSALONIKI

UNIVERSIDADE DE ÉVORA

SAPIENZA UNIVERSITÀ DI ROMA

PANEL OF JURY

President: Doctor Nicola Schiavon

Principal Researcher at University of Évora, Portugal

Opponent: Doctor Catarina Miguel

Researcher at University of Évora, Portugal

Member: Professor Doctor Federico Di Rita

Professor at Sapienza University of Rome, Italy

Member: Professor Doctor Donatella Magri

Professor at Sapienza University of Rome, Italy

Member: Professor Doctor Panagiotis Spathis

Professor at Aristotle University of Thessaloniki University, Greece

Member (Supervisor): Doctor Penka Girginova

Researcher at University of Évora, Portugal

Member (Co-Supervisor): Professor Doctor Cristina Galacho

Professor at University of Évora, Portugal

Abstract

This research work aims to evaluate the effectiveness of laboratory synthesised nanoparticles for the conservation of iron gall ink induced corrosion on paper. Nanoparticles of $Ca(OH)_2$ and $Mg(OH)_2$ were synthesized in HERCULES Laboratory and characterized using X-ray diffraction (XRD), thermogravimetric analysis (TGA), scanning electron microscopy (SEM) and Fourier transform infrared spectroscopy (FTIR). Three types dispersions of nanoparticles (NPs) ($Ca(OH)_2$, $Mg(OH)_2$ and a combination of $Ca(OH)_2$ / $Mg(OH)_2$) in 2-propanol were prepared and applied on IGI paper samples by spraying. A set of untreated and treated samples were aged in ambient conditions while another set of treated samples were artificially aged in order to observe the longer-term effect of treatment with NPs dispersions.

The paper samples were characterized using technical photography, 3D-digital microscopy, scanning electron microscopy coupled with energy dispersive spectroscopy (SEM-EDS), pH measurement, colorimetry and Fourier transform infrared spectroscopy-attenuated total reflectance (FTIR-ATR). The paper samples were characterized before and after treatment (and after accelerated aging, to study the effectiveness of the NPs dispersions towards paper deacidification.

The presence of NPs on the paper samples was confirmed by SEM images, EDS and FTIR analysis. 3D-digital microscopy confirms the absences of changes in surface texture of the ink after treatment. The initial acidic pH values of IGI papers have increased to an alkaline level after treatment with NPs dispersions as determined by the pH measurements. Colorimetric studies indicate there is a change in lightness and yellowness of the samples after treatment but it is not perceived by the naked eye.

This study projects the potential of the use of the laboratory synthesised NPs dispersions for deacidification of paper samples containing IGI induced corrosion.

This project also aims to contribute to the Development Goal 11 (SDG11) of 2030 Agenda for Sustainable Development. Within this goal, Target 11.4 pursues to "strengthen efforts to protect and safeguard the world's cultural and natural heritage"

Keywords: *Nanolime; cultural heritage preservation; paper conservation; iron gall ink SDG11.4.*

Resumo

O trabalho apresentado teve como principal objetivo a avaliação da eficácia de dispersões de nanopartículas, sintetizadas no laboratório HERCULES, para a conservação de documentos de papel degradados por ação da tinta de ferrogálica.

Nanopartículas de hidróxido de cálcio, $Ca(OH)_2$, e de hidróxido de magnésio, $Mg(OH)_2$, foram sintetizadas e caracterizadas por recurso às técnicas analíticas de difração de raios X (DRX), análise termogravimétrica (ATG), microscopia eletrónica de varrimento acoplada a espectroscopia de raios X dispersiva de energia (MEV-EDS) e espectroscopia de infravermelho com transformadas de Fourier (FTIR).

Foram preparados três tipos de dispersões de nanopartículas ($Ca(OH)_2$, $Mg(OH)_2$ e uma mistura de $Ca(OH)_2$ / $Mg(OH)_2$) em 2-propanol e aplicadas, por pulverização, em amostras de papel manuscritas com tinta ferrogálica. Um conjunto de amostras (não tratadas e tratadas) foi envelhecido em condições de temperatura e pressão ambiente enquanto um outro conjunto de amostras tratadas foi submetido a envelhecimento artificial acelerado a fim de se observar o efeito, a longo prazo, do tratamento com as dispersões de NPs.

As amostras de papel foram caracterizadas, antes e após tratamento, por recurso às técnicas de fotografia, microscopia digital 3D, microscopia eletrónica de varrimento acoplada a espectroscopia de raios X dispersiva de energia (MEV-EDS), potenciometria com elétrodo de vidro combinado, colorimetria e espectroscopia de infravermelho com transformadas de Fourier de reflectância total atenuada (FTIR-ATR).

Após tratamento com as dispersões de NPs foi possível confirmar a presença das NPs nas amostras de papel, pelas técnicas de SEM-EDS e FTIR. Foi também possível inferir a ausência de alteração da textura superficial da tinta ferrogálica, por microscopia digital 3D, e uma ligeira variação de luminosidade e do aumento do contributo da cor amarela, por colorimetria, não sendo estas percetíveis a olho nu.

Os valores iniciais de pH das amostras de papel manuscritas com tinta ferrogálica aumentaram, após tratamento com as dispersões da NPs, para valores situados na zona básica.

Este estudo evidencia a potencial utilização de dispersões NPs, sintetizadas em laboratório, para desacidificação de amostras de papel contendo tinta ferrogálica permitindo a sua estabilização e preservação.

Adicionalmente o trabalho realizado pretende contribuir para o objetivo de desenvolvimento sustentável 11 (ODS11) da Agenda 2030 da ONU, nomeadamente, para a meta 11.4 que preconiza o fortalecimento de esforços para proteger e salvaguardar o património cultural e natural do mundo.

Keywords: *Nanocal; Preservação do Património Cultural; Conservação de papel; Tinta Ferrogálica; ODS 11.4.*

Acknowledgements

This thesis has been made possible by the generous cooperation and sympathetic interest of many individuals whom I wish to acknowledge my deep sense of gratitude.

I record my sincerest gratitude to my supervisor, Dr. Penka I. Girginova, for her unlimited support and guidance throughout the duration of this thesis. Her endless patience and dedication to the work, constant supervision and complete presence through every stage of this work cannot be thanked enough. I also record my heartfelt gratitude to my co supervisors Prof. Cristina Galacho and Prof. Teresa Ferreira for all the care and support they extended towards me in this research period. I am grateful for everything I learnt from all three of them ranging from basic chemistry all the way to nanomaterial synthesis and paper conservation. Their passion for scientific research has been instilled in me too.

I record my appreciation to the team of HERCULES Laboratory for their help, especially to Dr. Luis Dias for helping with the settings of the SEM equipment which was essential for this research. I also record my thanks to Ana Machado from Laboratório José de Figueiredo, Lisboa, for the climate chamber which was a crucial part of this thesis, and to Dr Miguel Potes and Dr Samuel Bárias from Institute of Earth Sciences – University of Évora, for providing the data related to the atmospheric conditions near the Laboratory. I would also like to thank Eng. Manuel Magalhães / Colormetrix Lda for his help in resolving the problem with the colorimetry equipment.

I express my deepest thanks to Gláucia Wanzeller Martins for being a constant support system from the start of my thesis journey and for patiently teaching me how to use all the equipment that I required in the lab and for always being available whenever I needed help. I also record my heartfelt thanks to Margarida Nunes for guiding me through all the twists and turns I faced while interpreting my data. I also express my gratitude to my colleague Sayan Roy for all the help he extended in the technical photography sessions.

I am grateful to the Erasmus Mundus ARCHMAT consortium especially to programme coordinator Prof. Nicola Schiavon for giving me the opportunity of a lifetime to be a part of an international family and opening many doors for future endeavours.

I express my deepest love and gratitude to my fellow Archmatians for being there in the highs and in the lows throughout this journey. All the coffee breaks shall be cherished for life. I have learnt and evolved much in this journey for which I thank everyone I crossed paths with. I express my gratitude to Mr. and Mrs. Rahmath Ilahi for giving me the wings to fly and live my dreams half way across the world. Lastly, I record my everlasting gratitude to the Almighty for all the blessings He has bestowed.

Table of contents

List of Symbols and Abbreviations

IGI	Iron gall ink
NPs	Nanoparticles
XRD	X-ray diffraction
TGA	Thermogravimetric analysis
SEM	Scanning electron microscope
EDS	Energy dispersive spectroscopy
FTIR	Fourier transform infrared spectroscopy
ATR	Attenuated total reflectance

List of Figures

List of Tables

List of Appendices

Chapter 1:

Introduction

Cultural heritage are remains of the past which still have a role in the present. It is the doorway to understand the past as we go deep into the roots of culture in an attempt to piece together the source of our current state of existence. Initially, cultural heritage was associated with the protection and preservation of remains that could either be found beneath the soil or above it (UNESCO convention 1972), but over the course of time, it began to include various subfields such as tangible and intangible cultural heritage (UNESCO convention 2003). Within the classification of tangible heritage exists a category of movable cultural heritage, and written documents are an example of it.

Written cultural heritage is reminiscent of the intellect of the people of the past and covers a wide range of fields ranging from fiction to science, arts, economics, and legal and religious documents. The material used to keep these written records changed throughout time and region. The earliest form of written records was the clay tablets used by the Mesopotamian civilization, which further progressed to stone, bone and hide, papyrus, parchment and then paper (Gascoigne, 2001; Clayton, n.d.). The credit for the invention of paper is attributed to Ts'ai Lun, arbitrarily dated back to A.D. 105 in China (Hunter, 1947). And from there, it spread across the world through trade routes and soon became the most popular writing mode. Paper and papermaking techniques arrived in Europe along with the Arabs in the 11th century and increased in popularity in Europe with the wane of Islamic rule (Corregidor, 2019; Hoffman, n.d).

As there was a change in the material that was written on, there were also changes in the inks used throughout time. As a writing medium obtained by mixing a binding agent such as gum Arabic or animal glue with a pigment or a dye, ink can be further classified into plant ink, a solution of tannins derived from tree bark and gallnuts or other vegetal matter containing tannins. When the tannins in the plant ink react with iron ions, they form Iron gall ink (IGI) (Nehring, 2021). IGI was one of the most reproduced inks in Europe from the Middle Ages till the 19th century and was nicknamed "common ink". Though IGI was known to Europeans as early as the 3rd - 4th centuries, it gained popularity after the 10th century CE. Due to its characteristic properties, namely being easy to manufacture and hard to remove from the surface where it was applied, IGI eventually replaced carbon inks, the most popular ink of the time (Eusman, 1998).

The earliest evidence of IGI is in The Book of Proverbs in Akhmimic, preserved at the Staatsbibliothek in Berlin (Berlin, Ms.or.oct 987), dated to 3rd-4th centuries CE, the

Vercelli Gospel (Codex Eusebii Evangeliorum) at the Museo del Tesoro del Duomo in Vercelli dating probably to the 4th century CE, Codex Sinaiticus (4th century CE), the Vienna Dioskurides (Vienna, Codex Vindobonensis Med. gr. 1) from the 6th century CE and the Lindisfarne Gospels (8th century CE) (c.f. Ghigo, 2020).

Since the 12th century, iron gall ink has been commonly used in Europe in manuscripts, maps, and documents, among others. Some of the iconic documents written with IGI are the Magna Carta (13th century CE), manuscripts penned by Henry VIII (16th century CE) and the works of famous diarists such as John Evelyn (17th century CE), to more commonplace letters, notes, musical scores and records (Garside & Miller, 03 June 2021). IGI was not used exclusively for writing; several well-known artists used it to make exquisite drawings (Rembrandt, Van Gogh and Victor Hugo, to name a few) (Marieflemay, 2013).

1.1. **Chemistry of Iron Gall Ink**

IGI belongs to the group of metallic inks. The essential constituents required to prepare an iron gall ink are iron (II) sulphate- in literature, often referred to as vitriol, green vitriol, copperas, green copperas and Roman vitriol- and a plant material containing tannins (e.g. oak galls) as the colouring matter, gum Arabic as the binder and a solvent like water or wine, which would be the vehicle (Reissland & Graaff, 2001).

In order to increase the gallic acid concentration, the gallotannic acid can be hydrolysed by boiling the galls (Eusman, 1998). Iron (II) sulphate- pure or with impurities- is ground and added to the extracted solution. The mixture colour changes immediately. The water-insoluble pigment, responsible for its colour, results from a chemical reaction where iron (II) ions react with gallic acid or other polyphenols (hydrolysable tannins) to form a product which oxidises in the air to a dark-coloured complex, a ferric gallate and other Fe^{3+}-phenolic compounds (Teixeira, 2021). Sulphuric acid is formed as a by-product.

After this step, gum Arabic is added as a binder and a liquid suitable for writing is made (Zamorano, 2018). As the freshly applied ink dries, it continues reacting with atmospheric oxygen, and the colour of the ink develops and becomes darker and darker (Marieflemay, 2013).

Certain additives were added to the ink recipe to obtain specific desired properties. For instance, sugar or honey was added as plasticising agents, alcohol, cloves and vinegar were used as preservatives to increase the shelf life of the ink and pigments such as indigo and logwood were added to enhance the colour (Marieflemay, 2013).

1.2. Iron Gall Ink and Paper Degradation

One of the main problems conservators face in preserving written cultural heritage is paper degradation. The main factors influencing the extent of damage on paper artefacts can be divided into internal and external factors. The external factors are associated with storage and use, such as climatic conditions, air pollution, UV/IR/Vis light exposure, transport, exhibiting and handling for studies and research. The internal factors include the composition of the ink, composition of the paper, sizing, and thickness. Among the internal factors, the composition of the ink and the paper principally determines the condition of the artefacts (Reissland & Graaff, 2001). Identifying the main causes of the degradation of paper materials is essential to help assessing the documents ageing stability and aid in the development of suitable preservation strategies (Kolar, 2005). One such conservation issue is the corrosion of paper due to the presence of IGI, which leads to the depolymerisation of cellulose, which in turn results in the decrease of mechanical strength.

The natural ageing process of paper is based on two main degradation processes: acid-catalysed hydrolysis and metal-catalysed oxidation of cellulose. Meanwhile, in the making of IGI, most of the time, there is an excess of iron (II) sulphate; as a result, not all the iron (II) sulphate is used up in the reaction to form iron (III) complex and free iron (II) ions that remain present in the solution leads to iron (II) catalysed oxidation of cellulose. The excess of sulphate ions will lead to the sulphuric acid formation which has a key role in the acid-catalysed hydrolysis of cellulose. This results in chain scission and crosslinking of the cellulose polymer, consequently leading to fluorescence, change in colour and loss of mechanical strength of paper (Reissland & Graaff, 2001).

1.3. Conservation measures against Ink corrosion

The target of conservation, according to the International Council of Museums, Committee for Conservation (2008), is to slow down the deterioration and extend the useful life of the artefact. There are several strategies available for paper conservation, targeting various aspects of deterioration, which are further dedicated on understanding the targets and limitations of the specific implementation. Several treatment methods and preventive measures have been taken to inhibit ink corrosion in paper documents (which is discussed in detail in the following chapter), wherein the treatment and preventive methods are employed to improve the chemical and physical condition and the aesthetic appearance of art and archival materials.

As mentioned in section 1.2., the acid-catalysed hydrolysis makes the paper more acidic, which leads to the loss of mechanical strength of paper documents thereby making deacidifying of paper documents a requisite. Deacidification involves neutralization of the acid content and deposition of an alkaline substance (alkaline or alkali reserve) that will neutralize the acidity that may develop in the future (e.g.,

pollution) (Zervos & Alexopoulou, 2015). The best methods of deacidification are based on non-aqueous solvents wherein less polar fluids are the preferred solvents as they minimize the risk of ink solubility (Ion, 2017). Several methods of paper consolidation have also been studied in order to increase the mechanical stability of degraded paper.

Some of the earliest treatment methods were impregnation with Zapon (cellulose nitrate), neutralization using ammonia vapours and collodion consolidation (Zervos & Alexopoulou, 2015). These methods were followed by different types of laminations, such as transparent paper and starch paste and with acetate or PVC films. This resulted in destructive and irreversible interventions. The use of aqueous treatment of sodium phytate for consolidation along with deacidification by magnesium bicarbonate was proposed by Neevel *et al.* (Neevel, 1995) and later developed by others ((Henniges, 2008); Kolar, 2005; Kolar, 2007; Potthast, 2008). Aqueous deacidification with calcium hydroxide, magnesium hydroxide, calcium bicarbonate and magnesium bicarbonate results in immediate neutralization, but the excess alkalinity also leads to depolymerization of cellulose and discolouration of inks (Zervos & Alexopoulou, 2015). Traditional non-aqueous deacidification methods such as Wei'To and Bookkeeper's methods are based on $Mg(OH)_2$ being generated *in situ* after the treatment application and sometimes resulting in an inhomogeneous distribution of the alkaline reserve (Ion, 2017). Therefore, a better method of introducing alkaline material to the ink-corroded paper with a more homogenous distribution of hydroxides without the intermediate formation of oxides has led to the application of nanomaterials for treatment and as preventive measures against IGI-induced paper corrosion.

Nanostructures represent a stage of matter between agglomerated molecules and structures and are typically characterized by a large surface area that affects their physicochemical properties (Ion, 2017). Applications of nanotechnology to paper deacidification have recently provided clear evidence for the vast potentiality of this emerging science for cultural heritage conservation. Nanodispersions of solids, micelle solutions, gels and microemulsions offer new reliable ways to restore and preserve works of art by synthesis of systems specifically tailored to fight the deterioration processes which threaten the preservation of the world cultural heritage, including written documents (David, 2020; Ion, 2017). They provide an efficient alternative to the traditional conservation measures due to their unique features which include the possibility of altering the nanomaterial morphology and particle distribution conveniently to make it suitable to remedy conservation problems. In the case of paper artefacts, the tiny dimensions of nanoparticles (NPs) should facilitate their penetration in the paper sheet by the deacidifier with the help of non-aqueous dispersions (Wójciak, 2015).

1.4. Objective of Study

This research was conducted at HERCULES Laboratory at the University of Évora, Portugal, in partial fulfilment of the requirement of the Erasmus Mundus Joint Master's degree (EMJMD) in Archaeological Material Science (ARCHMAT). The research concept emerged in the frame of different multidisciplinary fields of research conducted in HERCULES Laboratory. The recent advances in innovative methods of nanoparticles synthesis (Girginova, 2020) intended for the conservation of cultural heritage and already investigated in relation to mortar conservation (Baiza, 2021) are extended into the treatment of paper degradation caused by IGI corrosion- the investigations on causes and conservation of the same are ongoing in the Laboratory (Claro, 2019; Claro , 2021; Nunes, 2022;).

This research aimed to 1) to characterise the laboratory synthesized nanoparticles and 2) compare and evaluate the efficacy of laboratory synthesized nanoparticles for the treatment of IGI induced corrosion on paper. Therefore, two kinds of metal hydroxide nanoparticles, $Ca(OH)_2$ and $Mg(OH)_2$, were synthesized following the synthesis conditions adapted in the research group (Girginova, 2020). They were later characterized using thermogravimetric analysis (TGA), Fourier transform infrared spectroscopy (FTIR), X-ray diffraction (XRD) and scanning electron microscopy – energy dispersive spectroscopy (SEM-EDS).

Paper mock-ups written and painted with IGI and artificially aged for different time periods to induce different levels of degradation were treated with 3 different nanoparticles dispersions in 2-propanol: $Ca(OH)_2$, $Mg(OH)_2$ and a combination of both. A set of treated papers was aged at ambient conditions. Another set of treated paper samples had further undergone accelerated ageing to observe the effect of the treatment in the long run. The efficiency of each of the treatments was investigated by monitoring the changes in the paper samples after treatment with NPs in comparison with the behaviour prior to the treatment using the analytical techniques already mentioned such as SEM-EDS and FTIR-ATR, and other techniques as colorimetry, 3D digital microscopy and pH measurement.

1.5. Research objectives

Several research objectives were formulated in order to attain the goal of this research study:

- To create a bibliographic overview of different methods of treatment of paper degradation caused by IGI corrosion in general and specifically of nanomaterials used in the conservation of paper artefacts containing IGI.
- To successfully synthesize nanoparticles of $Ca(OH)_2$ and $Mg(OH)_2$ in HERCULES Laboratory and characterize them using various analytical techniques.

- To apply three types of dispersions of nanoparticles of $Ca(OH)_2$ NPs, $Mg(OH)_2$ NPs and a combination of both dispersed in 2-propanol on the paper samples having different levels of induced degradation.
- To further expose parts of the treated paper samples to accelerated ageing and observe the effect of the treatment with the NPs.
- To compare the effectiveness of each of the nanoparticle dispersions on different types of ink and different levels of induced degradation due to the different aging times in the accelerated artificial aging chamber.
- To evaluate the influence of each kind of laboratory synthesized NPs in deacidification of paper containing IGI induced corrosion.

1.6 **Thesis structure**

This thesis has been divided into six chapters, summarized as follows. ***Chapter 1*** (Introduction) provides a brief introduction to IGI and the chemistry behind the formation of the ink. The various factors affecting the degradation of papers with IGI and the different conservation measures are also mentioned in this chapter, along with the purpose of the study. ***Chapter 2*** (Short review on Iron Gall Ink Conservation) provides a literature review of various studies conducted on IGI and the different methods of treatment of papers with IGI corrosion leading to the previous works that employ nanomaterials for IGI-induced corrosion. ***Chapter 3*** (analytical techniques) provides brief information and the purpose of the different analytical techniques that were used in this study. ***Chapter 4*** (Materials and Methods) addresses the methodology of this research work along with equipment specifications. ***Chapter 5*** (Results and Discussion) discusses the study's main results and ***Chapter 6*** (Conclusion) discusses the conclusions obtained from the study.

Chapter 2
Short review on Iron Gall Ink Conservation

2.1. Iron Gall Ink conservation studies

2.1.1. *Studies until the 20th century*

For several centuries, iron gall ink-induced decay, referred to as ink corrosion, has been acknowledged as one of the major threats to the written cultural heritage. As early as 1765, the English chemist William Lewis published a treatise on the stability of iron gall inks (Kolar, 2007). One of the earliest attempts to address the problems of ink corrosion in written cultural heritage and propose conservation measures took place in 1898 in St Gallen, Switzerland, during the International Conference for Preservation and Conservation Access of Antique Manuscripts (Reissland, 1997).

Papers were treated with cellulose nitrate (Zapon) dissolved in acetone by immersion, brush or spray and left to dry. This method was first proposed in 1899 by Dr Schill. A decade later, it was warned that paper treated with Zapon was highly flammable since the decomposition of Zapon affected the paper support leading to its yellowing (Reissland, 1997).

Franz Ehrle proposed the use of pure, salt-free gelatine for IGI degradation in 1899 to replace the loss of paper, by filling it with thin layers of gelatine until the thickness of the artefact is obtained. It was a time-consuming method, and the sensitivity of gelatine to humidity risked adherence to paper in case of long-term contact between papers (Reissland, 1997).

The use of ammonia vapours to neutralize the free acid before applying cellulose nitrate (collodion) with castor oil as a solvent for mechanical stabilization was also proposed at the conference of 1899. A drawback of this method was the considerable shrinkage of the impregnated papers. Same as the Zapon-impregnated papers, the documents treated with collodion were also highly flammable, and the neutralization with ammonia did not seem to have a long-term effect (Reissland, 1997).

2.1.2. *Studies from the 20th century onwards*

An irreversible method which consisted in embedding the damaged papers in acetate or PVC films was proposed by Nils Gärting in 1963 for exceptional cases due to the severe yellowing and damage by acetic or hydrochloric acid emitted by the film material (Gärting, 1963).

Hans Heiland mentions that ink-corroded manuscripts during the Third Reich were embedded between transparent papers (Pergamin-papers), and 30 years later, by

1964, a severe yellowing of the documents was observed. Unfortunately, the glue used was not identified though it is opined to be starch (Heiland, 1964; Reissland, 1997).

Deacidification

The studies conducted prior to the twentieth century were focused more on enhancing the aesthetic and mechanical strength of the manuscript. In the mid-twentieth century, William Barrow recognized acid hydrolysis as one of the main causes of paper deterioration and iron-gall ink corrosion. In 1965, he proposed deacidifying paper by washing it twice with water containing 0.15% of calcium hydroxide the first time to neutralize the acid and 0.2% calcium bicarbonate in the second wash to eliminate the hydroxide excess. The precipitate of calcium carbonate has a stabilizing effect on cellulose and also acts as a buffer against the absorption of any acid later on. This treatment made the paper heavier and stiff and reduced its strength significantly. This method was unsuitable for the treatment of bound documents (Melo, 2022; Smith, 1966; Zervos & Alexopoulou, 2015). The deacidification of paper materials has undergone a long process of change and development over many years and can be classified into aqueous and non-aqueous deacidification methods.

Mass deacidification is a process of paper conservation wherein a bound volume or stack of loose sheets can be neutralized and buffered as a whole. The neutralizing agent is introduced into the volume as a gas or a liquid penetrating it completely. The gas or liquid is pulled into the paper under vacuum, the paper is deacidified, and the waste products are pulled out and destroyed (Harris, 1983). Gaseous treatments based on diethyl zinc is another method invented by C. Williams and G.B. Kelly in the 1970s, which was utilized for mass de-acidification. However, it involves high costs, and significant safety and maintenance precautions, as diethyl zinc ignites in contact with air and is explosive in contact with water (Baglioni, 2005).

Non-Aqueous Deacidification

Methoxy magnesium methyl carbonate, ethoxy magnesium ethyl carbonate, magnesium methyl carbonate and magnesium ethyl carbonate are four Wei T'O solutions used as deacidification agents. R.D. Smith first proposed this method in 1974, wherein the solution is applied in a mixture of methyl alcohol and freons (later replaced by hydrochlorofluorocarbons), which then hydrolyses by moisture to form $Mg(OH)_2$, methyl alcohol and CO_2, which immediately provides an alkaline reserve. One of the major drawbacks of this method is that methyl alcohol is a toxic solvent and poses a danger to the conservator applying it (Green & Leese, 1991).

Another non-aqueous method includes the Bookkeeper method, introduced in 1993 for large-scale deacidification, involving the dispersion of micro-sized particles of MgO in fluorinated solvents (Stauderman, 1996). It is probably the most used method for deacidification, wherein magnesium oxide is converted to magnesium hydroxide by reaction with moisture which results in a significant decrease in the rate of paper degradation (Baglioni & Giorgi, 2006). The main advantages of this method are the ease of application, solvent inertness, no preconditioning, and a controlled hydrolysis process that grants neutralization without exposing cellulose to strong alkalinity. However, light whitening of the paper due to large particle size often leads to insufficient alkaline reserve in the inner (gutter) margins, and the use of highly concentrated fluorinated solvents to stabilize MgO are some drawbacks of this method (Baglioni, 2012; Baglioni , 2006).

Battelle's deacidification method involves magnesium and titanium ethoxide in hexamethyldisiloxane solutions. Magnesium ethoxide and titanium ethoxide hydrolyse easily in the presence of water, soaking the paper. The overall chemical reaction is a two-step process: a metal hydroxide is formed under environmental air influence, and the subsequent reaction produces magnesium carbonate ($MgCO_3$) and titanium dioxide (TiO_2). The magnesium carbonate and the residual metal hydroxides neutralize the acids present in the paper. However, despite these positive results, it was found that the Battelle process suffers from a number of side effects that hamper a large-scale application since a large part of the tested material showed a significant and immediate decrease in paper strength as a result of the deacidification treatment. There were also undesired side effects in the deacidified materials, such as discolorations, white deposits, Newton rings, bleeding of inks and dyes, and a different ''touch'' of the paper (Behrens, 2013 c.f. Baglioni & Giorgi, 2006). Other methods have been developed, still focusing on the hydrolysis of Mg-organic salts to obtain the in situ formation of $Mg(OH)_2$, such as the Sable, the CSC Book Saver and the Papersave, which was developed by Battelle Ingenieurtechnik GmbH (hence the name "Battelle process") and uses a complex of magnesium and titanium alcoholate in hexadimethyldisiloxane (HMDO) (Gulik, 1997**).**

The use of supercritical fluids as solvents is another method wherein the advantage of manipulating solvent strength by adjusting the fluid temperature and pressure exists. The surface tension of the fluid reaches zero at the critical point, where liquid droplets are no longer formed. In recent decades, this method has been used to neutralise acidic paper, and the most commonly used fluid is supercritical carbon dioxide (Weng, 2019). It has been studied widely because of its inherent innocuity, low cost and environmentally benign nature, but its weak dissolving capability limits its wide application. The more critical issue is that water in carbon dioxide can produce acidic substances, which may be harmful to paper conservation (Baglioni, 2005; Weng, 2019).

Aqueous deacidification and other methods

Neevel elaborated on the use of phytate as a deacidification method in 1995, wherein it was known that metal phytates, particularly sodium phytate, increased the mechanical strength of papers containing IGI due to its natural antioxidant properties. However, this method was further developed by adding magnesium phytate solution, which has several advantages. However, one of the main limitations of phytate treatment is that the complexing agents are usually metal-specific (Neevel, 1995). The phytate method was further developed over time, using this method along with calcium bicarbonate, application of gelatin sizing, and also replacing sodium with magnesium phytate for paper deacidification (Zervos & Alexopoulou, 2015).

Another method is based on the application of tetrabutylammonium bromide (TBAB) to paper samples containing IGI. Malesic *et al*, conducted a study on stabilization treatment using the interleaving papers or folders that were impregnated with alkaline buffer and antioxidants, resulting in an intense stabilization action in the presence of both iron and copper ions. The degradation rate was also considerably lower than untreated samples, and no migration of iron ions from the ink lines to the surrounding paper could be observed, despite the 90% RH. One limitation of using TBAB is that the inks tend to appear slightly darker after the treatment (Malesic, 2014).

A. Potthast and colleagues discuss the use of gelatine and they mention that it reduces ion mobility, forms a protective layer between inks, shows stabilizing effect and is often used as a resizing agent as a part of the conservation treatment (A. Potthast, 2008).

Rouchon and colleagues also tested the use of halides to treat iron gall ink-damaged papers, but in this case, salts (NaCl, NaBr, $CaBr_2$) were used in combination with $CaCO_3$ as a buffer, and the iron gall inked documents were compressed between two interleaves charged with the active compound. However, high RH conditions (above 80%) for several days are required for the migration of the active compounds from the interleaves to the documents to occur. These conditions may additionally induce the migration of iron and acidic compounds out of the ink line and across the paper itself (Rouchon, 2013).

Biomass interleaving paper (BIP), which is produced from aquatic plants' Duckweed *Lemna gibba* and Water hyacinth *Eichorniacrassipes*, has been proposed as a conservation treatment by Mohammed and team (Mohammed, 2018), wherein each model inked paper coupon is placed upside down on one of BIP strips under pressure. This treatment proved efficient in neutralizing the acidic inked paper, and the production of BIP from non-living plant biomass is cost-efficient and non-invasive. However, the high and fluctuated humidity in storage conditions causes discolouration of iron gall ink and a little darkness of IGI possibly due to Fe^{3+} desorption (Mohammed, 2018).

Calcium hydroxide is one of the most used deacidification compounds in paper conservation due to the long-term physicochemical stability between calcium and cellulose. Still, using aqueous solutions of calcium hydroxide is too chemically aggressive on the cellulose fibre of the paper. The aqueous solutions of bicarbonates (pH≈8.5) or hydroxides involve the presence of free, highly mobile hydroxyl ions that allow fast neutralization of acids. The drawbacks of this method appear when hydroxyls are used in excess since it can result in depolymerization of aged, oxidized cellulose even at room temperature, and the aqueous alkaline environment can alter inks, e.g., through leaching or discolouration (Baglioni, 2005; Weng, 2019). An alternative is to disperse the hydroxide in non-aqueous solvents. This allows a gradual and safe release of OH^- ions from the particles, rather than the sudden delivery of free, highly mobile ions as occurs in the aqueous solutions. The neutralization between the OH^- ions (from particles) and the H^+ ions (coming from acidic species) take place on the surface of the particles through a layer of water that comes from environmental humidity and fibres moisture (Baglioni, 2015). An alternative is to use nanosized particles of calcium hydroxide for paper conservation.

2.2. **Nanomaterials and Iron Gall Inked paper conservation**

Nanomaterials have been employed for IGI conservation for their increased surface area that is available to react compared with their bulk analogues which would ensue in the enhanced potential for neutralization. In addition, the nanoparticles, applied in lower amount comparing to their bulk counterparts, are expected to penetrate the interdigitated cellulose fibre net and reach more easily to the thickness of the treated paper as deeply as possible (Weng, 2018). Several studies were conducted on using nanomaterials to conserve iron gall ink-induced corrosion on paper. Paper samples have been treated with nanomaterials by different kinds of application methods. The samples have been immersed in NPs dispersions such as $Ca(OH)_2$ and $Mg(OH)_2$ in 2-propanol (Sequeira, 2006; Wójciak, 2015); and NPs of silver and zinc oxides (Fouda, 2019). In alternative, NPs dispersions were also brushed on to the paper (e.g. $Ca(OH)_2$ and $Mg(OH)_2$) (Poggi, 2010; Poggi; 2011; Poggi, 2016); and applied by spray (Afsharpour, 2011).

Various combinations of nanoparticles of alkaline metals and carrier solvents of non-aqueous treatment methods have been experimented in the conservation of cellulose-based art materials (Weng, 2019). In addition, biosynthesized NPs of ZnO and Ag have been studied as efficient strategy against microbial deterioration in manuscripts (Fouda, 2019). The results showed that the low concentration of NPs used can protect cellulosic fibres from bacterial deterioration, however, this treatment led to increased darkness in the treated papers.

Afsharpour (Afsharpour, 2011) attempted layering cellulosic nanocomposite of TiO_2 as a protective coating on the surface of paper fibers as it can protect the paper from damaging effects of UV radiation, air pollutants, mold and bacteria, which resulted in

good stability of papers against bacterial growth. A drawback of this procedure could be the degradative effect of organic solvent on the inks and colours used in the historical paper documents (Afsharpour, 2011).

$Ca(OH)_2$ NPs dispersed into 2-propanol were sprayed on yellow paper made in the 14^{th}, 17^{th}, 19^{th}, and 20^{th} centuries (Poggi, 2014). The test showed that the pH of the aged paper increased from 5 to 8, demonstrating a satisfactory deacidification effect. In addition, the paper retains alkalinity for a long time, as indicated by 4 months of accelerated aging (c.f. Zhu, 2021).

Poggi *et al.,* (Poggi, 2010) reviewed the efficacy of applying nanomaterials for deacidification and inhibition of Fenton reaction to that of with Bookkeeper method. There was little to no colour change in the treated samples, and one of the main advantages of this method is that it is possible to prevent two degradation pathways (oxidation and hydrolysis) in a single step. Yet, it was determined through gravimetric measurements that the aqueous treatment led to a considerable loss (~50%) of the applied iron gall ink (Poggi, 2010).

Another study, involved the application of alkaline earth metal hydroxide nanoparticles dispersed in alcohols to inhibit ink-induced degradation of paper objects. The dispersions were applied using a brush on both sides of the samples and left to dry in air for 10 days in order to neutralize the acidity and to be converted to respective alkaline earth metal carbonates, which would be the alkaline reserve deposit within the paper. The solvent, 2-propanol, used for the nanoparticle application does not affect water-sensitive object components, therefore, making the dispersion less harmful to the paper compared to aqueous deacidification solutions (Poggi, 2011). A similar study of the use of nano $Ca(OH)_2$ in different dispersions of ethanol and 2-propanol was conducted, and the resulted changes were observed in terms of pH and mechanical strength (Ali, 2019).

An attempt was also made to study the deacidification with calcium hydroxide nanoparticles that were obtained via a solvothermal reaction by applying it using a micropipette and directly dropping onto the samples. After treatment, the pH of the samples was neutral and remained constant upon the aging, thereby inhibiting the depolymerization of cellulose (Poggi, 2014).

Bastone *et al.*, treated an ancient book in Italy with nano $Ca(OH)_2$ that was dispersed in a water-isopropanol mixture and monitored its pH for a long time. After treatment, the pH of the book increased from 6.2 to 8.2 and decreased only after 1 year (Bastone, 2017). Similarly, Sequeira *et al.* (Sequeira, 2006) studied the efficiency of nano $Ca(OH)_2$ in 2-propanol over traditional treatment with a saturated aqueous $Ca(OH)_2$ solution. It was known that the IGI samples maintain their coloration closer to the original after the non-aqueous $Ca(OH)_2$ nanoparticles treatment, contrary to the aqueous treatment that changes the ink aesthetics considerably.

Bicchieri *et al.* (Bicchieri, 2017), synthesized nano calcium carbonate and calcium nano-propanoate for conservation of library materials. This provides a safety strategy for treatment as they are not aggressive to the support and also promising for their eco-sustainability.

In the study conducted by Xu *et al.*, cellulose nanocrystals were grafted along with the addition of nano $Ca(OH)_2$ and nano $CaCO_3$. This resulted in improved mechanical properties of paper and an increase in pH (Xu, 2020). However, cellulose nanocrystals are expensive, and the grafting process is time-consuming (Zhu, 2021).

The above-discussed literature has proven the potential of nanoparticles for application in paper conservation in general and IGI-induced degradation in particular for biological protection, deacidification and consolidation in comparison to the traditional methods of conservation. However, many methods have drawbacks such as ink loss, discoloration, or the method itself being expensive, time and energy consuming along with problems associated with the selection of the best solvent, application mode and proper concentration of dispersion which would, in turn, affect the behaviour of NPs upon application. Further research would lead to a better understanding of IGI, its related degradation and the role of eco-friendly, sustainable nanomaterials for the conservation of the same.

Chapter 3:

Applied Analytical Techniques

3.1. X-Ray diffraction

X-ray diffraction (XRD) is a material characterization technique that provides information regarding crystalline structure, the nature of the phase, lattice parameters and crystalline grain size (Mourdikoudis, 2018). When a beam of X-rays strikes a crystalline solid, reinforced diffractions peaks of radiation with varying intensities are produced. This occurs when the wavelength of the X-rays is equal to the distance between the planes of atoms in the crystalline solid (Stuart, 2007). Two waves in phase reach the crystal at an angle θ and are diffracted at the same angle by adjacent layers. Constructive interference of the X-rays occurs at an angle θ if the path length difference is equal to a whole number of wavelengths, $n\lambda$, where n is a integer number and λ is the wavelength which can be described using Bragg's Law [1],

$$n\lambda = 2d \sin\theta \qquad \text{[Eq. 1]}$$

where d is the distance between the layers of atoms (Stuart, 2007).

Powder diffraction is a very powerful tool for the identification of crystal phases and when applied to cultural heritage materials, it is commonly used to determine the phases relative to specific production processes, to trace the provenance of materials, to understand the details of the manufacturing techniques, or to evaluate the degradation state of the object (Artioli, 2013). This technique was used in this study to characterize the mineralogical phases of the synthesized nanomaterials.

3.2. Thermogravimetric analysis

Thermogravimetric analysis (TGA) is a thermal method that involves the measurement of the weight loss of a material as a function of temperature or time. It can be used to quantify the mass change in a material associated with transitions or degradation / decomposition processes with the increase in time and temperature (Stuart, 2007).

In the context of cultural heritage studies, initially, this analytical technique was used to determine firing temperatures of archaeological ceramics but over time the use of thermal analysis expanded to various fields of cultural heritage such as studies related to the characterization of the painting media, the waterlogged wood recovered in archaeological excavations, the parchment used in ancient documents, the mortars employed in historic buildings, heritage stones, the synthetic polymer coatings with

high potential for the conservation and restoration of textiles with cultural value, or the thermal analysis of mock ups as well as historic tapestries (Pires & Cruz, 2007).

Within the purview of the current study, the variations in weight as a function of the temperature obtained can be used to identify the composition of nanomaterials, determine the effect of additives and assess the thermal stability (Rami, 2020). The weight loss percentage at different temperature ranges indicates the presence of various phases of the nanomaterial in the synthesized sample and therefore this technique can be used for quantitative analysis.

3.3. Scanning electron microscopy-Energy dispersive spectroscopy

A *Scanning electron microscope* is a versatile equipment that produces detailed magnified images of the surface of an object with the help of a beam of electrons. It can magnify objects 100,000 times, and high-resolution three-dimensional images can be produced (Stuart, 2007). An electron gun fires a beam of electrons at the sample. This beam passes through a series of magnetic lenses that focus the electrons on a very small spot. The action of the electron beam can stimulate the emission of high-energy backscattered electrons (BSE) due to elastic interactions whereas inelastic interactions can promote low-energy secondary electrons (SE) from the surface of the specimen. BSEs originate from deeper areas of the sample, whereas SEs come from surface regions. A detector counts and amplifies these signals for the computer which provides a three-dimensional image of the object's surface on a monitor (Price & Burton, 2011). SEM can be used to observe the morphological characteristics (Mourdikoudis, 2018) and therefore, it can be employed to examine the materials used in heritage manuscripts as it is particularly helpful for ascertaining the state of deterioration of such materials (Stuart, 2007).

Scanning electron microscopy may also be combined with *Energy dispersive spectroscopy* (EDS) in order to carry out elemental analysis of very small samples. EDS involves the examination of the X-rays that are released by the secondary electrons in an inelastic collision. These X-rays allow elements to be identified (Stuart, 2007). The EDS analysis helps to understand the distribution of chemical elements across the sample.

3.4. Fourier transform infrared spectroscopy-Attenuated total reflectance

Fourier transform infrared spectroscopy (FTIR) is a technique based on the measurement of the absorption of electromagnetic radiation with wavelengths within the mid-infrared region (4000–400 cm^{-1}) (Mourdikoudis, 2018). In a FTIR spectrometer, the radiation emerging from a source is passed through an interferometer to the sample before reaching a detector (Stuart, 2007). Each part of a molecule has specific singular

resonant vibrational modes that can be identified through FTIR and therefore revealing the constituent elements and their bonding arrangements (Baudot, 2010).

However, depending on the sampling method, FT-IR spectroscopy can be used in different modes such as transmission and reflection. Reflectance techniques may be used for samples where the destruction of the sample needs to be avoided or when the surface properties are of interest. *Attenuated total reflectance* (ATR) spectroscopy utilises the phenomenon of total internal reflection (Stuart, 2007). During reflection, the infrared radiation penetrates a short distance into the sample before being reflected back. The intensity of the radiation that penetrates the sample decays exponentially with the distance from the surface, giving the analysis a very short ability of penetration and making it particularly effective for the study of surfaces and most suited for analysing paper surfaces (Ferreira, 2009).

FTIR spectroscopy is a well-established analytical technique that has been used in the cultural heritage field for identifying and characterising original materials, degradation and restoration/conservation products, and monitoring of cleaning treatments. ATR-FTIR spectroscopy is a very suitable method for the investigation of cultural heritage materials due to its minimal requirements for sample preparation and its provision for high resolution. Applications of ATR-FTIR spectroscopy on cultural heritage have been explored and the findings are significant to archaeology and conservation management of cultural heritage (Liu & Kazarian, 2022). In this study, the technique has been employed to analyse the synthesized nanomaterials, the change in the paper samples before and after application of nanoparticles and in paper samples on the regions with and without ink.

3.5. Technical photography

The use of imaging has played an essential role in the science-and-art interface because it is extremely useful to examine and document the conservation status of artistic and cultural heritage objects, and it should be performed as a first step in the study (Rizzutto, 2015). Photography is one of the oldest non-destructive imaging techniques and is considered to provide an accurate pictorial record. It provides accurate pictorial record (Verhoeven, 2016). The purpose of using photographic documentation in this work was to observe the morphological and chromatic features of the paper samples prior to the treatment and to be able to compare the features before and after consolidation.

3.6. pH measurement

The pH of an artifact is an important consideration when selecting suitable conservation treatments, storage conditions, and accompanying exhibition materials. Measuring pH is therefore a common procedure in the assessment and documentation

of cultural objects. A pH meter with an electrode (when immersed in a drop of water on the surface of the sample), can determine the pH of the surface with high accuracy and repeatability (Rota, 2021). Its evaluation is important because acidity affects the permanence of the paper.

3.7. Colorimetry

Colorimetry is a technique that allows to quantify and describe colours through spectrophotometry. The data is represented in colour spaces, namely using CIEL*a*b* systems where "L" coordinate corresponds to brightness, "a" colour ranging from red (positive values) to green (negative values) and "b" ranges from yellow (positive values) to blue (negative values) (Ohta & Robertson, 2005). The introduction of colorimetry in the study of cultural heritage has led to the analysis of colour fading on surfaces of artefacts subsequently assisting in understanding the cause of discolouration and evaluating the effectiveness of preventive and conservation measures that do not alter colour of the surface (Plutino & Simone, 2021).

Total colour variations (ΔE*) can be calculated according to Eq. 2,

$$\Delta E^*_{Lab} = [(\Delta L^*)^2 + (\Delta a^*)^2 + (\Delta b^*)^2]^{1/2} \quad \text{[Eq. 2]}$$

where ΔE^*_{Lab} represents the total colour difference, ΔL^* represents the lightness-darkness variation; Δa^*describes the redness-greenness variation; and Δb^* describes the yellowness-blueness variations. The parameters variation was calculated according to [Eq.3], [Eq. 4] and [Eq. 5] (Feller, 2002),

$$\Delta L^* = L^*(sample) - L^*(standard) \quad \text{[Eq. 3]}$$

$$\Delta a^* = a^*(sample) - a^*(standard) \quad \text{[Eq. 4]}$$

$$\Delta b^* = b^*(sample) - b^*(standard) \quad \text{[Eq. 5]}$$

3.8. 3D-Digital microscopy

The Digital microscope is used to acquire 3D images of the sample with a maximum magnification of up to 5000x with multiple illuminations. It enables 3D analyses including height, depth and profiles of a large range of materials such as pigments, cracks, and loss of material. It can also provide information on the morphological features of the paper surface.

3.9. Micro-Raman spectroscopy

Raman spectroscopy is a technique that studies how radiation (ranging between Visible to near-infrared region) is scattered by a sample (Stuart, 2007). The Raman spectroscopy provides information on the structure of natural compounds such as gemstones and minerals, the provenance of raw materials and technological productions (Caggiani & Colomban, 2020). In this study, it has been used to analyse the crystals formed on the surface of paper samples prior to treatment during the sample storage.

3.10. Accelerated aging

A climatic chamber allows temperature and relative humidity parameters to be controlled and recorded throughout a certain duration of time commonly used for conducting artificial aging. An artificial aging test intends to accelerate the process of natural aging, satisfying all the variables of the degradation process which would otherwise occur in natural aging conditions (Porck, 2000). The goals of accelerated ageing studies include the prediction of rates of degradation at room temperature (or similar); comparison of the stability of a variety of samples at some chosen conditions of aging; and studies of degradation mechanisms (Strlič, 2005).

Chapter 4:

Materials and Methods

4.1. Materials

The paper samples containing IGI used in this study were already prepared prior to the start of this master's thesis in the scope of the doctoral research work conducted by Margarida Nunes (PhD ref: SFRH/BD/147528/2019) under the IronIC project (PTDC/ART-HIS/32327/2017), both funded by *Fundação para a Ciência e Tecnologia* (FCT). All the related information about the ink and samples' preparation and artificial aging carried out previously is described in the Appendix A1.

4.1.1. Sample description

The batches of samples painted with inks R1 and R2 to be used in this study are:

- zero aging (t0) samples,
- artificially aged samples for 4 weeks (t4);
- artificially aged samples for 5 weeks (t5).

Since there are two different recipes involved, the samples were named as <recipe>_<aging time> such as R1_t0, R1_t4, R1_t5, R2_t0, R2_t4 and R2_t5 (Table 4.1).

Table 4.1.: Untreated sample description

Sample	*Sample name*	*Ink recipe*	*Paper aging before treatment*	*Sample image*
1	R1_t0	R1	0 days	
2	R1_t4	R1	4 weeks	
3	R1_t5	R1	5 weeks	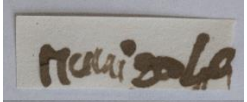
4	R2_t0	R2	0 days	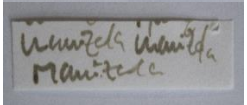
5	R2_t4	R2	4 weeks	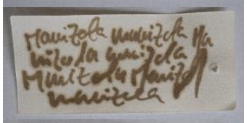
6	R2_t5	R2	5 weeks	

4.1.2. Nanoparticle synthesis

In this study, nanoparticles of calcium hydroxide, $Ca(OH)_2$, and magnesium hydroxide, $Mg(OH)_2$, were synthesised by chemical precipitation from an aqueous solution method (Girginova, 2020; Daniele & Taglieri, 2012). The chemicals involved in the synthesis were used as purchased without any further purification (Appendix 2, Table A2.1.)

Synthesis of calcium hydroxide ($Ca(OH)_2$) nanoparticles:

For synthesising $Ca(OH)_2$ NPs following the abovementioned methodology, aqueous solutions of calcium chloride ($CaCl_2$) and sodium hydroxide (NaOH) were prepared using calcium chloride anhydrous and sodium hydroxide in ultrapure water (Mili Q) in a concentration of 0.4 mol/dm^3 and 0.8 mol/dm^3, respectively.

Equal volumes of aqueous solutions of $CaCl_2$ (100 mL, 0.4 mol/dm^3) and NaOH (100 mL, 0.8 mol/dm^3) were heated separately under magnetic stirring until they reached a temperature of 90 ℃. As the solution of $CaCl_2$ was heating up (30 ℃), 530 μL of Triton X-100 ($(C_2H_4O)_nC_{14}H_{22}O$) were added to it as a non-ionic surfactant to reduce the synthesis time and to prevent agglomeration of the particles during the reaction (Daniele & Taglieri, 2012). The NaOH solution is added dropwise to mixture at 90 ℃ in the set up shown in figure 4.1a. As the reaction takes place [Eq. 6], the mixture turns milky white with the formation of the calcium hydroxide The reaction continued to take place for an hour at a temperature of 90 ℃ after which the mixture was left to cool down. Then, the white precipitate of calcium hydroxide (Figure 4.1b) was washed with Mili Q water within a cycle of sonication (Ultrasonic bath), centrifugation and decantation subsequently repeated until the by-product sodium chloride (NaCl) was removed.

$$CaCl_2\,(aq) + 2NaOH\,(aq) \xrightarrow[Triton\ X-100,90\ ℃]{} Ca(OH)_2\,(s) + 2NaCl\,(aq) \qquad \text{[Eq. 6]}$$

The presence/absence of NaCl was determined by the silver nitrate aqueous solution ($AgNO_3$) test following the reaction [Eq. 7]. Once the white precipitate of silver chloride (AgCl) was not observable, Milli Q water was substituted by ethanol for the last wash cycle, followed by a drying process at a temperature of 75 ℃.

$$NaCl\,(aq) + AgNO_3\,(aq) \rightarrow NaNO_3\,(aq) + AgCl\,(s) \qquad \text{[Eq. 7]}$$

Synthesis of magnesium hydroxide ($Mg(OH)_2$) nanoparticle:

Magnesium hydroxide ($Mg(OH)_2$) NPs were synthesised in the same manner as that of $Ca(OH)_2$ NPs, where an aqueous solution of magnesium chloride ($MgCl_2$) was prepared using magnesium chloride in ultrapure water (Mili Q) with a concentration of 0.4 mol/dm^3. Equal volumes of aqueous solutions of $MgCl_2$ (100 mL, 0.4 mol/dm^3) and NaOH (100 mL, 0.8 mol/dm^3) were heated separately under magnetic stirring until they reached a temperature of 90 ℃. As the solution of $MgCl_2$ was heating up (30 ℃), 0.05 g of hexadecyltrimethylammonium bromide (CTAB) was dissolved in 5 mL H_2O and added to it as a cationic surfactant to improve the dispersion of particles (Girginova, 2020) as described in the reaction below [Eq. 8]. The NaOH solution is added dropwise to mixture at 90 ℃ in the set up shown in figure 4.1a. Once $Mg(OH)_2$ NPs have precipitated, the abovementioned washing cycles occur, followed by drying in the oven.

$$MgCl_2(aq) + 2NaOH\,(aq) \xrightarrow[CTAB,90\,℃]{} Mg(OH)_2\,(s) + 2NaCl\,(aq) \qquad \text{[Eq. 8]}$$

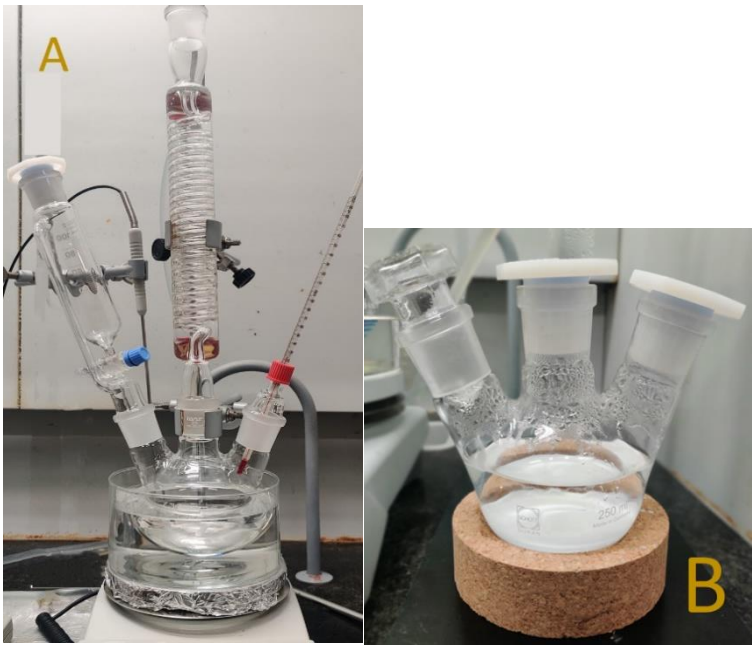

Figure 4.1: Syntheses set up representing:(A) $Mg(OH)_2$ synthesis; and (B)The white precipitate of $Ca(OH)_2$ NPs after slow cooling.

Both of the abovementioned synthesis were repeated twice to produce enough amount of NPs for consolidation and to ensure reproducibility (Table A2.2., Appendix A2).

4.1.3. Treatment of paper samples with NPs dispersions

Before applying nanoparticles dispersions on to the paper samples, specific criteria had to be decided such as, the application method, and the dispersions concentration and quantity to be applied. An error in choice in any of the above parameters could result in adverse effects on samples which are not desired. Therefore, trial runs on a non-important set of samples needed to be done to rule out the difficulties that could occur before experimenting on the selected sets of samples.

4.1.3.1. Defining parameters for NPs application

A set of trial applications were conducted to understand the suitable concentration and the number of applications of the synthesised NPs that would be acceptable to avoid aesthetical change and deacidify effectively IGI containing papers without causing possible cellulose alkaline depolymerization. The number of applications corresponds to the number of sprays applied on the same inked surface of a sample. For conducting a trial application, R2_t4 paper samples were considered.

A total of three different kinds of dispersions of NPs of calcium hydroxide, magnesium hydroxide and mixed (a combination of an equal amount of both calcium and magnesium hydroxides) in 2-propanol with two concentrations (1.0 g/L and 2.5 g/L) were prepared.

Each dispersion was sprayed on samples employing a different number of applications such as 2&2 (two times in the front and two times in the reverse of the paper), 3&3 (three times on each side), 6&6 (six times on each side) and 8&8 (eight times on each side). The preliminary observations were made based on visual examination and pH measurements after the samples were dried (table 4.2).

Table 4.2: Trial application observations.

Nanomaterial	*Dispersion Concentration/ g/L*	*Number of Applications*	*pH before treatment*	*pH after treatment*	*Visual observation (after 10 days)*
$Ca(OH)_2$	1.0	2&2	1.97	2.71	No visible change
		3&3	2.15	4.51	No visible change
		8&8	3.95	5.6	White haze over darker ink
	2.5	2&2	2.15	2.95	No visible change
		3&3	2.73	4.24	Darker ink
		6&6	2.63	8.45	Darker ink
		8&8	2.11	9.50	White haze over darker ink
$Mg(OH)_2$	1.0	2&2	1.97	2.85	No visible change
		3&3	2.15	4.33	Darker ink
		8&8	3.95	5.53	White haze darker ink
	2.5	2&2	2.15	4.01	No visible change
		3&3	2.73	6.1	Darker ink
		6&6	2.63	6.83	Darker ink
		8&8	2.11	8.19	White haze over darker ink
Mixed $Ca(OH)_2$ + $Mg(OH)_2$	1.0	2&2	1.97	3.07	No visible change
		3&3	2.15	4.45	Darker ink
		8&8	3.95	7.81	Darker ink
	2.5	2&2	2.15	6.75	No visible change
		3&3	2.73	5.52	Darker ink
		6&6	2.63	6.15	Darker ink
		8&8	2.11	7.02	Darker ink

A white layer was noticed on the surface of the paper when the dispersion was sprayed on the sample in an excessive amount. Therefore, preventing white haze formation was the primary concern while selecting the adequate concentration and number of applications.

The whitish layer was more prominent in the higher concentration (2.5 g/L) when samples were sprayed 8 times. This concentration attained a higher (more alkaline) pH value than the lower concentration (1.0 g/L) which took 8 applications to achieve a neutral pH value. However, the whitish layer also starts to appear with this number of applications. The samples sprayed with 3&3 applications and less did not reach a basic pH value implying that a higher number of applications was required. Therefore, it was necessary to select a number higher than 3&3 in order to deacidify but lower than 8&8 to avoid the white layer formation. This led to the selection of 2.5 g/L as the dispersion concentration and 4 as the number of applications in an

attempt to achieve a basic pH value for all the paper samples and, to a greater extent, to avoid the formation of the white layer with the obvious change in samples' colour.

4.1.3.2. Nanoparticles application

The dispersions of the nanoparticles were prepared with 2-propanol as the dispersing solvent with a concentration of 2.5 g/L. The dispersion process was assisted by sonication (US bath). Three types of dispersions were prepared (Table 4.3, Figure 4.2a). The dispersions were applied to the paper samples with the help of a spray bottle and were sprayed from an approximate distance of 4 cm from the sample in a horizontal orientation (Figure 4.2 b and c). The samples were sprayed four times on one side, and once the solvent evaporated the samples were flipped and sprayed four times on the reverse to ensure maximum penetration of the nanoparticles into the paper. The samples were treated at temperature, T, 26 ºC and relative humidity, RH, 49 % (data for T and RH were measured outdoors at Évora, Sertório; courtesy of ICT - Instituto de Ciências da Terra, University of Évora; URL: http://www.icterra.pt/estacoes/sertorio).

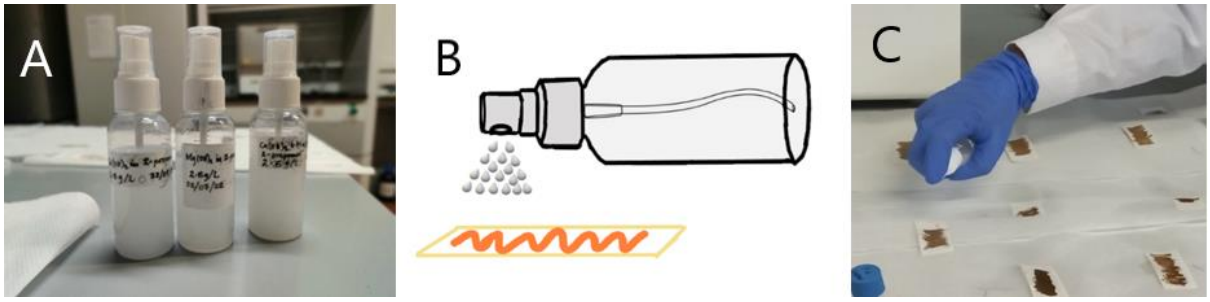

Figure 4.2: Experimental details: (a) Nanoparticle dispersions; (b Representation of the dispersions application on paper; (c) Nanoparticles dispersions application on paper with IGI.

Table 4.3: Nanoparticle dispersion types.

Dispersion	*NPs*	*Solvent*	*Concentration / g/L*
1	$Ca(OH)_2$	2-propanol	2.5
2	$Mg(OH)_2$	2-propanol	2.5
3	Mixed ($Ca(OH)_2$ + $Mg(OH)_2$)	2-propanol	2.5

A total of two sets of samples, Batch 1 and Batch 2, (Table 4.4) were treated with the three different dispersions as described in Table 4.3. One set of samples (batch 1) was aged under ambient conditions after treatment at 24 ˚C ± 3 ˚C and RH 57% ± 10%. The other set (batch 2, treated at T 22 ˚C and RH 61%) was further aged in the climate chamber at T 80 ˚C and RH 65% (at Laboratório José de Figueiredo). A schematic

representation of the paper samples from R2 is shown in Figure 4.3 (identical for R1 samples). Triplicate samples were used in each set and treated with respective dispersions.

Table 4.4: Specifications of paper samples after treatment.

	Sample Name	*Ink recipe*	*Paper Aging period before treatment*	*Nanomaterial applied*
1	R1_t0_Ca	R1	Unaged	$Ca(OH)_2$
2	R1_t0_Mg	R1	Unaged	$Mg(OH)_2$
3	R1_t0_Mixed	R1	Unaged	$Ca(OH)_2$+ $Mg(OH)_2$
4	R1_t4_Ca	R1	4 weeks	$Ca(OH)_2$
5	R1_t4_Mg	R1	4 weeks	$Mg(OH)_2$
6	R1_t4_Mixed	R1	4 weeks	$Ca(OH)_2$+ $Mg(OH)_2$
7	R1_t5_Ca	R1	5 weeks	$Ca(OH)_2$
8	R1_t5_Mg	R1	5 weeks	$Mg(OH)_2$
9	R1_t5_Mixed	R1	5 weeks	$Ca(OH)_2$+ $Mg(OH)_2$
10	R2_t0_Ca	R2	Unaged	$Ca(OH)_2$
11	R2_t0_Mg	R2	Unaged	$Mg(OH)_2$
12	R2_t0_Mixed	R2	Unaged	$Ca(OH)_2$+ $Mg(OH)_2$
13	R2_t4_Ca	R2	4 weeks	$Ca(OH)_2$
14	R2_t4_Mg	R2	4 weeks	$Mg(OH)_2$
15	R2_t4_Mixed	R2	4 weeks	$Ca(OH)_2$+ $Mg(OH)_2$
16	R2_t5_Ca	R2	5 weeks	$Ca(OH)_2$
17	R2_t5_Mg	R2	5 weeks	$Mg(OH)_2$
18	R2_t5_Mixed	R2	5 weeks	$Ca(OH)_2$+ $Mg(OH)_2$

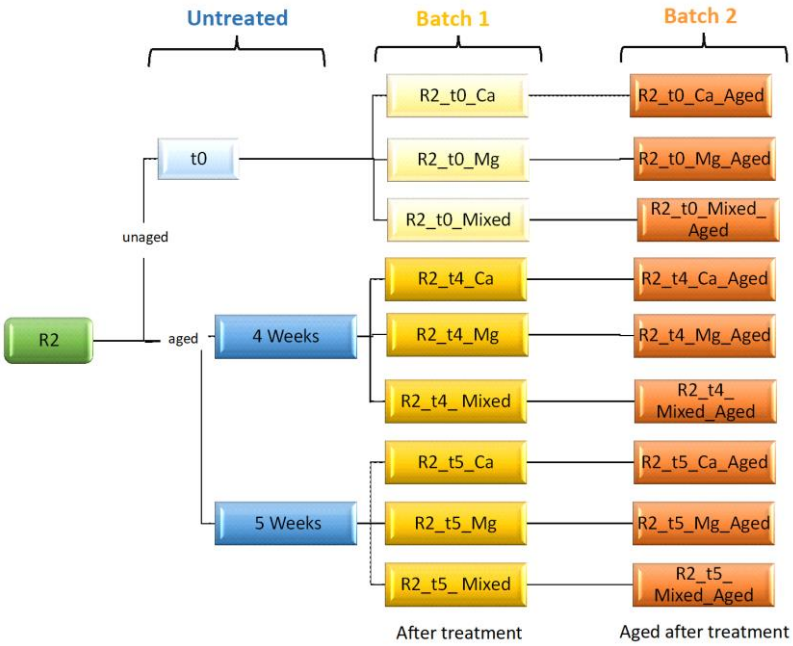

Figure 4.3: Schematic representation of IGI paper samples with R2 ink, involved in this study.

4.2. Characterization Techniques

The NPs were characterized with X-Ray diffraction, thermogravimetric analysis, scanning electron microscope and Fourier transform infrared spectroscopy. The paper samples were characterized before and after treatment with colorimetry, pH measurement, scanning electron microscopy coupled with energy dispersive spectroscopy, 3D- digital microscopy and Fourier transform infrared spectroscopy with attenuated total reflectance.

4.2.1. X-Ray diffraction (XRD)

Crystalline phases of the dried NPs was studied by XRD with a BRUKER AXS D8 Discovery XRD with monochromatized Cu Kα radiation (λ1=1.54056 Å e λ2=1.54439 Å) operating at 40 kV and 40 mA in the 2θ range 3–75º with a step size of 0.05º (2θ) and 1s per step (increment: 0.05º, time 1.000 s, steps = 1438). The DIFRAC.SUITE.EVA software identified the mineral phases with Powder Diffraction Files of the International Center for Diffraction Data-2. For XRD analysis the samples were prepared by powdering dried nanomaterials and then placed the powder in a polymeric sample holder.

4.2.2. Thermogravimetric analysis (TGA)

For the thermal analysis, Simultaneous Thermal Analyzer STA 449 F3 Jupiter (NETZSCH) equipped with a silicon carbide furnace (RT-1550 °C) was used. Around 25-30 mg of powder sample was placed in a platinum crucible and heated under an inert atmosphere of Nitrogen (Air Liquide Alphagaz compressed N_2) with a flow rate of 70 mL/min. The heating program was set to start at 40 ℃ and then increase it with a uniform heating rate of 10°C/min until reaching the temperature of 1000 ℃.

4.2.3. Scanning electron microscopy-Energy dispersive spectroscopy (SEM-EDS)

SEM-EDS analysis of the synthesized samples has been performed using a Hitachi S-3700N (Hitachi High Technologies, Berlin, Germany) Scanning Electron Microscope coupled with an energy dispersive X-ray spectrometer BRUKER XFlash 5010 SDD EDS. The analysis was performed under variable pressure, operated with accelerating voltages of 20 kV (BSE) and 10 kV (SE).

SEM images of NPs samples were captured under SE mode (magnified x8.00k, x25.0k, x27.0k). The samples were prepared by placing a drop of NPs dispersed in ethanol on to a glass piece attached to the SEM sample holder by carbon tape. Once the ethanol

has completely evaporated, the samples were coated with a metallic conductive layer of gold/palladium with Quantum Q5150RES/sputter coater SC 7620 Polaron.

For characterizing paper samples, the analysis was performed under variable pressure, operating with accelerating voltages of 20 kV. Treated and untreated paper samples were fixed onto the sample supports with the help of double-sided carbon tape.

The EDS elemental data was acquired as point microanalyses and elemental distribution maps with ESPIRIT Compact Software. The SEM images for all the samples were acquired in backscattering electron (BSE) mode (magnifications x200, x700, x1.50k) focusing on the regions of the samples where inked and non-inked surfaces could be captured. In addition, samples from Batch 1 R1_t4 and R2_t4 (treated with all of the three dispersions) were metallized and images were captured in secondary electron (SE) mode (x8.00k) to observe the distribution of the NPs in the cellulose paper fibres and ink.

4.2.4. Fourier-transform infrared spectroscopy (FTIR)

The FTIR spectra was obtained with PerkinElmer Spectrum 10.5.2 equipment in transmission mode in the range 400–4000 cm^{-1} with 32 scans and a spectral resolution of 4cm^{-1} when the NPs were analysed. The obtained spectra were converted to absorbance and analysed in NIOS2 Main 00.02.0079 software. The potassium bromide (KBr, FTIR grade) pellets for the analysis were prepared from dried NPs powder.

The FTIR spectra were obtained with a single-reflection diamond ATR module using a Brüker Alpha spectrometer when the paper samples were analysed. The spectra were acquired in the absorbance mode, in the range of 4000 to 375 cm^{-1} with 128 scans and a spectral resolution of 4 cm^{-1}. They were recorded and analysed using OPUS/Mentor software (version 6.5). A total of 6 points were measured from each sample which consisted of 3 inked points and 3 paper points without ink which was then averaged separately resulting in two measurement values for the same sample (inked region and un-inked region).

4.2.5. Technical photography in the visible range

A Sony α 6400 camera with APS-C type (23.5x15.6 mm) Exmor® CMOS sensor was used for the study. The images were captured by placing the camera on a column stand and using natural daylight. Datacolor grayscale, including white, 18% grey, and black reference patches, were used while clicking the images. The picture of the grayscale was later used to white balance the image in the Adobe Photoshop 2021 software.

4.2.6. 3D-Digital microscopy

The images were acquired with an HRX-01 Hirox digital microscope equipped with a 5 MP sensor to suit 4K resolution and motorised HR lenses. The wide and mid objective lenses with corresponding varying magnifications have been used in this study to observe the morphological features of the paper.

4.2.7. Colorimetry

This technique was used to observe and monitor any colour change in the paper and IGI before and after treatment with NPs. A Data Colour Check Plus II colorimeter was used with SCE and Standard Illuminator D65 / 10° parameter and aperture size XUSAV (3 mm). The values obtained in the CIEL*a*b* space colour for every value is an average of three analysis (three light flashes). Four points (3 inked points and 1 white part) on each sample were analysed. The average of each point was calculated with standard deviation in consideration. To calculate ΔE*, based on the equations [Eq. 2], [Eq. 3], [Eq. 4] and [Eq. 5], for Batch 1, the untreated sample was considered as the 'standard'. To calculate ΔE* for Batch 2, the treated sample (Batch 1) was considered as 'standard'.

4.2.8. pH measurement

A HI-99171 portable pH meter together with a HI-14143 electrode was used to measure the pH of paper samples before and after the application of NPs and the samples' progress in time. A drop of conductive electrolyte solution for pH measurement (HI-70960-0) was applied on the paper surface before placing the electrode to enable the measurement. Three points on each paper sample were measured, and the average was calculated with the standard deviation in consideration. The effectiveness of the deacidification of the paper samples with NPs dispersions was ascertained by this technique. This technique was used to evaluate the deacidification potential of the NPs dispersion on IGI paper samples.

4.2.9. Micro Raman spectroscopy

An Alpha300 Witec™ dispersive Raman spectrometer (Oxford Instrument®, United Kingdom) equipped with a Leica DM microscope to focus the laser on the sample surface with a 50x standard objective (NA 0.75) was used for Raman analysis. The experiments were conducted using a 785 nm laser (diode-type, 125 mW, 1200 1/mm grating). The laser power on the sample surface was 2.74 mW. The Raman spectra were collected in the region 100 – 1750 cm^{-1}, with a spectral resolution of 1 cm^{-1}. The number of accumulated scans for each recorded spectrum was 25, and the exposure time was 3 s. All Raman spectra were recorded after instrument calibration on the internal Si-reference standard (520.6 ± 0.1 cm^{-1}) and were performed at room

temperature. All spectra were recorded and processed using Witec software (Witec™).

4.2.10. Climate chamber and accelerated aging

For the purpose of this study the paper samples (batch 2) were aged in moist heat artificial ageing performed at 80 °C and 65% RH (ISO 5630/3:1986) for one week in a FITOCLIMA 150 EDTU, Cimaplus IV climate chamber (José de Figueiredo Laboratory).

Chapter: 5

Results and Discussion

5.1. Nanoparticles Characterization

As mentioned in the previous chapter, two types of nanoparticles, calcium hydroxide $Ca(OH)_2$) and magnesium hydroxide ($Mg(OH)_2$, were synthesised in the HERCULES Laboratory in accordance with the following reactions [Eq. 1] and [Eq. 2]

$$CaCl_2(aq) + 2NaOH(aq) \xrightarrow[\text{Triton X}-100,90\,℃]{} Ca(OH)_2(s) + 2NaCl\,(aq) \qquad \text{[Eq. 1]}$$

$$MgCl_2(aq) + 2NaOH(aq) \xrightarrow[CTAB,90\,℃]{} Mg(OH)_2(s) + 2NaCl\,(aq) \qquad \text{[Eq. 2]}$$

The synthesis yield of $Ca(OH)_2$ and $Mg(OH)_2$ NPs (Appendix A1.2) are approximately, 45 % and 41 %, respectively, which is coherent with the reported values for this reaction (Girginova, 2018). The synthesis reproducibility in terms of yield was also confirmed.

The synthesised NPs were further characterized using four analytical techniques, namely, X-Ray Diffraction (XRD), Fourier Transform Infrared spectroscopy (FTIR), Thermogravimetric analysis (TGA) and Scanning electron microscope-Energy dispersive spectroscopy (SEM-EDS) to understand their, crystalline, molecular structure, composition and morphology respectively.

5.1.1. TGA

To confirm the composition of the NPs and to ascertain the absence of surfactants, TGA-DTG was conducted.

Calcium hydroxide: The thermograms of $Ca(OH)_2$ NPs (Figures 5.1 and 5.2) presents two temperature ranges where significant weight loss has occurred. The weight loss in the first temperature range between 350-550℃ corresponds to the thermal decomposition of calcium hydroxide [Eq. 3], thus enabling the identification and quantification of $Ca(OH)_2$.

$$Ca(OH)_2(s) \rightarrow CaO\,(s) + H_2O(g) \qquad \text{[Eq. 3]}$$

The calcium hydroxide content expressed as $Ca(OH)_2$ % (w/w) is calculated (Table: 5.1) in accordance with [Eq. 4],

$$Ca(OH)_2\,(\%) = [P(H_2O) * M(Ca(OH)_2)]\,/M(H_2O) \qquad \text{[Eq. 4]}$$

where P(H_2O) is the percentage of mass change between 350-550℃, which corresponds to the decomposition of $Ca(OH)_2$,; M($Ca(OH)_2$ represents the molar mass of calcium hydroxide (74.093 g/mol),; and M(H_2O) represents the molar mass of water (18.01 g/mol).

The second temperature range where significant weight loss is observed occurred between 600-900℃ corresponding to the loss of CO_2 due to the thermal decomposition of $CaCO_3$ [Eq. 5], thus enabling the identification and quantification of $CaCO_3$ in the sample.

$$CaCO_3(s) \rightarrow CaO(s) + CO_2(g) \qquad \text{[Eq. 5]}$$

The calcium carbonate content expressed as $CaCO_3$ %(w/w) is calculated with the following equation [Eq. 6],

$$CaCO_3\ (\%) = [P(CO_2) * M(CaCO_3)]\ /M(CO_2) \qquad \text{[Eq. 6]}$$

where P(CO_2) is the percentage of mass change between 600-900℃ due to the decomposition of $CaCO_3$; M($CaCO_3$) represents the molar mass of calcium carbonate (100.082 g/mol); and M(CO_2) represents the molar mass of carbon dioxide (44.02 g/mol).

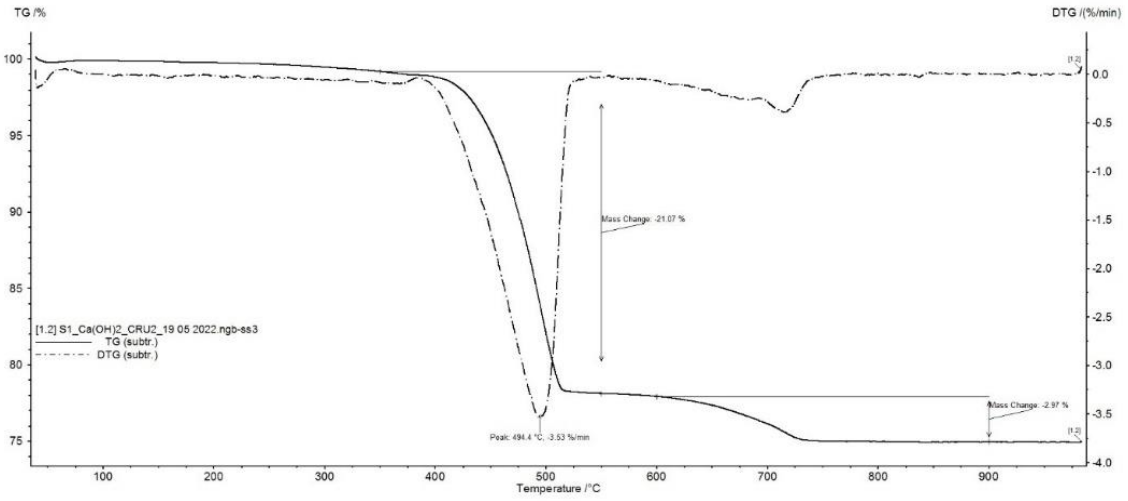

Figure 5.1: TGA-DTG curves of $Ca(OH)_2$ NPs (S1).

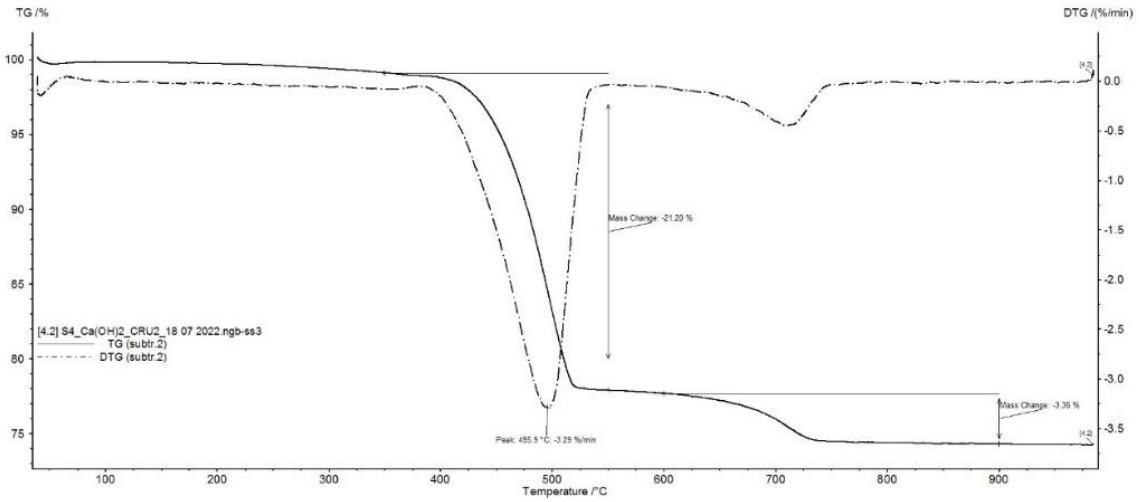

Figure 5.2: TGA-DTG curves of $Ca(OH)_2$ (S4).

Magnesium hydroxide: The thermal analysis of $Mg(OH)_2$ NPs (Figures: 5.3 and 5.4) presents two temperature ranges where significant weight loss has occurred. The first temperature range of 300-450℃ corresponds to the weight loss from the thermal decomposition of magnesium hydroxide [Eq. 7], thus enabling the identification and quantification of $Mg(OH)_2$.

$$Mg(OH)_2(s) \rightarrow MgO\ (s) + H_2O(g) \qquad \text{[Eq. 7]}$$

The magnesium hydroxide content expressed as $Mg(OH)_2$ % (w/w) is calculated in accordance with the following equation [Eq. 8],

$$Mg(OH)_2\ (\%) = [P(H_2O) * M(Mg(OH)_2)]\ /M(H_2O) \qquad \text{[Eq. 8]}$$

where, $P(H_2O)$ is the percentage of mass change between 300-450℃, which corresponds to the decomposition of $Mg(OH)_2$, $M(Mg(OH)_2)$ represents the molar mass of magnesium hydroxide (58.3197 g/mol), and $M(H_2O)$ represents the molar mass of water (18.01 g/mol).

The second temperature range where significant weight loss is observed between 600-900 ℃ which corresponds to the loss of CO_2 in the thermal decomposition of $MgCO_3$ [Eq. 9] and thus enabling the identification and quantification of $MgCO_3$ in the sample.

$$MgCO_3(s) \rightarrow MgO(s) + CO_2(g) \qquad \text{[Eq. 9]}$$

The magnesium carbonate content expressed as $MgCO_3$ % (w/w) is calculated (Table 5.1) in accordance with the following equation [Eq. 10],

$$MgCO_3\ (\%) = [P(CO_2) * M(MgCO_3)]\ /M(CO_2) \qquad \text{[Eq. 10]}$$

where, $P(CO_2)$ is the percentage of mass change between 600-900℃, which corresponds to the decomposition of $MgCO_3$, $M(MgCO_3)$ represents the molar mass of magnesium carbonate (84.3139 g/mol), and $M(CO_2)$ represents the molar mass of carbon dioxide (44.02 g/mol).

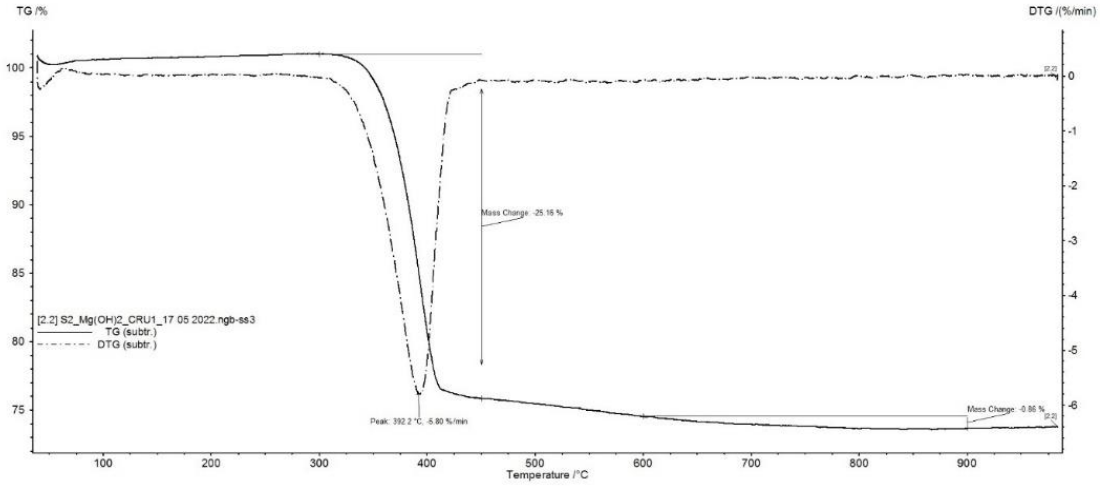

Figure 5.3: TGA-DTG curves of $Mg(OH)_2$ NPs (S2).

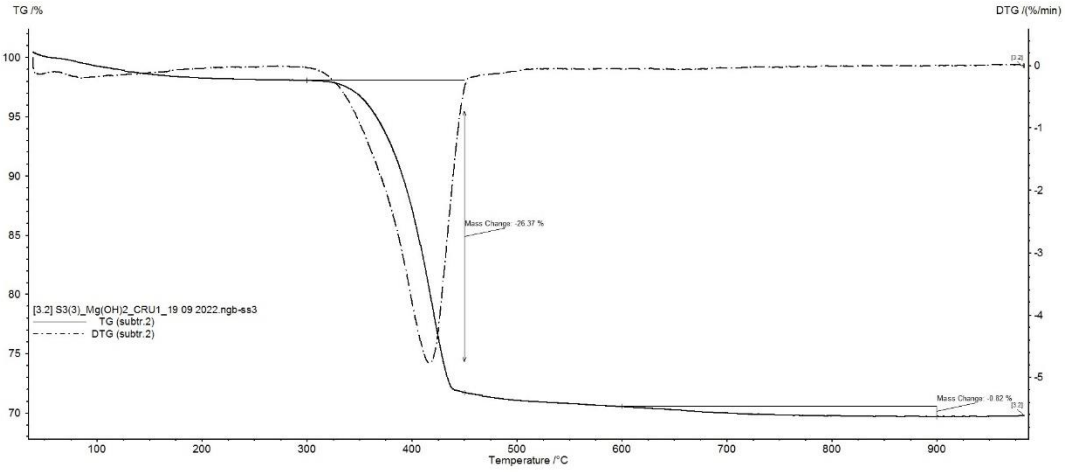

Figure 5.4: TGA-DTG curves of $Mg(OH)_2$ (S3).

Table 5.1: Hydroxide and carbonate content obtained from TGA.

Sample	*$Ca(OH)_2$ / %(w/w)*	*$CaCO_3$ / % (w/w)*	*$Mg(OH)_2$ / %(w/w)*	*$MgCO_3$ / %(w/w)*
S1	86.68	6.80	-	-
S2	-	-	85.68	1.64
S3	-	-	85.49	1.57
S4	87.21	7.69	-	-

The TGA results confirmed that the surfactants Triton X-100 and CTAB are not present in $Ca(OH)_2$ and $Mg(OH)_2$ NPs, respectively. It can be attributed to their removal from successive washing cycles (Dhaouadi, 2011; Rojas, 2019).

5.1.2 XRD

The XRD of the powder samples were performed to identify the crystalline phase structure of the nanoparticles synthesised.

Calcium hydroxide: The diffractogram pattern (Figure 5.5) shows characteristic peaks of the main crystalline phase, calcium hydroxide, $Ca(OH)_2$ and low-intensity peaks for the crystalline phase of calcium carbonate, $CaCO_3$.

$CaCO_3$ indicates a partial carbonatation of the nanolime by atmospheric carbon dioxide and humidity when exposed to air during the drying process and analysis (Michalopoulou, 2020), which is coherent with the results obtained by TGA.

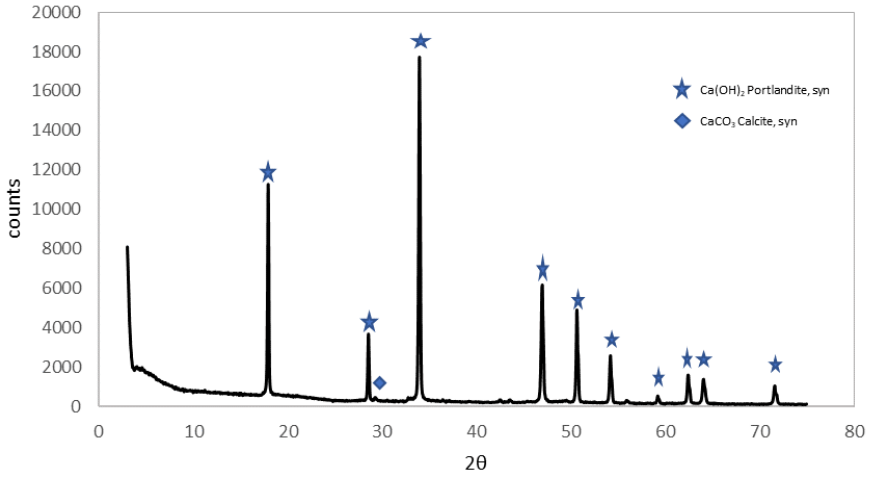

Figure 5.5: XRD pattern of $Ca(OH)_2$ NPs (S4).

Magnesium hydroxide: The diffractogram pattern (Figure 5.6) shows the characteristic peaks of the crystalline main phase magnesium hydroxide, $Mg(OH)_2$. No peaks associated with the crystalline magnesium carbonate phase, $MgCO_3$, were found. This is probably due to a minimal amount of this phase, as inferred from the TGA results.

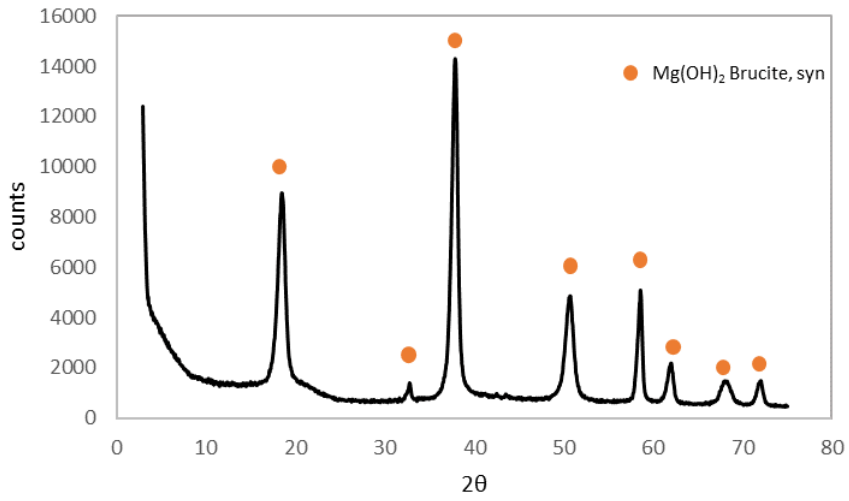

Figure 5.6: XRD pattern of $Mg(OH)_2$ NPs (S3).

The absence of CTAB was also confirmed by XRD due to the lack of the characteristic peaks of the surfactant in $Mg(OH)_2$ pattern (Dhaouadi, 2011).

5.1.3 FTIR

FTIR analysis was conducted to further verify if the surfactant is present in the NPs.

Calcium hydroxide: The sharp bands at 3642 and 3644 cm^{-1} are associated with the OH^- stretching of $Ca(OH)_2$, and the bands at 1457, 1455, 868 and 869 cm^{-1} are indicative of $CaCO_3$ (Girginova, 2020) (Figure 5.7a). In sample S4 (Figure 5.7b), the peaks assigned to the carbonate (CO_3) such as 1455 and 868 cm^{-1} are more evident than in S1, which confirmed that the $Ca(OH)_2$ NPs synthesized in S4 carbonated in the higher degree presumably during drying or storing processes, as observed by the TGA analysis.

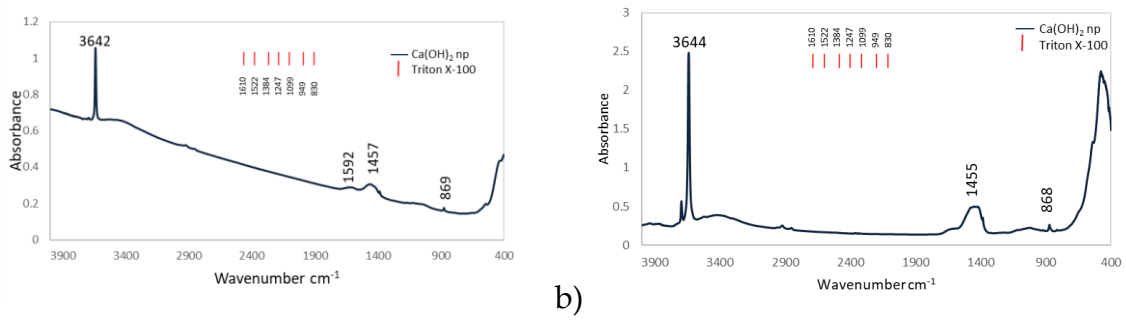

a) b)

Figure *5.7: FT-IR spectra of $Ca(OH)_2$ NPs: a) S1. b) S4. The red dash represents Triton X-100 peak values (Girginova, 2020 and references therein).*

Magnesium hydroxide: The sharp peaks at 3700, 3699, 3642 and 3431 cm^{-1} correspond to the stretching of O-H. The peaks at 1633 and 1436 cm^{-1} are due to the bending vibration

of the water molecules and the characteristic vibration of Mg-OH bond (Asgari-Vadeghani, 2016; Dhaouadi, 2011; Girginova, 2020; Hanna, 2019). The band at 444 cm^{-1} is associated with the lattice mode region of $Mg(OH)_2$ (Oliveira & Hase, 2001). In the S3 NPs spectrum (Figure 5.8b), the peaks attributed to CO_3 - 1383 indicate that the NPs produced in this synthesis carbonates in a higher degree when compared to S2. The absence of peaks at 2920 and 2850 cm^{-1} attributed to the -CH_2 and -CH_3 stretching modes and peaks in the region 1700~1400cm^{-1}, corresponding to the-CH_2 and -CH_3 groups bending modes of the organic surfactant confirmed that the surfactant (CTAB) has been completely washed out (Dhaouadi, 2011) (Figure 5.8).

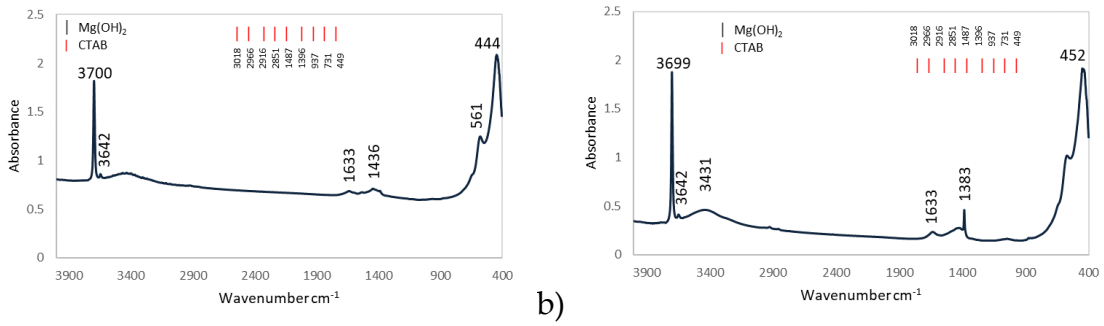

a) b)

Figure 5.8: FT-IR spectra of $Mg(OH)_2$ NPs: a) S2. b) S3. The red dash represents the obtained CTAB peak values.

5.1.3 SEM

SEM-EDS analysis was conducted to analyse the morphological features and elemental composition of the synthesised NPs.

Calcium hydroxide: The nanoparticles of $Ca(OH)_2$ present a hexagonal plate-like shape and appear to be clustered together (Figure 5.9a). The analysis of the SEM images shows that the particles obtained from the two syntheses (S1 and S4) display different space orientations and inhomogeneous size distribution (Figure 5.9b). The mean diameter is 483±204 nm (observed d_{min} of 146 nm and d_{max} of 948 nm) and the mean thickness is 207±89 nm.

Magnesium hydroxide: The $Mg(OH)_2$ NPs show hexagonal plate-like shape, smaller in a narrower size distribution compared to the $Ca(OH)_2$ NPs (Figure 5.10a). The $Mg(OH)_2$ NPs are grown forming flower-like clusters, where each hexagonal platelet has a different orientation (Figure 5.10b). The mean particle diameter measured is142±27 nm (observed d_{min} of 104 nm and d_{max} of 204 nm) and mean thickness of 43±8 nm.

a) 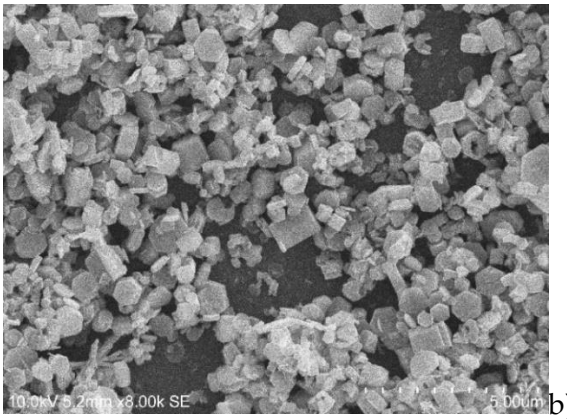

b) 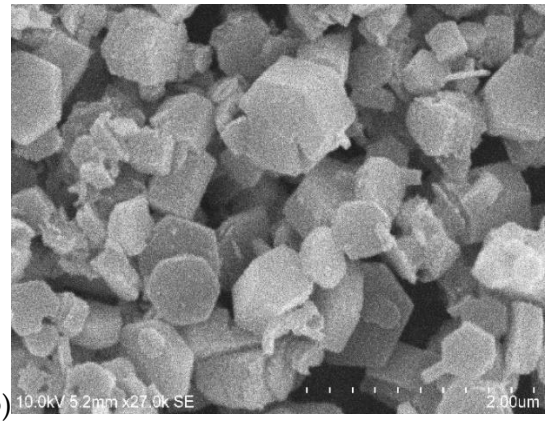

Figure 5.9: SEM images of the laboratory synthesized $Ca(OH)_2$ nanoparticles: a) Magnification 8.0 k. b) Magnification 27.0 k.

a) 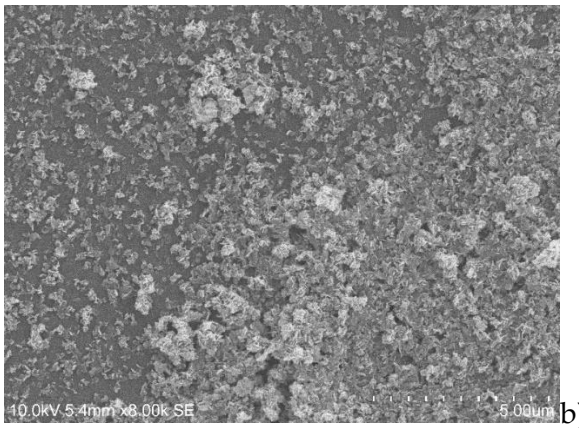

b) 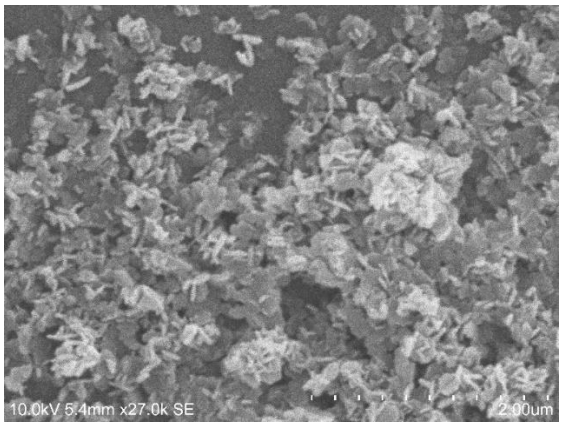

Figure 5.10: SEM images of the laboratory synthesized $Mg(OH)_2$ nanoparticles: a) Magnification 8.0 k. b) Magnification 27.0 k.

5.2. Paper characterization and evaluation of NPs dispersions on IGI on paper

5.2.1. Characterization of paper samples before treatment with NPs

This section discusses the characterization of paper samples before the application of the NP dispersions in order to understand the features of the paper and to be able to observe the changes that may occur after the application of the NPs.

5.2.1.1. 3D-Digital microscopy

The images acquired with the 3D-digital microscope helped understanding the surface texture of the ink on the paper and the paper itself. The images were acquired in two magnifications: x20 and x140 with wide and mid objectives, respectively. The images for R2 samples are present in figure 5.11 and for R1 are in Appendix A3.1. The distribution of ink on the paper fibres can be seen vividly in the images, being darker in the more concentrated parts and gradually becoming lighter at the border of the ink line. Besides, the ink changes colour from approximately black for samples t0 to brown on samples artificially aged (t4 and t5). More time in the chamber (t5 vs t4) led to samples with slightly darker hues of brown.

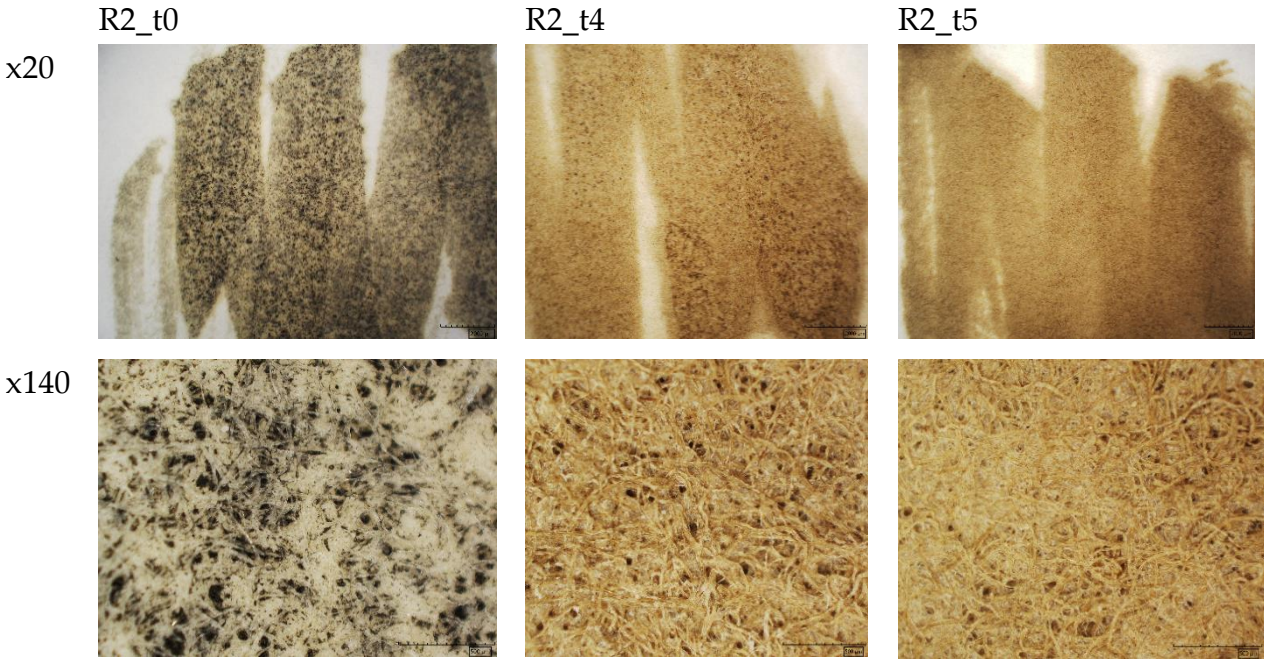

Figure 5.11: 3D-digital microscope images of untreated R2 samples (t0, t4 and t5) in two magnifications (x20 and x140).

5.2.1.2. SEM

SEM images of paper samples were captured, locating parts of the sample where cellulose fibres with and without ink can be observed in a single frame (Figure 5.12).

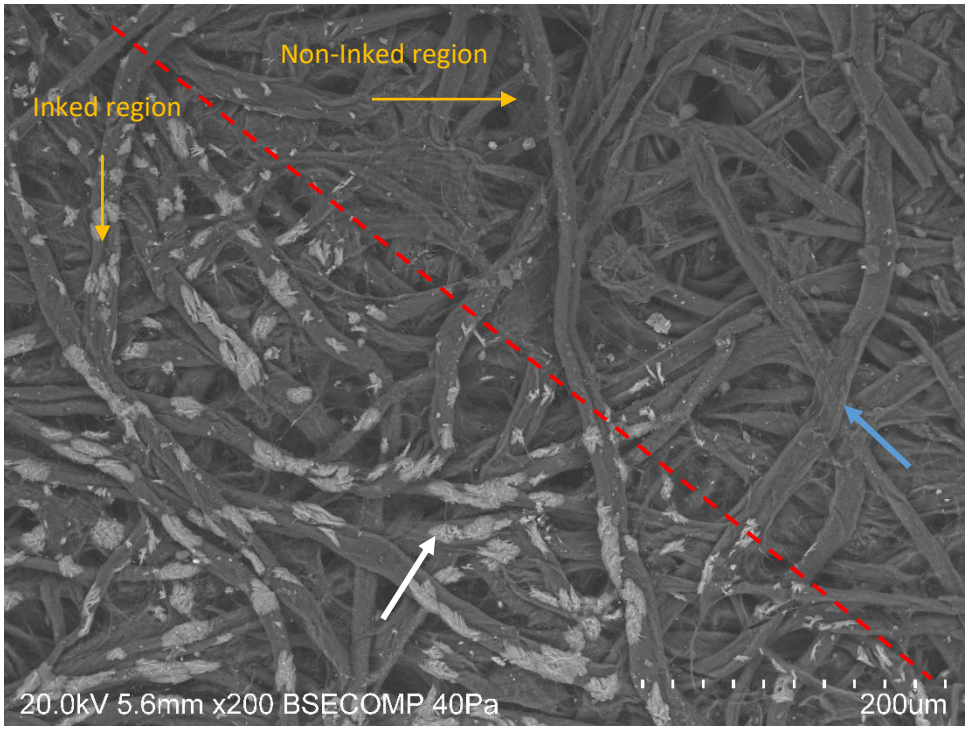

Figure 5.12: SEM image of R2_t4 differentiating parts of the paper with and without IGI. (White arrow - ink particles; blue arrow - cellulose fibres.)

In unaged samples (t0), an ink film can be observed on the top of the fibres. On the contrary, aged samples (t4 and t5) present spiked crystals on the top of the fibres in the inked part and the film disappeared (figure 5.13), showing a totally different morphological features of the aged ink when compared to unaged ink. The SEM behaviour for R1 samples is similar and the results are present in Appendix A3.1.

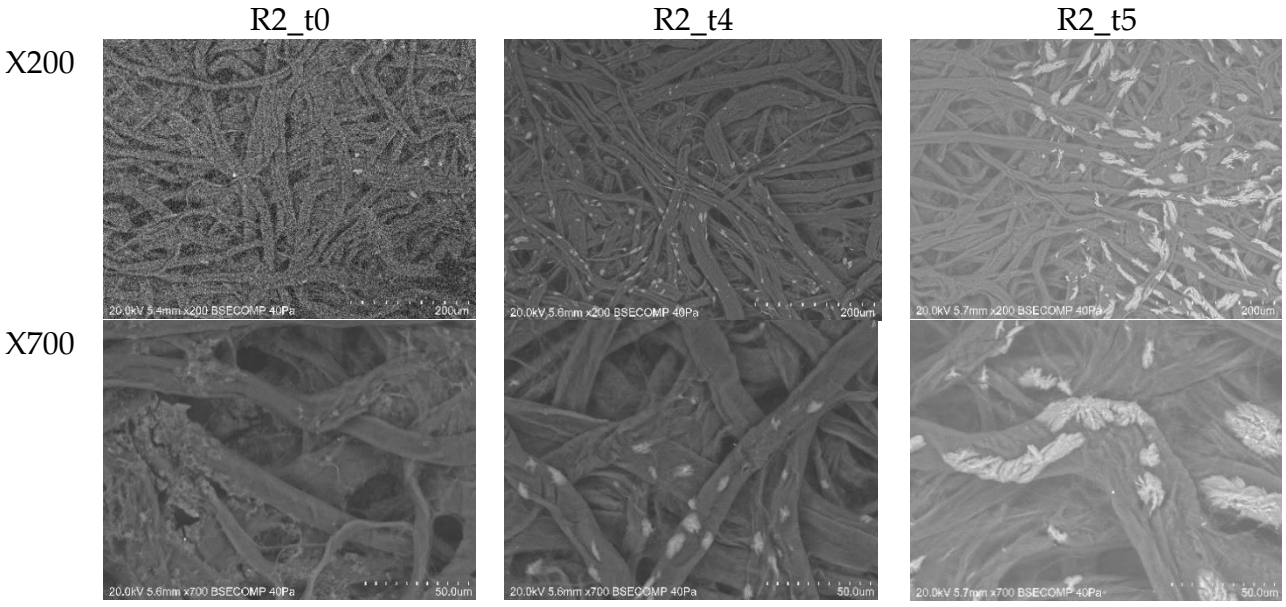

Figure 5.13: SEM images of untreated R2 samples (t0, t4 and t5) in two magnifications (x200 and x700).

5.2.1.3. pH measurements and colorimetry

The initial pH value of the inked paper was measured (Table 5.2). Three measurements were made on each sample, in equivalent points of the inked area, and the average and standard deviation of the values is considered. The samples are very acidic (generally pH ≤ 3) due to IGI. The pH of inked samples from R2 is more acidic in the unaged samples (t0) when compared to R1 which is attributed to the presence of vinegar in the recipe for R2 (see Appendix A1.1). however, the aged samples (t4 and t5) have similar pH regardless of the ink type (Table 5.2).

Colorimetry was used to compare the colour coordinates for the ink before and after the treatment with NPs and to estimate the total colour variation. The L*, a* and b* values were measured in three equivalent points of each sample using a colorimeter and the mean and standard deviation are presented in Table 5.2. The Whatman paper used in this study has colour coordinates of L* 98.79, a* -0.05 and b* 0,44 which corresponds to almost completely white. The unaged samples with R2 ink (R2_t0) is much darker than the corresponding sample from R1 as seen from the L* values but after aging, the samples have similar L* values. R2_t0 sample is more yellow (as seen from b* values) and slightly more red (as seen from a* values) compared to R1_t0 and this behaviour continuous after aging as well. Therefore, unaged R2 ink is darker than R1, and aged R2 ink is more yellow and slightly more red than aged R1 ink.

Table 5.2: pH values and colorimetry coordinates of untreated samples for both inks.

Sample	*pH*	*L**	*a**	*b**
R1_t0	3.0 ±0.1	73.56±0.31	-0.92±0.03	5.52±0.02
R1_t4	2.1 ±0.1	53.13±0.54	6.04±0.05	16.95±0.10
R1_t5	2.3 ±0.1	52.3±0.59	6.99±0.02	18.52±0.06
R2_t0	2.7 ±0.1	58.32±0.27	-0.58±0.03	8.65±0.19
R2_t4	2.5 ±0.2	53.6±0.12	7.66±0.02	21.45±0.06
R2_t5	2.3 ±0.1	53.47±0.03	8.34±0.01	22.52±0.02

5.2.1.4. FTIR

FTIR-ATR is used for identifying the organic and inorganic components present in the paper samples. The samples were analysed prior to treatment to characterize the IGI and the paper support and to observe and compare any changes that could possibly happen after treatment with NPs.

The cellulose OH stretching band is visible in the 3300 cm^{-1} range, with C-H stretching band at 2900 cm^{-1} region (Zidan, 2017). The OH bending mode of water molecule of IGI and cellulose is visible at 1610-1635 cm^{-1}. This band also overlaps with C=O stretching band of cellulose. The peak at 1310 cm^{-1} is associated with the symmetric stretching of hydrolysable tannins from the IGI (Ursescu, 2009). The range between 1200 and 900 cm^{-1} covers the C-O and C-C stretching, anti-symmetric bridge C-O-C, as well as C-C-H and O-C-H deformation vibrations from cellulose and the peak at 1030 cm^{-1} is associated with the C-O stretching of gum Arabic from the IGI (Proniewicz, 2001; Manso & Carvalho, 2009). The peak at 1104 cm^{-1} and 980 cm^{-1} is associated with asymmetric and symmetric stretching of S-O, respectively, from iron sulphate in IGI (Kaminari, 2018; Ursescu, 2009). The peaks at 813 and 484 cm^{-1} may indicate the presence of oxalates formed in the IGI (Ferrer & Sistach, 2013). The spectrum of R2_t4 sample is shown in figure 5.14, with the above-mentioned peaks and bands marked. The assignment to the bands is presented in table 5.3.

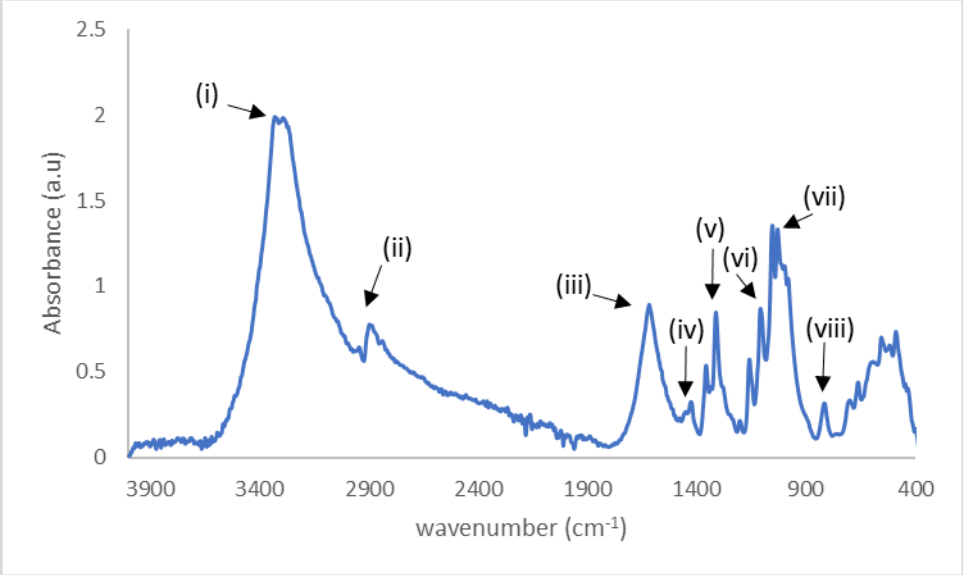

Figure 5.14: FTIR-ATR spectrum of R2_t4 before treatment (i to viii – peak numbering assigned in Table 5.3).

Table 5.3: FTIR-ATR bands and tentative assignments.

Peak nº	***Wavenumber (cm^{-1})***			***Tentative assignment****	
	t0	***t4***	***t5***		
(i)	3331	3328	3318	ν O-H	hydroxyl group of cellulose,
(i)	3269	3288	3294	ν O-H	hydroxyl group of Arabic gum
(ii)	2888	2892	2882	ν C-H	hydrocarbon group in cellulose
(iii)	1611	1616	1617	δ(O-H-O)	adsorbed water
				ν(C=O) (-COOH dimers)	polyphenolic compounds (e.g. tannins from different vegetable sources)
(iv)	1429	1429	1430	ν(C-C) aromatic ν(S-O)	polyphenolic compounds $FeSO_4$ (vitriol)
	1356	1356	1356	ν_s O-C-O	metal oxalates
(v)	1311	1312	1311	δ(C-OH) ν_s(C-O) of the ester function of hydrolysable tannins	polyphenolic compounds
				ν_s O-C-O	metal oxalates
	1279	1284	1283	νC-O	ester, ether or phenol groups
	1158	1158	1159	ν_{as}(C-O-C)	Arabic gum (sucrose)
(vi)	1106	1104	1104	ν_{as}(S-O)	$FeSO_4$ (vitriol)
				ν_s(-CO)	Arabic gum
(vii)	1031	1029	1029	δC-C	Arabic gum
				ν_s(-CO)	polyphenolic compounds
	987	983	981	ν_s(S-O)	$FeSO_4$ (vitriol)
	840	-	827	γ(CH2) δ(C-C-OH) δ(-OH, in carboxyl)	Arabic gum
(viii)	-	814	813	δ(C-C)	metal oxalates
	-	484	484	ν_s(Fe-O)	metal oxalates

**(Díaz Hidalgo, 2018; Kaminari, 2018; Rouchon, 2012; Ursescu, 2009)*

In figure 5.15, the FTIR spectra of all R2 untreated samples are shown (R1 in Appendix: A3.2), wherein the main noticeable difference is in the intensity of the peak at 1610-1635 cm^{-1}. This band is weak and broad in the case of the unaged sample (t0) but becomes stronger in aged samples (t4 and t5). The cellulose oxidation of paper, catalysed by iron ions present in IGI, is indicated by this peak (Ursescu, 2009) which increases with increasing paper degradation by IGI.

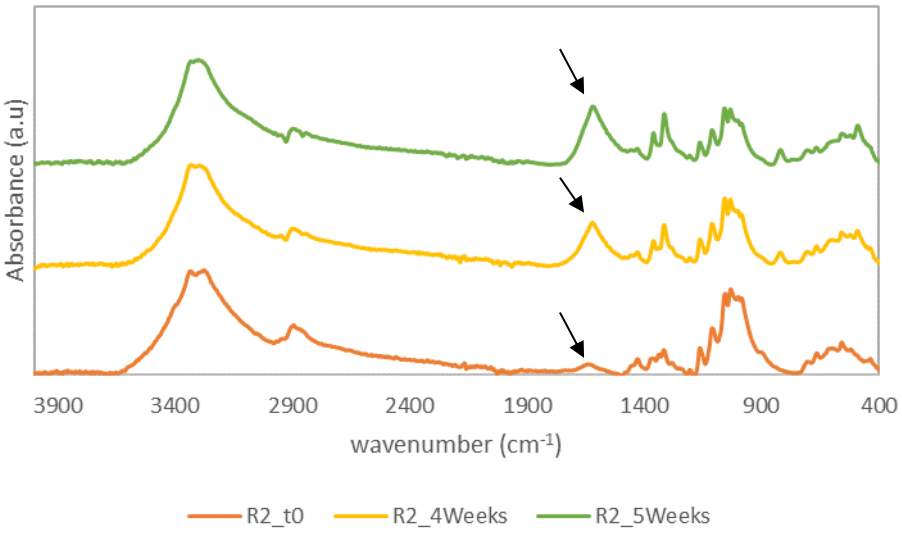

Figure 5.15: FTIR spectra of R2 paper samples before treatment (t0, t4 and t5), indicating the change in intensity of peak 1610-1635 cm^{-1} with an increase in aging time.

Crystal formation on IGI paper: Analysis with 3D-Digital imaging, SEM/EDS and micro-Raman spectroscopy

When sample R1_t4 was analysed by 3D-digital microscopy before the application of nanoparticle dispersions, certain white particles were discovered on the surface of the sample, as depicted in figure 5.16-left. This sample was further analysed by SEM-EDS and Raman spectroscopy to evaluate the shape and the composition of the crystals that formed on the surface of the paper with IGI ink. Raman spectra are in accordance with sulphate compound, and EDS mapping confirmed the presence of Fe represented in figure 5.17. Combination of both techniques suggest the presence of iron sulphate crystals. The morphological features of the crystals are different from the ink particles which can be seen in the SEM image (Figure 5.16-right). The paper samples were kept at air temperature T(av) = 16.6±6 ℃ and relative humidity RH 70.4±19.6 % measured outdoors (http://www.icterra.pt/estacoes/sertorio, courtesy of Évora Geophysics Centre (CGE), (ICT - Instituto de Ciências da Terra)). Due to the high humidity in the laboratory, crystals formed on the surface of the paper sample when the sulphate ion

present bonded to the free iron ions present in the ink (Camera, 2007), while they were stored prior to the start of this study.

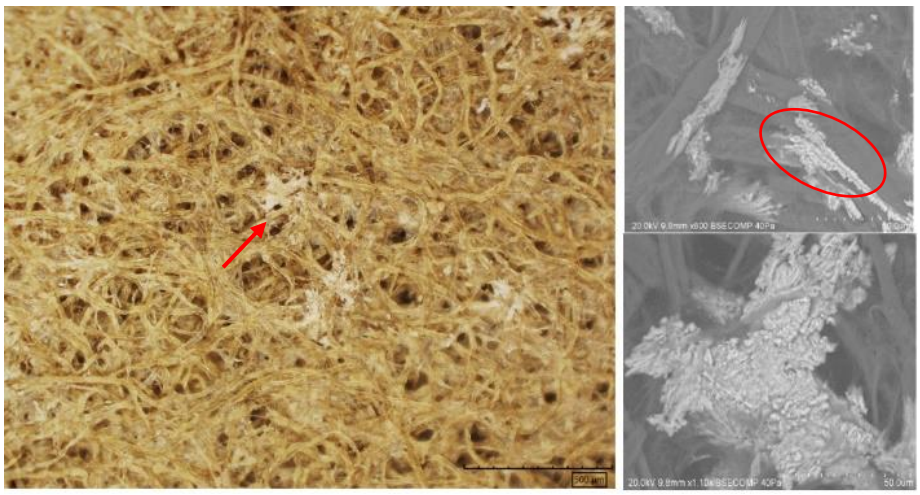

Figure 5.16: Crystals on R2_t4 sample in 3D-digital microscope(left) and SEM (top right – magnification x800; bottom right- magnification x1.10k) with red arrow and red circle showing the crystals.

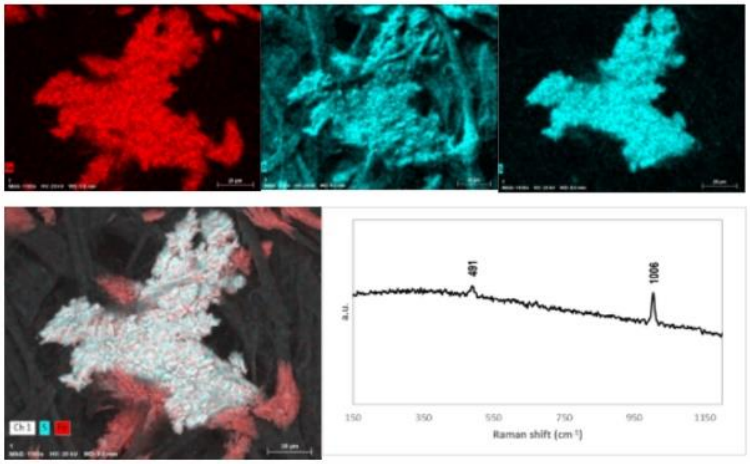

Figure 5.17: EDS mapping of the crystal (top left- Fe; top middle- O; top right- S) confirming the presence of Fe and S and micro-Raman spectra suggesting the presence of SO_4^{2-}.

5.2.2. Characterization of paper samples after treatment with NPs

This section presents the results of the analysis conducted on the samples mentioned as Batch 1 and Batch 2 in the figure 4.3 (representing R2) and the corresponding samples from R1. The pH measurement and colourimeter analysis were conducted on all samples from Batch 1 and Batch 2. SEM-EDS, FTIR and 3D-digital microscopy were used to characterise all the samples from Batch 1 and selected samples treated with

each of the three dispersions (R1_t4 and R2_t4) were analysed from Batch 2. The results measured for samples prepared with ink R1 and their analogues with R2 did not show significant differences; therefore, the results from R2 samples have been selected to be present here, and the remaining are placed in Appendix A4.

5.2.2.1. Photographic documentation

Photographic documentation of samples was taken in visible range after treatment (Batch 1) and also after accelerated aging of treated samples (Batch 2). The images of samples from R1_t4 and R2_t4 are shown in Table 5.4 and the details for other samples are present in Appendix: A4.1. No visible change in terms of colour was noticed in samples from Batch 1 whereas; the samples from Batch 2 present colour alteration that can be noticed by visual inspection. The ink colour became darker after accelerated aging.

Table 5.4: Images of samples of R1 and R2 (t4; treated and untreated) from Batch 1 and Batch 2

	Untreated	Batch 1 *(treated)*	Batch 2 *(treated and aged)*
R1_t4_Ca			
R1_t4_Mg			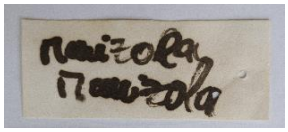
R1_t4_Mixed			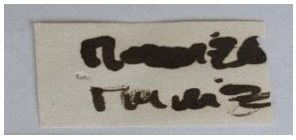
R2_t4_Ca		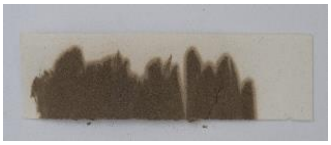	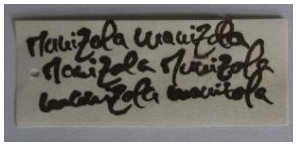
R2_t4_Mg	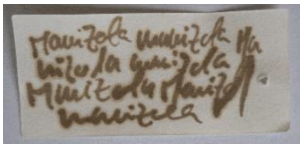		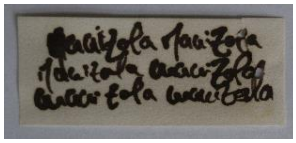
R2_t4_Mixed			

5.2.2.2. 3D digital microscopy

Two magnifications were used for the observations: x20 with the wide objective and x140 with the mid objective. The samples analysed were:

- Batch 1 was observed three times in a period of 6 weeks, wherein observation #1 is immediately after the application, #2 is three weeks after the application, and #3 is six weeks after the application.
- Batch 2 (R1_t4 and R2_t4) with three different treatments, observed 2 weeks after accelerated aging.

The samples do not show any significant changes in the paper surface between the untreated and Batch 1. However, there is a difference in terms of colour in Batch 2, when compared to Batch 1. In fact, this has already happened with untreated samples t4 and t5 (figure 5.11), where the latter presented darker hues, which is expected after the accelerated aging and is more likely from the degradation of IGI as mentioned in the work by Malesic (Malesic, 2014).

The three NPs $Ca(OH)_2$, $Mg(OH)_2$ and mixed treatments seemed not to produce any significant morphological and textural change in the ink surface as can be observed in the 3D-digital microscopic images in Figure 5.18, where images for samples R2_t4_Ca, R2_t4_Mg and R2_t4_Mixed, acquired before treatment, after treatment (Batch 1: #1, #2 and #3) and also images observed on samples subsequently aged under accelerated conditions after treatment (Batch 2) are presented. The images acquired for other samples are present in Appendix: A4.2 and A4.3.

The images acquired from the 3D-digital microscope show no change occurring on the surface texture of the paper fibres in regards to the treatments, indicating that the treatment with different NPs do not form any visible residues on the surface of the paper or alter it from a morphological point of view.

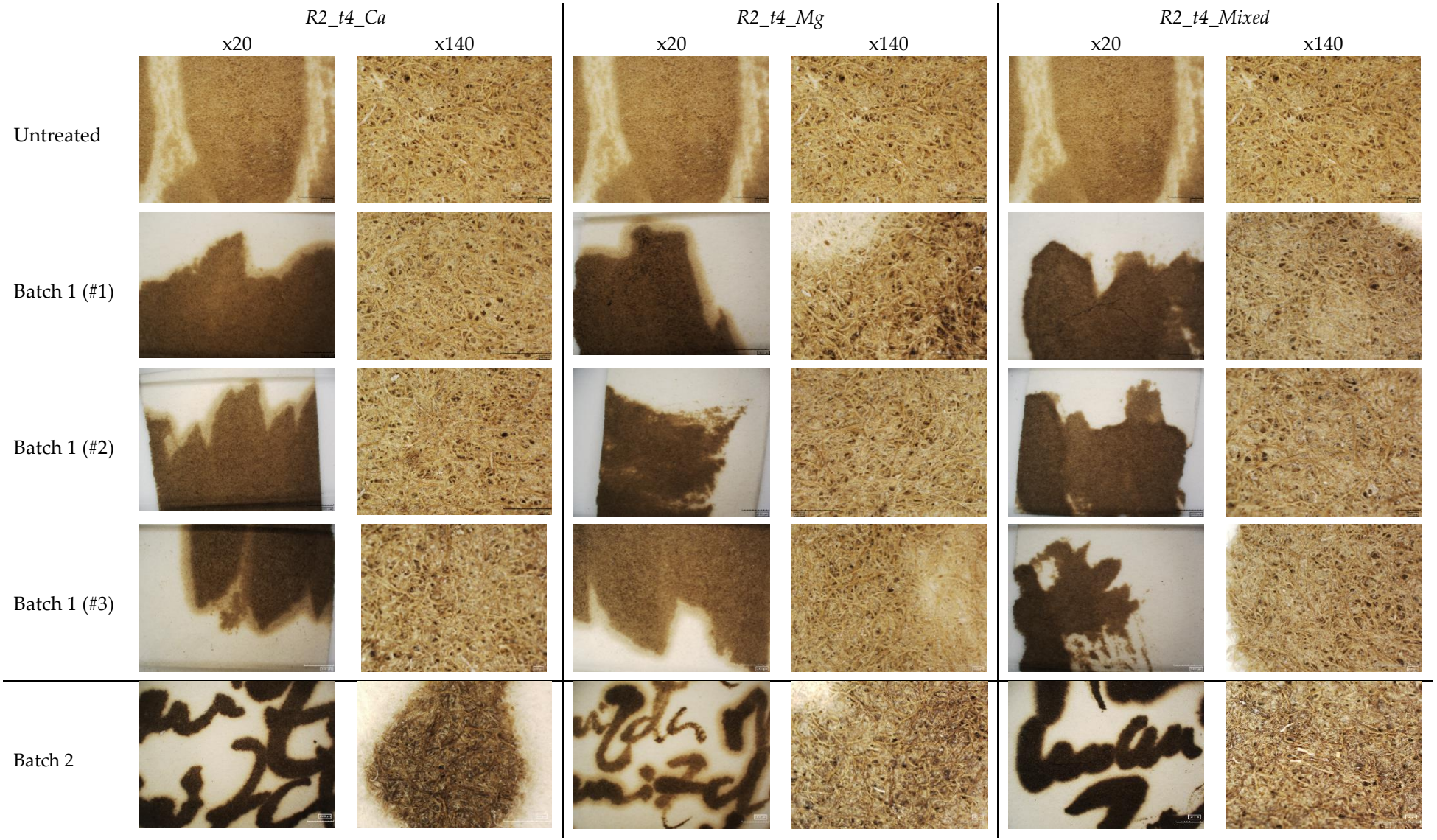

Figure 5.18: 3D-digital microscopy images (x20 and x140) of R2_t4 (Ca, Mg, mixed) (#1 is observation conducted immediately after application, #2 is 3 weeks after application and #3 is 6 weeks after the application)

5.2.2.3. SEM-EDS

The paper samples were analysed to observe the morphology of cellulose fibres, the ink and the nanoparticles distribution on the paper samples in-depth. Images were captured before and after the samples' treatment with the NPs dispersions. The samples were observed three times over the course of two months for Batch 1 (mentioned as #1, #2 and #3) and once for Batch 2 (6 samples from this category were analysed: R1_t4 and R2_t4 with the three types of dispersions) after accelerated aging. Furthermore, EDS analysis (mapping and point analysis) was conducted to register the elemental distribution.

Treatment with $Ca(OH)_2$ NPs: The SEM images of sample R2_t4_Ca (Batch 1 and Batch2) are shown in Figure 5.19. The NPs appear in clusters within the paper structure, in between the fibres and in the empty spaces between the fibres as seen on the images on the right in figure 5.19 (indicated with red arrow). They are on the ink as well, which is visible in lower magnification as shown in figure 5.19-left. The $Ca(OH)_2$ NPs appear as small dots in the samples that are well (but in a non-uniform manner) dispersed on the fibres in magnification as low as x200 and the NPs appear as small clusters of hexagonal-shaped particles in the pores at a magnification as high as x8.00k similar to figure 5.17 (a and b) which is similar to the behaviour of NPs on cellulose reported in the literature (Poggi, 2002; Poggi, 2016). Samples from Batch 1 (#1 to #3) have the same particle morphology which is maintained even after accelerated aging (Batch 2), also shown in figure 5.19-bottom row. The lack of change in the morphology of the NPs and in the morphology of the paper fibres (both batches) suggests that the carbonatation of NPs have not yet occurred.

The EDS mapping displays the distribution of the NPs on the sample surface. The EDS point analysis of the white particles observed in SEM is confirmed to be Ca, indicating that the NPs are dispersed around the fibres, ink and in the empty spaces between the fibres (Figure 5.20). The weight percentage of Ca (Figure 5.20, Table in the set) is clearly higher than the Ca amount in the paper network of the untreated sample (Figure 5.21, Table inset). The presence of iron (Fe) and sulphur (S) is associated with IGI and weak presence of aluminium (Al) are probably external contaminants on the surface of the paper.

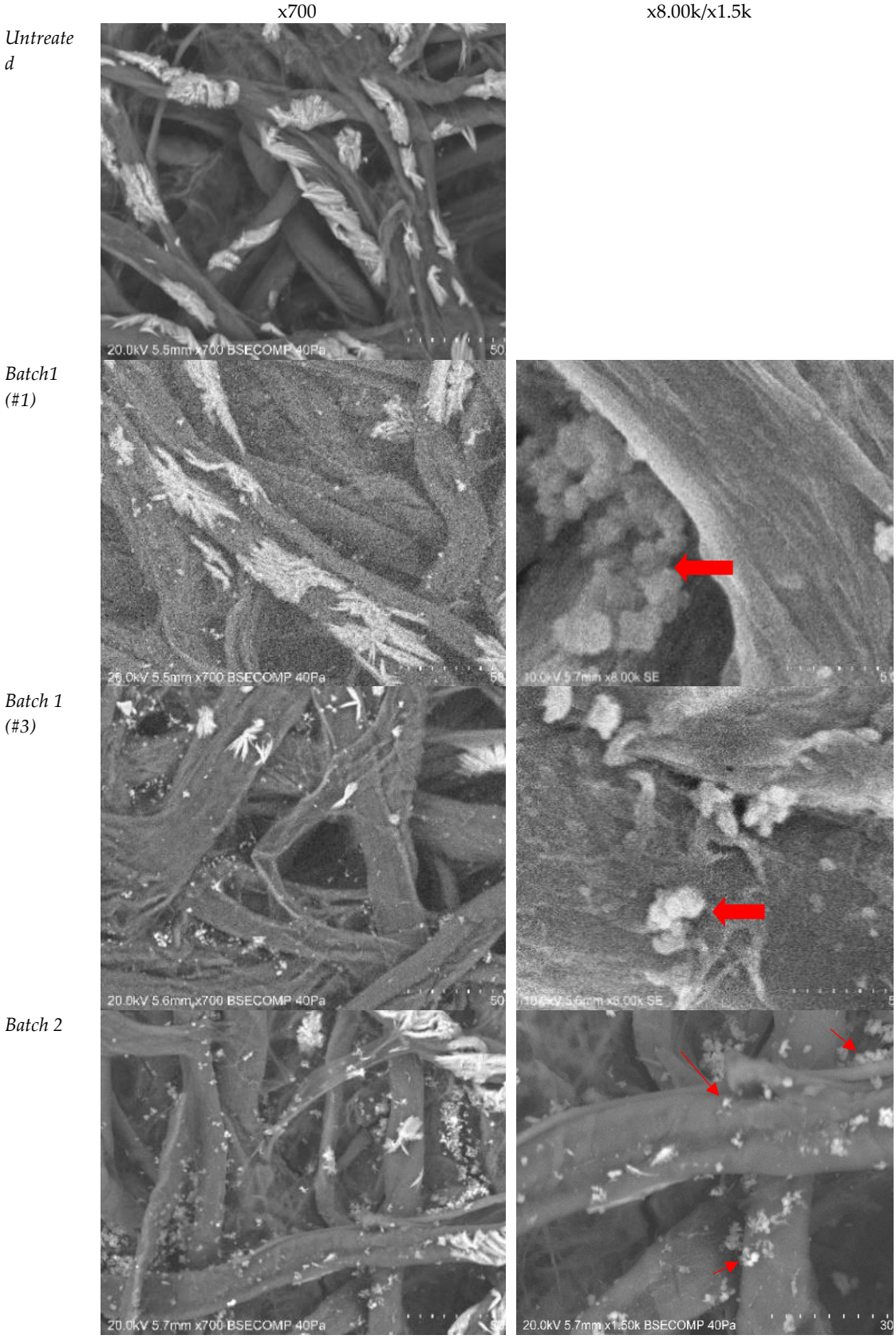

Figure 5.19: SEM images of R2_t4_Ca (Batch 1: #1, and #3 and Batch 2).

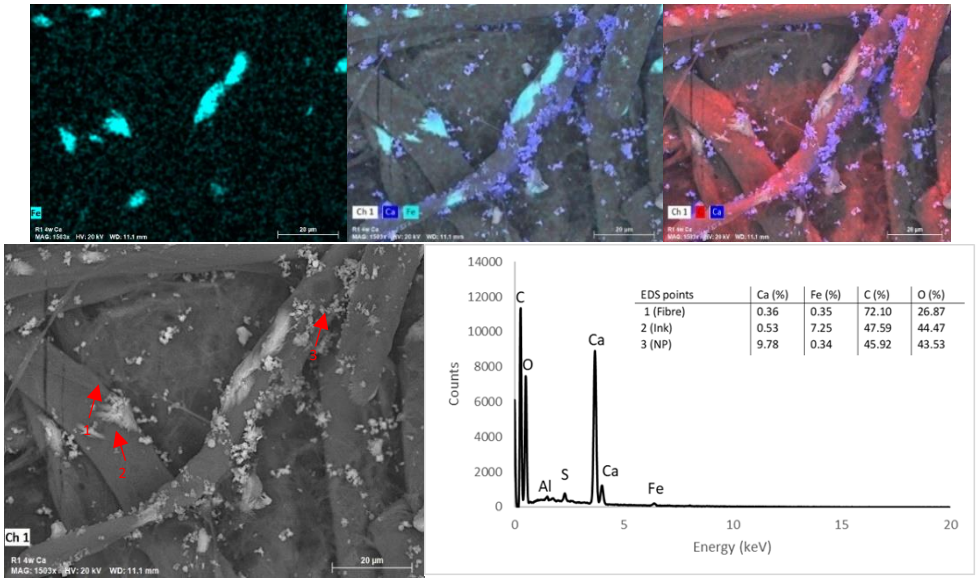

Figure 5.20: EDX mapping (top) of R1_t4_Ca (batch 1: #3) and corresponding EDX point analysis spectra (bottom, conducted at the red arrow marked point) and semi-quantification data (inset).

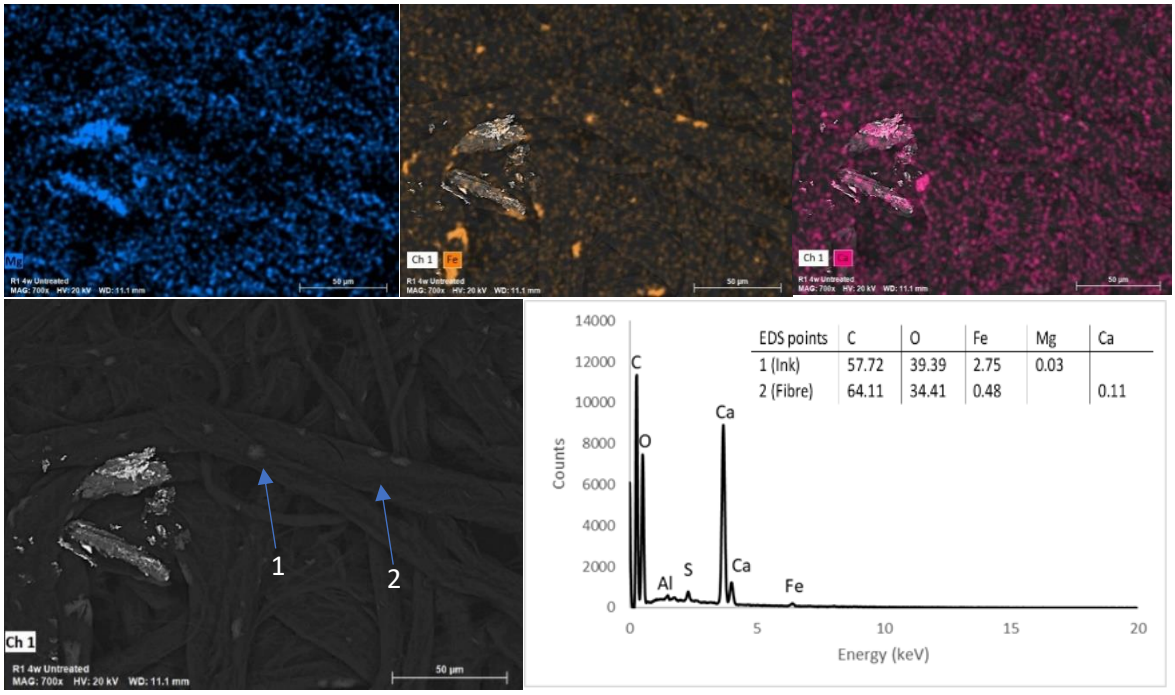

Figure 5.21: EDS mapping (top) of R1_t4 untreated and corresponding EDX point analysis spectra (bottom, conducted at the blue arrow marked point) and semi-quantification data (inset).

Treatment with $Mg(OH)_2$ NPs: The SEM images of sample R2_t4_Mg are shown in figure 5.22. The $Mg(OH)_2$ NPs appear as small floret-shaped particles on the fibres and in the spaces between the cellulose fibres at a magnification of x8.00k (Figure 5.22-right) the same as those observed in figure 5.18 (a and b). The NPs are strongly

agglomerated, which is not uncommon for similar NPs (e.g., Mg (Kwiatkowska, 2014)).

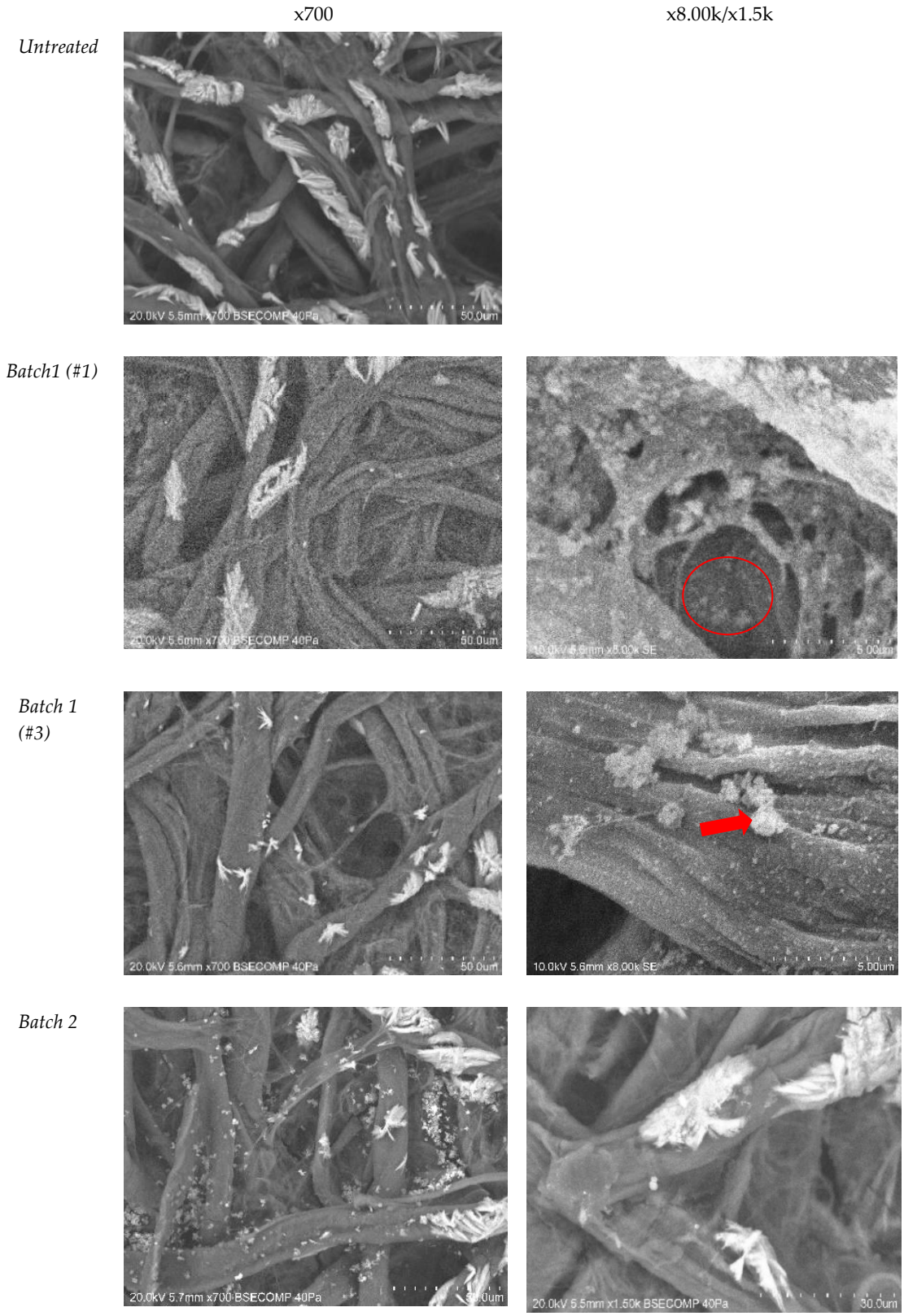

Figure 5.22: SEM images of R2_t4_Mg (Batch 1: #1, #3 and Batch 2).

The EDS analysis confirms the presence of magnesium in the paper sample. The $Mg(OH)_2$ particles are very small and appear clustered together in the empty spaces and on the surface of the fibres as can be seen in the elemental mapping distribution (Figure 5.23-top) which is clearly higher than in the untreated sample (Figure 5.21). The weak presence of calcium (Ca) and aluminium (Al) in the sample is probably due to external contamination of the paper sample (Figure 5.23-bottom).

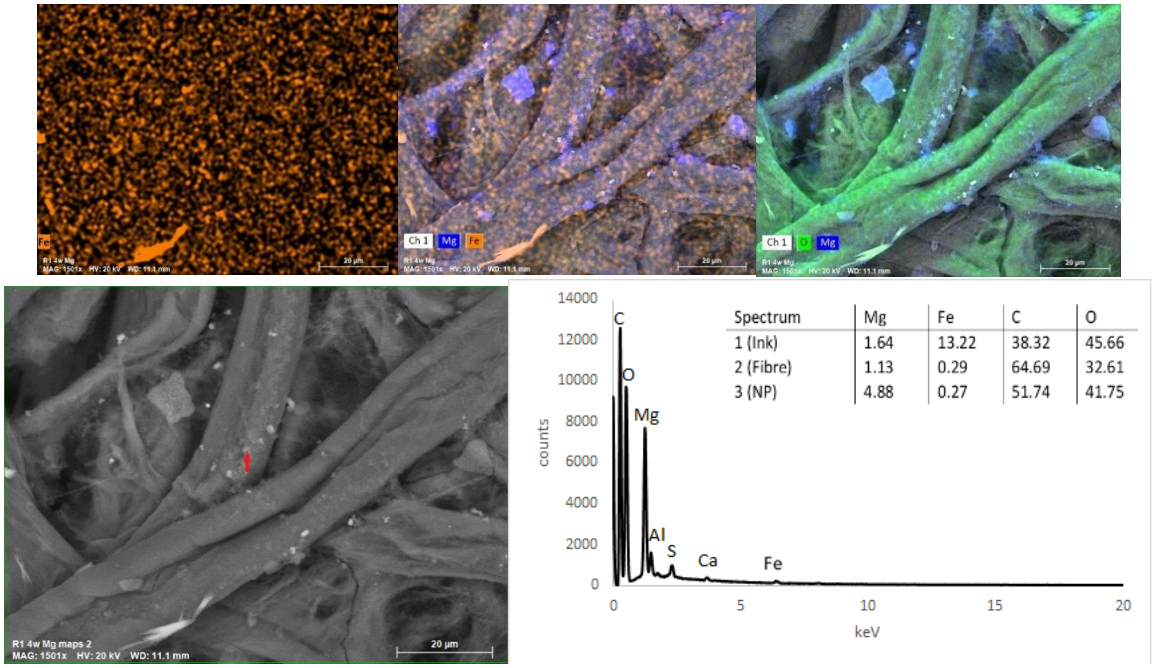

Figure 5.23: EDX mapping (top) of R1_4Weeks_Mg (batch 1: #3) and corresponding EDX point analysis spectra (bottom, conducted at the red arrow marked point) and semi-quantification data (inset).

Treatment with Mixed dispersion: The hexagonal shape and floret-like particles of $Ca(OH)_2$ and $Mg(OH)_2$ NPs respectively, are visible in the SEM images captures at a magnification of x8.00k. They are found as small clusters on the fibres and in the pores between the fibres (Figure 5.24). The $Ca(OH)_2$ NPs appear as dots while $Mg(OH)_2$ NPs appear as small patches on the fibres at a magnification of x700.

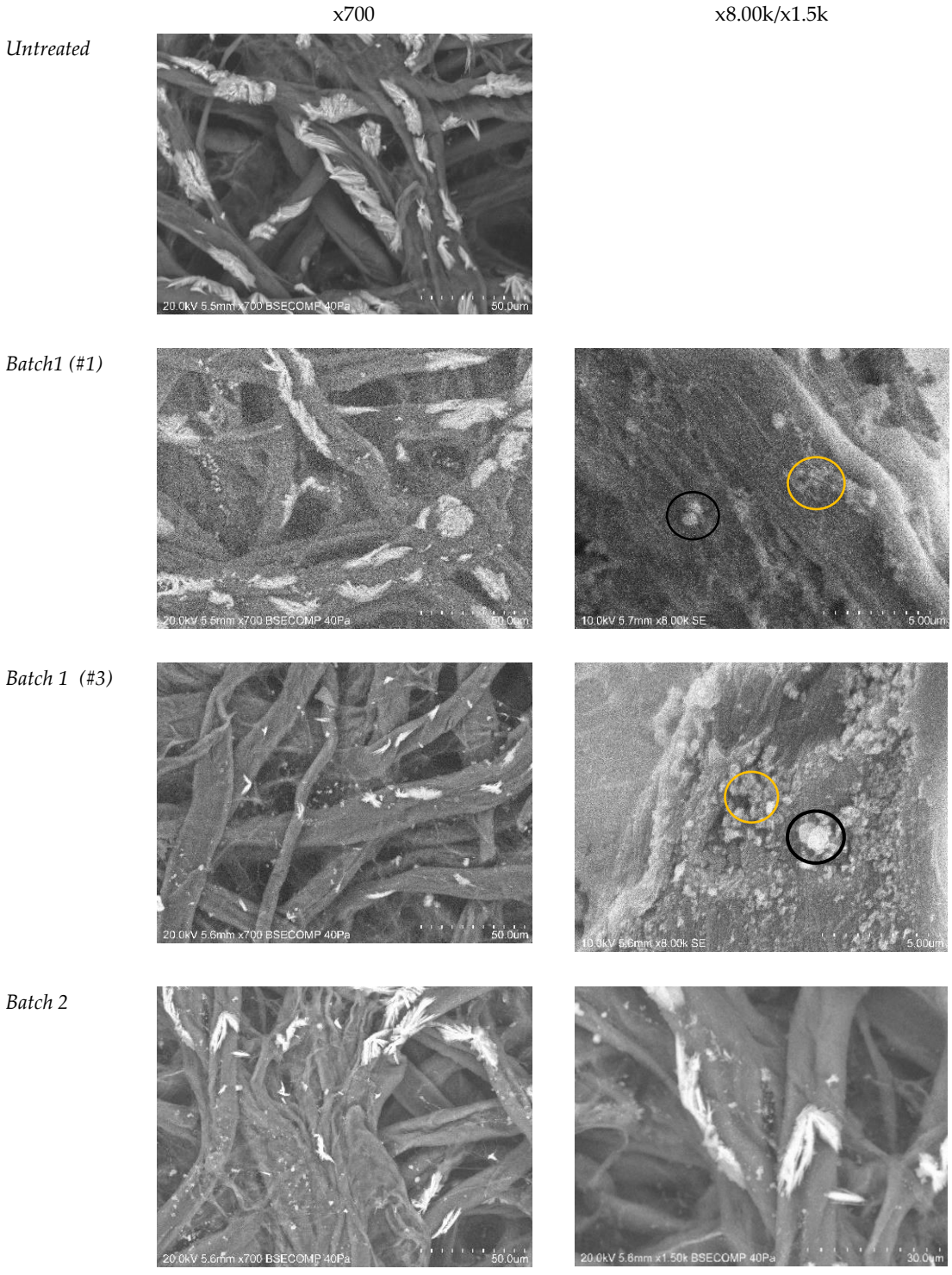

Figure 5.24: SEM images of R2_t4_Mixed (Batch 1: #1 , #3 and Batch 2) with $Ca(OH)_2$ NPs marked in black ellipse and $Mg(OH)_2$ NPs marked inn yellow ellipse.

The EDS analysis confirms the presence of both calcium and magnesium elements assigned to the hydroxide NPs in the treated paper sample. As observed in the EDS mapping, they appear clustered along the fibres and are also present in the empty

spaces between the fibres. The $Mg(OH)_2$ particles are very small and appear clustered together in the pores and on the surface of the fibres, as can be seen in the mapping distribution (Figure 5.25-top). Similarly, the larger $Ca(OH)_2$ NPs appear in clusters, non-uniformly distributed on the surface. The larger white particles seen around the fibres are $Ca(OH)_2$ NPs, while the smaller particles are $Mg(OH)_2$ NPs which is confirmed by the EDX point analysis result (Figure 5.25-bottom and Table 5.4). A minor content of aluminium and copper was found, which could possibly be due to external contamination of the paper sample.

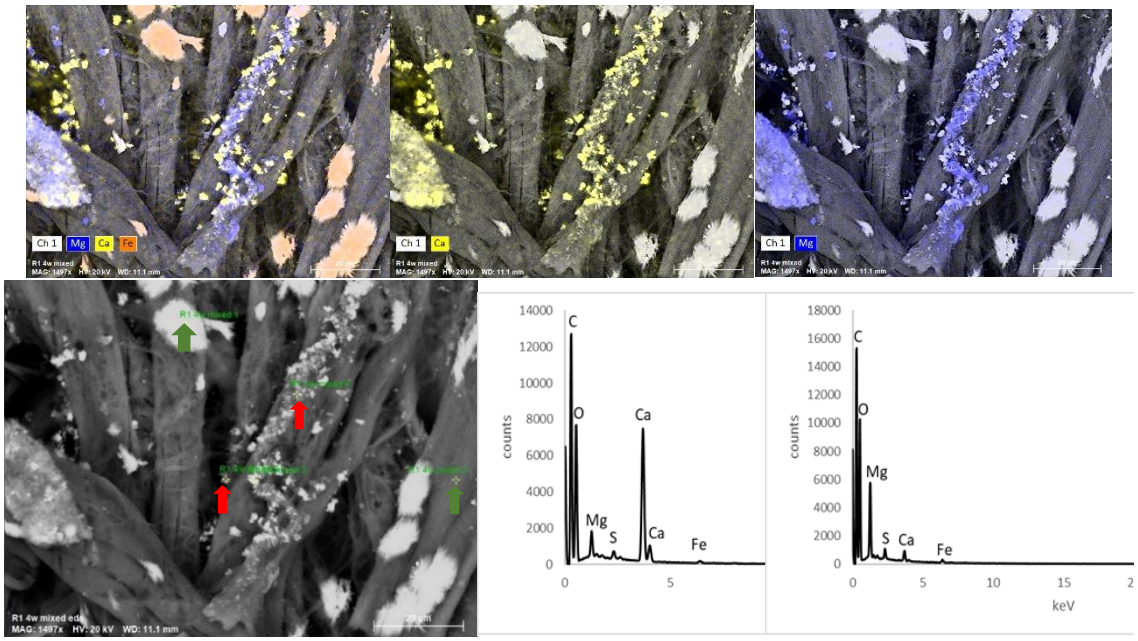

Figure 5.25: EDX mapping (top) of R1_t4_mixed (batch 1: #3) and corresponding EDX point analysis spectra (bottom, conducted at the red and green arrows marked points). The corresponding semi-quantification data is shown in Table 5.4.

Table 5.4: EDX point analysis of R1_t4_Mixed (batch 1: #3): semi-quantification data at the points analysed (fibre, ink and NPs as shown in Fig. 5.28).

	Element, Wt. %				
EDS point analysed	Ca	Mg	Fe	O	C
Fibre	0.76	0.35	1.12	39.85	57.03
Ink	0.15	0.20	17.16	50.80	31.39
$Ca(OH)_2$ NP	8.05	0.71	0.29	41.96	48.72
$Mg(OH)_2$ NP	0.90	2.93	0.56	41.44	53.41

The results from SEM-EDS confirmed the presence of the NPs in the paper samples which are only visible in high magnification (x1.5k and x8.00k) and not in lower magnification such as x200 which is coherent with the results in 3D-digital microscopy, where no visible change was observed in x140 magnification. The SEM-EDS analysis shows that the NPs of all kinds of dispersions are present across the paper samples in the pores between fibres and also on the fibres, confirming a wide, non-uniform distribution of small clusters of NPs on the paper samples. The clusters remained stable for the time of measurements and there is evidence that the particles have not carbonated until two months after the treatment. It is also evident from the results of Batch 2 that the samples have also not carbonated after one week of accelerated aging.

The SEM-EDS results for all the other samples are presented in Appendices A4.3 and A4.4.

5.2.2.4. pH measurement

pH measurements were made to evaluate the treatments' deacidification potential on papers containing IGI. Each paper sample was measured in three points and the average of the values was calculated keeping the standard deviation in mind. Each sample was analysed before and after treatment: Batch 1 (three times over a period of two months: #1: 1 week after treatment, #2: 4 weeks after treatment, and #3: 8 weeks after treatment) and Batch 2 after accelerated aging (Table 5.5). The pH measurements for untreated samples are 3±0.1 for R1_t0, 2±0.1 for R1_t4, 2.3±0.1 for R1_t5, 2.6±0.1 for R2_t0, 2.5±0.2 for R2_t4 and 2.3±0.1 for R2_t5.

Table 5.5: pH values measured on IGI on paper before and after the different nanoparticle treatments.

Sample	*Batch 1 (#1)*	*Batch 1 (#2)*	*Batch 1 (#3)*	*Batch 2*
Treatment with $Ca(OH)_2$ NPs treatment				
R1_t0_Ca	8.7±0.5	7.7±0.1	8.0±0.1	7.9±0.4
R1_t4_Ca	8.0±0.3	7.8±0.1	7.7±0.2	7.3±0.3
R1_t5_Ca	8.2±0.2	8.2±0.2	8.9±0.2	3.6±0.4
R2_t0_Ca	8.6±0.2	8.0±0.1	7.2±0.3	8.7±0.2
R2_t4_Ca	7.9±0.2	7.6±0.3	6.5±0.4	6.2±0.3
R2_t5_Ca	6.8±0.2	7.6±0.1	7.4±0.1	6.1±0.8
Treatment with $Mg(OH)_2$ NPs treatment				
R1_t0_Mg	8.2±0.1	7.0±0.2	9.0±0.5	8.5±0.3
R1_t4_Mg	8.0±0.2	7.5±0.1	9.0±0.1	6.9±0.8
R1_t5_Mg	8.1±0.4	8.0±0.1	8.4±0.5	7.0±0.2
R2_t0_Mg	8.7±0.6	8.1±0.2	8.0±0.1	8.3±0.3
R2_t4_Mg	7.6±0.1	7.7±0.2	6.8±0.5	8.0±0.5
R2_t5_Mg	7.5±0.1	8.0±0.4	7.5±0.4	7.4±0.3
Treatment with NPs Mixed NPs				
R1_t0_Mixed	8.0±0.1	7.7±0.4	10.0±0.1	9.9±0.2
R1_t4_Mixed	8.4±0.4	8.0±0.3	7.9±0.6	6.0±0.3
R1_t5_Mixed	7.9±0.2	8.0±0.2	8.3±0.1	6.2±0.3
R2_t0_Mixed	9.1±0.1	8.2±0.1	7.5±0.4	9.3±0.1
R2_t4_Mixed	7.2±0.1	7.5±0.2	5.2±0.6	6.3±0.9
R2_t5_Mixed	7.3±0.1	7.5±0.1	7.0±0.3	4.5±0.6

Treatment with $Ca(OH)_2$ NPs: A significant increase in the pH is observed on the paper samples treated with $Ca(OH)_2$ NPs. The pH after treatment increases by a minimum of 4 values towards alkaline values (between pH 6.8 and 8.7) from the initial untreated pH acidic value, as can been seen in Figure 5.26 and Table 5.5.

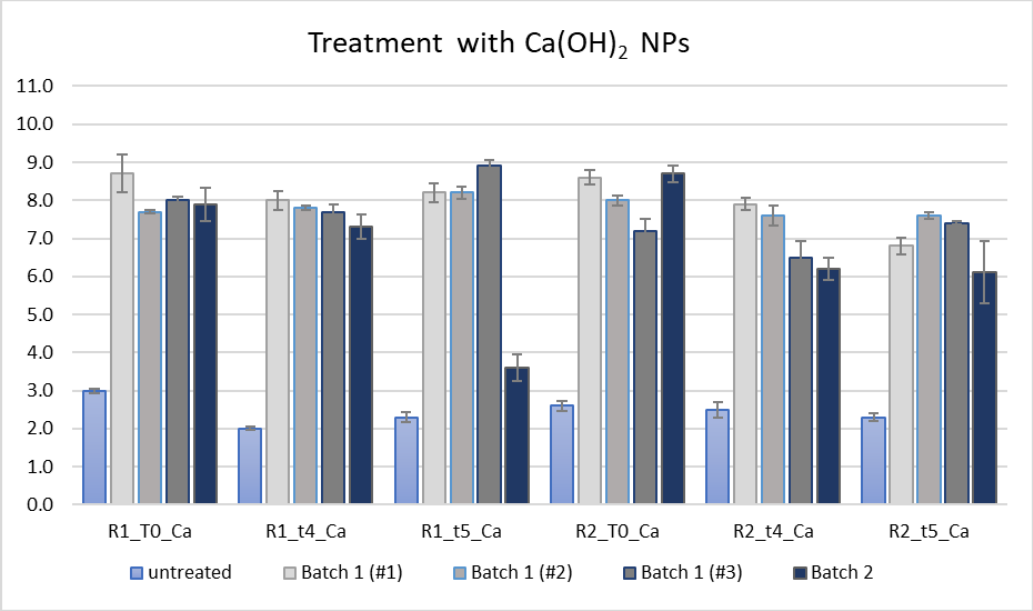

Figure 5.26: Graphical representation of pH values of samples treated with $Ca(OH)_2$ NPs (Untreated is pH before treatment; Batch 1: (#1), (#2), (#3) and Batch 2.

In the three measurements made in Batch 1, the pH slightly drops but remains stable and above pH value 7 except for R2_t4_Ca where the pH drops to 6.5±0.4 (but remains close to the neutral pH value). The highest value reached after $Ca(OH)_2$ treatment and natural aging under ambient conditions (Batch 1: #3) is in R1_t5_Ca with a value of 8.9±0.2. The lowest value achieved in Batch 1 is in R2_t4_Ca with a value of 6.5±0.4 (Batch 1: #3). The samples R1 seem to show smaller variation in the pH values between measurements #1 and #3 (Batch #1) than samples R2 where the variations are more noticeable, and the pH values are also lower. Indeed, R2 is a more aggressive ink, with a starting pH lower than R1 (Table 5.2, R1_t0 and R2_t0), given the presence of vinegar in its composition (Appendix 1: A1.1). A possible reason for the slight drop in the values of R2-inked samples between #1 and #3 could be the more rapid consume of the hydroxide and in a larger extent (considering the difference in the initial pH values). The neutralization of the acid groups in the samples prepared with ink R1 could occur in a longer-term process compared to the samples prepared with the ink R2.

The pH values after treatment/artificially ageing (batch 2) are lower than the values in Batch 1 (#3), with the exception of R2_t0. The sample R1_t5 appears to have the lowest pH in Batch 2, which is nevertheless higher than the initial pH value of the untreated sample. Considering the behaviour observed for samples in Batch 2, R1_t5_Ca and R2_t0_Ca are possibly outliers. One exciting aspect is that, within the error, the treatment undoubtedly increased the pH to values in the basic range, but it has not returned to the initial values for the untreated samples reflecting the effectiveness of the treatment with laboratory prepared $Ca(OH)_2$ NPs. Besides, R1 samples tend,

within the error, to present higher pH values. This may be due to the lower starting pH for the R2 recipe, with the addition of vinegar making it harder to deacidify the paper support. Another fundamental conclusion is that artificial aging of the treated samples did not lead to a decrease in the pH within the error, confirming the long-term effectiveness of the treatment with $Ca(OH)_2$ NPs,

Treatment with $Mg(OH)_2$ NPs: The paper samples treated with $Mg(OH)_2$ NPs also show an abrupt increase in pH to alkaline level from the initial untreated acidic level (Figure 5.27, Table: 5.5).

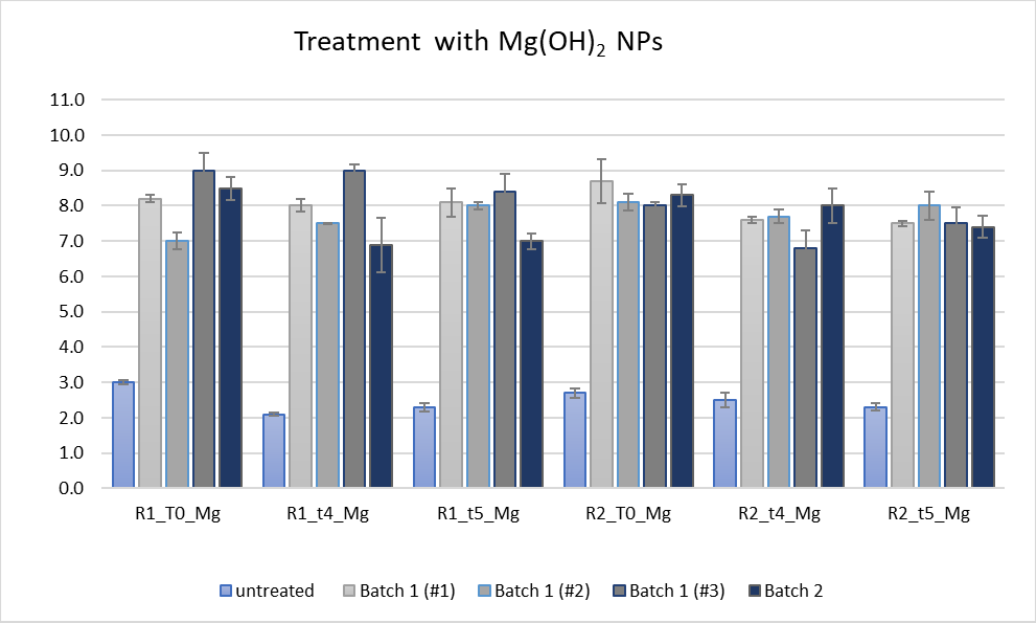

Figure 5.27: Graphical representation of pH values of samples treated with $Mg(OH)_2$ NPs (Untreated is pH before treatment; Batch 1: (#1), (#2), (#3) and Batch 2.

The pH values do not vary significantly on average and within the error on the three measurements in Batch 1, with pH remaining higher than 7 or around it. The highest pH values achieved by treatment with $Mg(OH)_2$ NPs were measured for samples (Batch 1) prepared with the ink R1, likewise as the samples treated with $Ca(OH)_2$ NPs. These values were also higher after treatment with the magnesium dispersion than with the calcium one (pH 9±0.5, 9±0.2 and 8.4±0.5, respectively; Batch 1: #3).

The pH has not returned to the initial value for any of the samples, remaining neutral for the samples of both batches reflecting on the effectiveness of the treatment with $Mg(OH)_2$ NPs. Once again, samples in Batch 2 are, within the error, similar to Batch 1, which also shows the treatments' long-term effectiveness.

Treatment with mixed ($Ca(OH)_2$/ $Mg(OH)_2$) NPs dispersion: Once again, there was an increase in the pH values. Within the error, the pH did not change for the three

measurements taken for each sample in Batch 1 (except for #2 and #3 in R1_t0_Mixed which are probably outliers considering the general tendency of the samples) and generally remained above 7 except. Also, likewise the other treatments, the pH values of the samples prepared with ink R2 decreased more than the values of R1-based samples. Overall, the mixed treatment seemed less effective in the long term, since the pH of Batch 2 samples tend to be lower than the average values of the samples from Batch 1 (Figure 5.28).

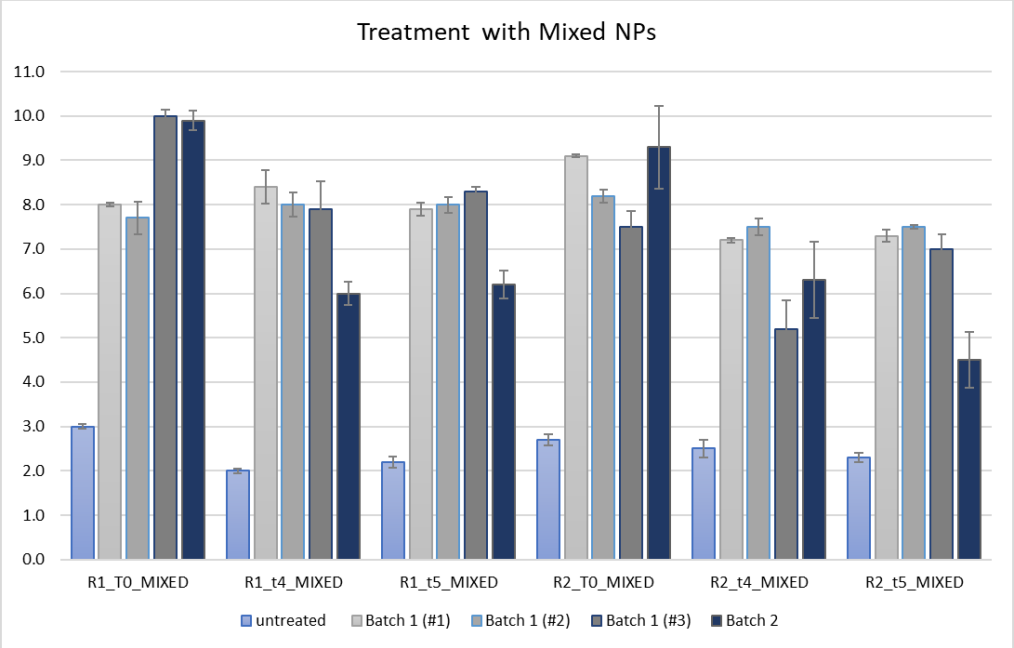

Figure 5.28: Graphical representation of pH values of samples treated with Mixed NPs (Untreated is pH before treatment; Batch 1: (#1), (#2), (#3) and Batch 2.

In agreement with the literature, the catalytic activity of iron ions is minimal when pH is around neutral values (Strlič, 2003); consequently, the control of paper acidity/alkalinity could provide a way to reduce the degradation rate of oxidation through Fenton reactions; and the ink-catalysed degradation of the paper cellulose could be also reduced with the deacidification treatment (Poggi, 2010). However, for pH>8.5 the rate of cellulose oxidative reactions increases (Poggi, 2010).

It can be observed that the pH value has abruptly increased to an alkaline level after the deacidification treatments regardless of which NPs were used in the treatment (Figure 5.29 and Table 5.5). The treatments with different NPs dispersions have resulted in neutral to basic pH value in almost all the paper samples. The lowest pH value achieved was by R2_t4 sample (5.2±0.6) in association with the treatment with mixed NPs dispersion. The highest pH value (sample R1_t0_Mixed) of 10±0.1,

susceptible of causing alkaline depolymerization was also associated to the mixed NPs dispersion.

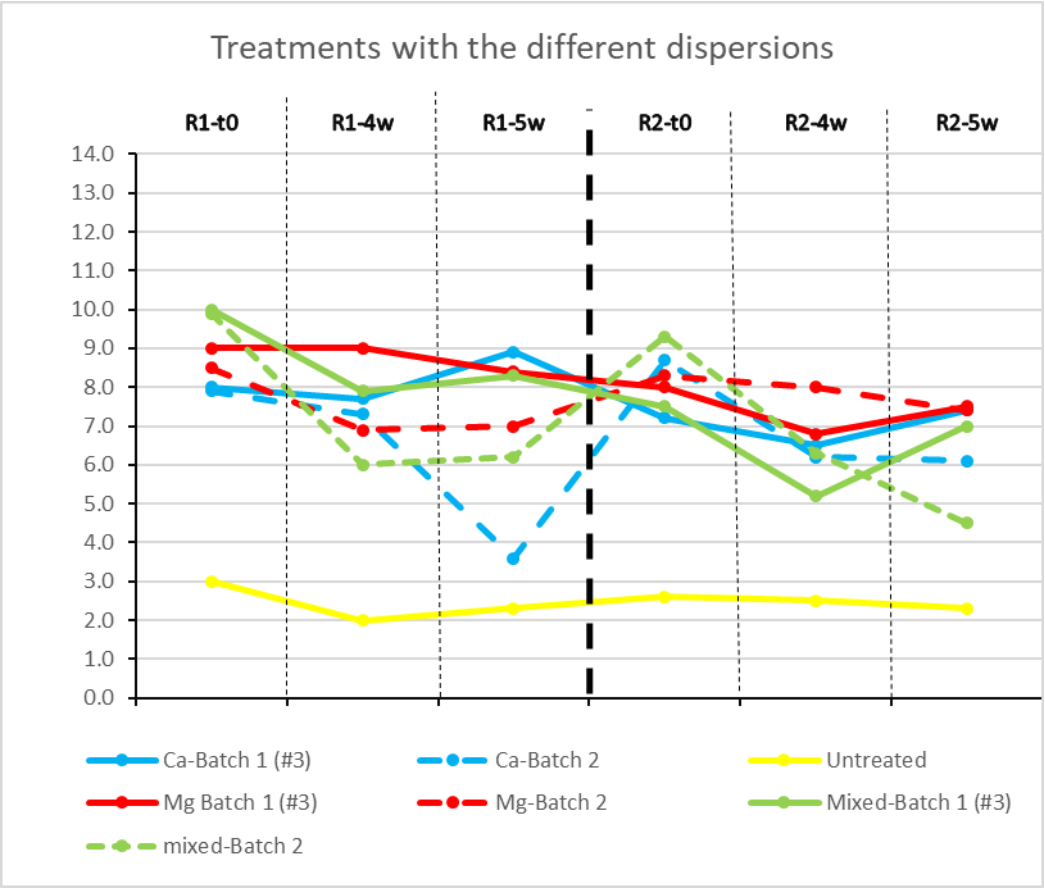

Figure 5.29. pH values measured for all types of dispersions applied (Batch 1-#3 and Batch 2).

All the samples experience a decrease in the pH in Batch 2 except for R2_t0 samples which, irrespective of the dispersions, maintains a neutral value even after accelerated aging. The samples R1_t5_Ca and R2_t5_Mixed have the lowest pH value in Batch 2 reaching acidic level again (table 5.5). As it was mentioned before, the pH achieved after treatment should be above neutral value, because the catalytic activity of iron ions is at the minimum value (Stauderman, 1996; Strlič, 2003; Poggi, 2010). At the same time the pH should not be too alkaline in order to avoid alkaline cellulose depolymerization (optimal values would be in the 8.5 range (Sequeira, 2006; Kwiatkowska, 2014)). Therefore, the achieved values after treatments with the three kinds of dispersions (between pH 6.5 and 9) can be seen as very effective and suitable, because the NPs provide necessary amount of OH- for deacidification to occur and at the same time the pH is the range of the optimal values. The treatments with $Ca(OH)_2$ and Mg $(OH)_2$ are similarly effective, mixed NPs dispersion provides the lower pH values (with a very small difference).

The SEM analysis suggested that the NPs are strongly agglomerated. In order to deposit the NPs dispersions in a more uniform way over the surface, the NPs can be

deagglomerated by homogenisation in ultrasonic bath before the treatment that might improve their deacidification capacity that, for the case of only one kind of NP applied has not influenced significantly the pH of papers (Wójciak, 2015).

The increase in pH is coherent with previous publications where varied concentrations of NPs in 2-propanol are used for the purpose of deacidification of paper samples (Sequeira, 2006; Giorgi, 2011; Poggi, 2016). The desired pH of neutral value which would slow down further degradation of IGI (Melo, 2022) is attained in each of the NPs dispersions that are used here.

5.2.2.5. Colorimetric studies

The samples treated with nanoparticles (Batch 1) were studied by colorimetric analysis to evaluate the colour changes (Table 5.6). Untreated samples were considered as reference (standards) to Batch 1 samples.

*Table 5.6: CIE*L*a*b* coordinates before (std) and after (sample) treatment with different NP dispersions and corresponding ΔE values for Batch 1.*

sample name	L^*_{std}	L^*_{sample}	a^*_{std}	a^*_{sample}	b^*_{std}	b^*_{sample}	ΔE
Treatment with $Ca(OH)_2$ NPs							
R1_t0_Ca	73.56 ± 0.31	81.12 ± 0.15	-0.92 ± 0.03	0.82 ± 0.01	5.52 ± 0.02	11.14 ± 0.35	9.6
R1_t4_Ca	53.13 ± 0.54	54.72 ± 0.14	6.04 ± 0.05	5.45 ± 0.03	16.95 ± 0.1	13.86 ± 0.35	3.5
R1_t5_Ca	52.3 ± 0.59	51.08 ± 0.25	6.99 ± 0.02	5.57 ± 0.05	18.52 ± 0.06	13.76 ± 0.49	5.1
R2_t0_Ca	58.32 ± 0.27	63.00 ± 0.14	-0.58 ± 0.03	1.89 ± 0.01	8.65 ± 0.19	17.33 ± 0.15	10.2
R2_t4_Ca	53.6 ± 0.12	56.15 ± 0.08	7.66 ± 0.02	5.5 ± 0.04	21.45 ± 0.06	16.71 ± 0.11	5.8
R2_t5_Ca	53.47 ± 0.03	55.53 ± 0.18	8.34 ± 0.01	5.67 ± 0.03	22.52 ± 0.02	16.73 ± 0.05	6.7
Treatment with $Mg(OH)_2$ NPs							
R1_t0_Mg	73.56 ± 0.31	82.29 ± 0.35	-0.92 ± 0.03	1.89 ± 0.02	5.52 ± 0.02	13.57 ± 0.09	12.2
R1_t4_Mg	53.13 ± 0.54	56.42 ± 0.22	6.04 ± 0.05	5.69 ± 0.08	16.95 ± 0.1	14.46 ± 0.06	4.1
R1_t5_Mg	52.3 ± 0.59	54.06 ± 0.06	6.99 ± 0.02	5.83 ± 0.13	18.52 ± 0.06	14.93 ± 0.35	4.2
R2_t0_Mg	58.32 ± 0.27	63.63 ± 0.47	-0.58 ± 0.03	3.06 ± 0.03	8.65 ± 0.19	19.73 ± 0.14	12.8
R2_t4_Mg	53.6 ± 0.12	57.15 ± 0.56	7.66 ± 0.02	5.89 ± 0.13	21.45 ± 0.06	17.38 ± 0.15	5.7
R2_t5_Mg	53.47 ± 0.03	50.74 ± 0.21	8.34 ± 0.01	5.91 ± 0.05	22.52 ± 0.02	16.26 ± 0.26	7.2
Treatment with Mixed NPs							
R1_t0_Mixed	73.56 ± 0.31	77.88 ± 0.24	-0.92± 0.03	1.39 ± 0.12	5.52 ± 0.02	11.83 ± 0.28	8.0
R1_t4_Mixed	53.13 ± 0.54	54.97 ± 0.22	6.04 ± 0.05	5.54 ± 0.03	16.95 ± 0.1	13.91 ± 0.14	3.6
R1_t5_Mixed	52.3 ± 0.59	54.75 ± 0.04	6.99 ± 0.02	5.38 ± 0.01	18.52 ± 0.06	13.92 ± 0.1	5.5
R2_t0_Mixed	58.32 ± 0.27	61.42 ± 0.08	-0.58 ±0.03	2.80 ± 0.03	8.65 ± 0.19	19.41 ± 0.12	11.7
R2_t4_Mixed	53.6 ± 0.12	51.01 ± 0.32	7.66 ± 0.02	5.47 ± 0.04	21.45 ± 0.06	15.95 ± 0.18	6.5
R2_t5_Mixed	53.47 ± 0.03	52.92 ± 0.24	8.34 ± 0.01	5.88 ± 0.16	22.52 ± 0.02	16.9 ± 0.15	6.2

The results of the colorimetric analysis for samples from Batch 2 are presented in Table 5.7. Samples treated and not aged (Batch 1) were considered the reference for Batch 2 samples.

*Table 5.7: CIE*L*a*b* coordinates of treated samples before (std- Batch 1) and after (sample- Batch 2) accelerated aging and corresponding ΔE values.*

sample name	L^*_{std}	L^*_{sample}	a^*_{std}	a^*_{sample}	b^*_{std}	b^*_{sample}	*ΔE*
Treated with $Ca(OH)_2$ NPs							
R1_t0_Ca	81.12±0.15	66.57±0.26	0.82±0.01	3.40±0.23	11.14±0.35	14.97±0.57	15.27
R1_t4_Ca	54.72±0.14	40.01±0.19	5.45±0.03	4.12±0.11	13.86±0.35	7.52±0.14	16.07
R1_t5_Ca	51.08±0.25	60.69±0.49	5.57±0.05	2.18±0.03	13.76±0.49	8.81±0.04	11.33
R2_t0_Ca	63.00±0.14	70.97±0.94	1.89±0.01	1.72±0.08	17.33±0.15	12.50±0.36	9.32
R2_t4_Ca	56.15±0.08	40.59±0.35	5.50±0.04	4.41±0.21	16.71±0.11	9.87±0.87	17.03
R2_t5_Ca	55.53±0.18	39.23±0.22	5.67±0.03	4.37±0.18	16.73±0.05	9.31±0.91	17.96
Treated with $Mg(OH)_2$ NPs							
R1_t0_Mg	82.29±.35	70.21±0.26	1.89±0.02	2.66±0.23	13.57±0.09	14.51±0.21	12.14
R1_t4_Mg	56.42±0.22	36.37±.39	5.69±0.08	4.4±.21	14.46±0.06	8.58±0.51	20.93
R1_t5_Mg	54.06±0.06	41.56±0.35	5.83±0.13	3.93±0.04	14.93±0.35	9.8±0.28	13.64
R2_t0_Mg	63.63±0.47	67.81±0.3	3.06±0.03	3.66±1.5	19.73±0.14	15.17±0.57	6.21
R2_t4_Mg	57.15±0.56	38.63±0.13	5.89±0.13	4.88±.04	17.38±0.15	11.13±0.09	19.57
R2_t5_Mg	50.74±0.21	39.44±.4	5.91±0.05	4.96±0.34	16.26±0.26	11.82±.58	12.18
Treated with Mixed NPs							
R1_t0_Mixed	77.88±.24	70.32±0.14	1.39±0.12	3.16±0.03	11.83±0.28	15.5±0.07	8.59
R1_t4_Mixed	54.97±0.22	36.14±0.21	5.54±0.03	4.55±0.11	13.91±0.14	7.85±0.24	19.81
R1_t5_Mixed	54.75±0.04	38.44±0.46	5.38±0.01	4.84±0.29	13.92±0.1	8.95±0.26	17.06
R2_t0_Mixed	61.42±0.08	68.46±0.18	2.8±0.03	2.03±0.19	19.41±0.12	12.35±0.89	10.00
R2_t4_Mixed	51.01±0.32	37.43±0.16	5.47±0.04	4.71±0.24	15.95±0.18	9.89±0.5	14.89
R2_t5_Mixed	52.92±0.24	36.18±0.18	5.88±0.16	5.22±0.07	16.9±0.15	10.66±0.14	17.88

Change in Lightness (L* values)

Batch 1: The unaged samples (t0) from R1 and R2 show a trend to become lighter after treatment as indicated in figure 5.30. In t4 samples, all samples (R1 and R2) have become lighter after respective treatments except R2_t4_Mixed which have lower L* values than the untreated sample indicating that it became darker after treatment. In the case of t5 samples, the samples have non-uniform changes in L* values. In R1_t5, the sample treated with $Ca(OH)_2$ has lower L* value than the untreated sample indicating it has become slightly darker after treatment, whereas the other two treatments have made the sample lighter as indicated by the values in Table: 5.6. in the case of R2_t5 samples, the sample treated with Mixed dispersion has almost the same L* value as the untreated sample of the same with a slight increase (Table 5.6) meanwhile, the treatment with $Mg(OH)_2$ NPs has resulted in the sample becoming

darker than untreated one. The treatment with $Ca(OH)_2$ has made R2_t5 lighter than before treatment.

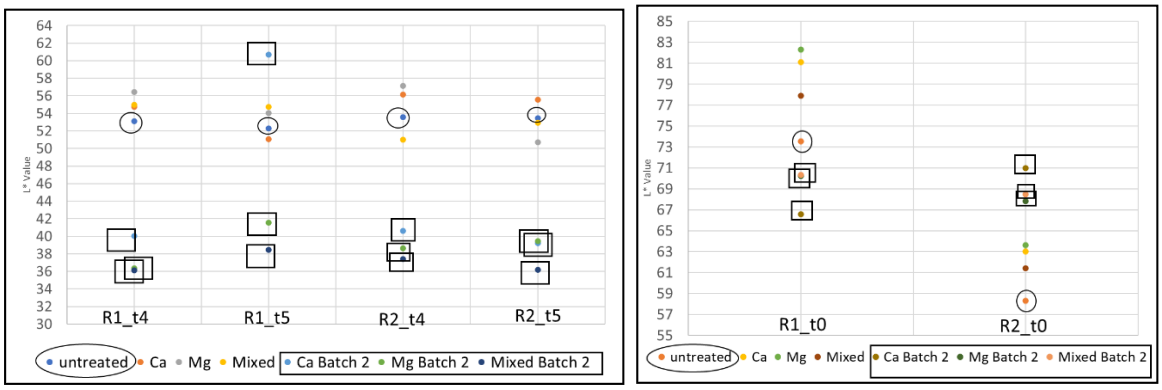

Figure 5.30 : L coordinate : Samples t4 and t5 (R1 and R2) (left); Samples t0 (R1 and R2) untreated, Batch 1 and Batch 2 (with circle indicating untreated, and square indicating the values from Batch 2 (after accelerated aging)) (Right).*

Comparing the ΔL values of samples treated with $Ca(OH)_2$ NPs (Figure 5.31a) shows that the samples that had the least degradation (R1_t0 and R2_t0) have a high increase in a ΔL and with an increase in aging, the ΔL value decreases within each type of ink (ΔL-R1_t0_Ca > ΔL-R1_t4_Ca > ΔL-R1_t5_Ca and ΔL-R2_t0_Ca > ΔL-R2_t4_Ca > ΔL-R2_t5_Ca). A similar trend in ΔL values of samples treated with $Mg(OH)_2$ NPs is seen (Figure 5.32a). However, the samples treated with Mixed do not show this trend in ΔL value. In R1 samples, 4 weeks sample has the lowest ΔL value indicating that the other samples (t0 and t5) have become more lighter after treatment. In the case of R2 samples, 4 weeks sample has the lowest ΔL value which is also negative, as can be inferred from figure 5.33a, indicating that the sample has become darker after treatment.

Batch 2: The samples after undergoing accelerated aging have shown significant change in L* value in comparison to untreated and Batch 1 (Figure 5.31b). All the samples irrespective of treatment have a decrease in L* value in Batch 2 in comparison to the untreated samples indicating the samples have been darker after aging, except R2_t0 (with three kinds of NPs dispersion) and R2_t5_Ca, where the L* value of each of the samples has become higher than the untreated sample, indicating that the sample became lighter after treatment and aging.

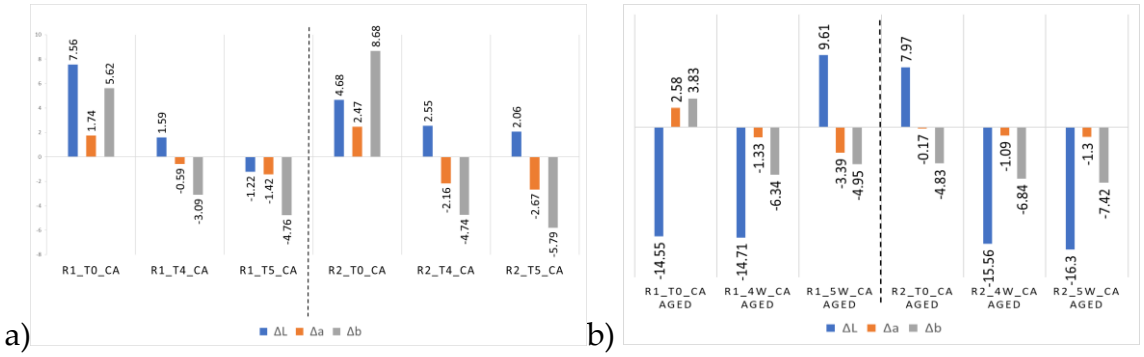

Figure 5.31: Graph of ΔL, Δa and Δb values of paper samples treated with $Ca(OH)_2$ NPs (a) Batch 1; (b) Batch 2.

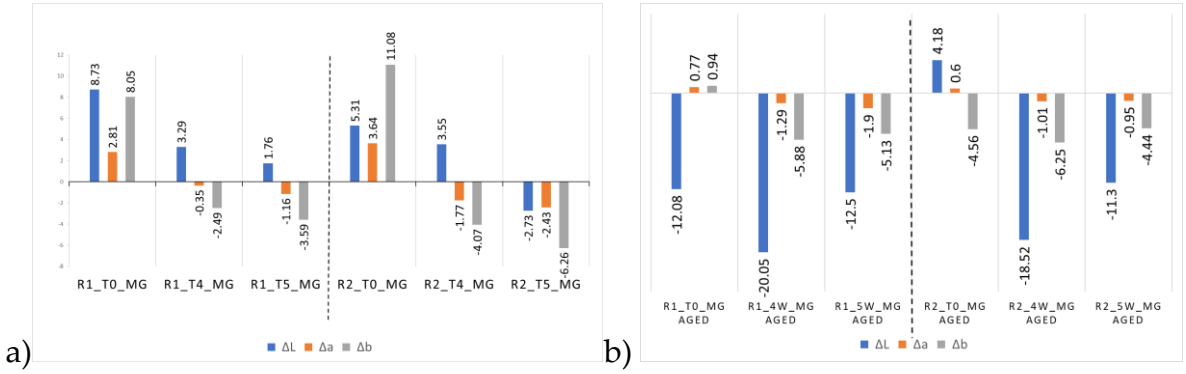

Figure 5.32 Graph of ΔL, Δa and Δb values of paper samples treated with $Mg(OH)_2$ NPs (a) Batch 1; (b) Batch 2

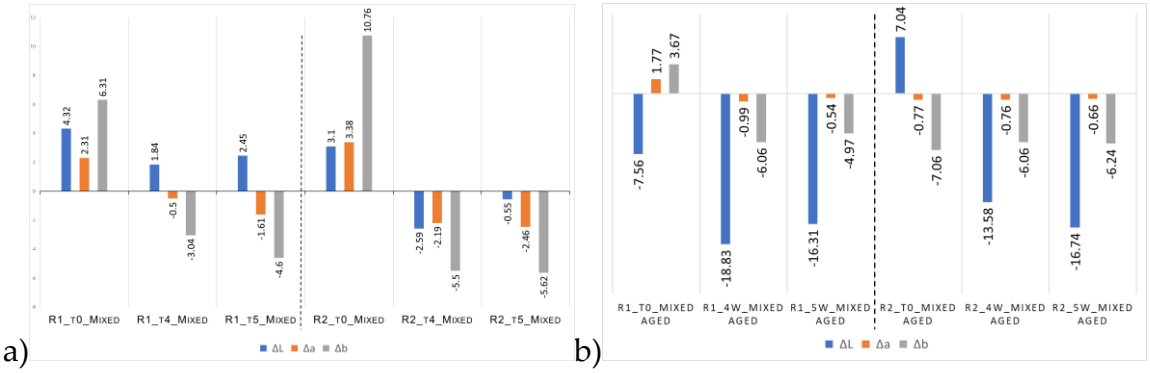

Figure 5.33: Graph of ΔL, Δa and Δb values of paper samples treated with Mixed NPs, (a) Batch 1; (b) Batch 2.

The ΔL values of Batch 2 samples treated with $Ca(OH)_2$ NPs are large negative values (Figure 5.31b) which is expected as aging makes IGI paper darker due to oxidation (Sequeira, 2006), however, the ΔL values of R1_t5 and R2_t0 are positive values (figure 5.31b) which is implied from figure 5.30 as the respective L* value is higher than that of Batch 1 (which is considered as reference for calculating ΔL values for Batch2, see table 5.7). The positive ΔL value of R2_t0 is consistent across all NPs dispersion treatments. In the case of $Mg(OH)_2$ NPs treatment in Batch 2, all samples have negative

ΔL values (except R2_t0) with the highest negative values appearing for 4 weeks samples (R1 and R2) indicating the samples became darker after treatment and aging (figure 5.32b). The same trend of negative ΔL value (except for R2_t0) is visible in the case of samples treated with mixed NPS dispersion but the highest negative ΔL value appears for R1_t4 sample (Figure 5.33b).

Redness of sample (a*)

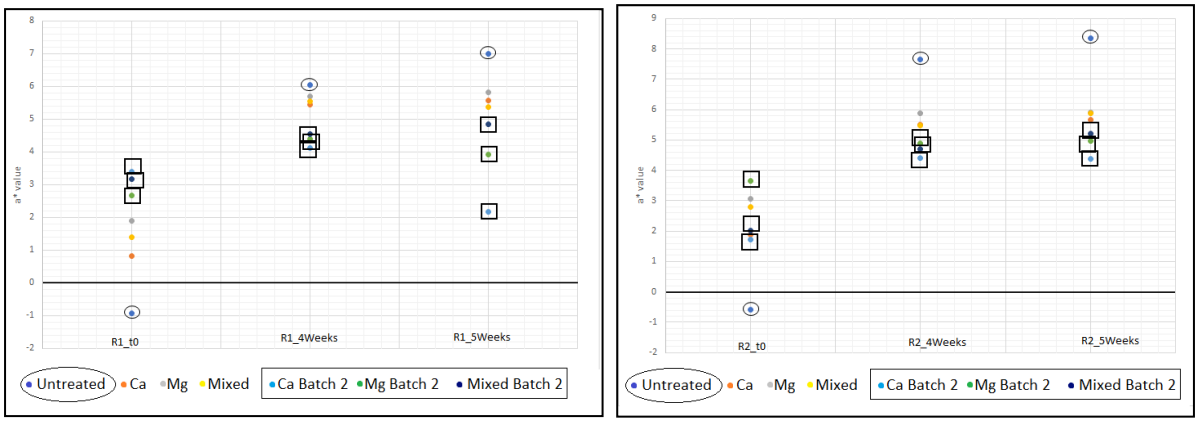

Figure 5.34 : a cordinates of samples (left): R1 (t0, 4 and 5 weeks); (Right): R2 (t0, 4 and 5 weeks) from before treatment (untreated- marked in black circle), Batch 1 and Batch 2 (Aged after treatment -values indicated by black square).*

Batch 1: There is an increase in a* value of unaged samples (t0) of R1 and R2 after treatment while there is a decrease in the a* value of aged samples (4 and 5 weeks) of R1 and R2 after treatment (Figure 5.34). This suggests that the samples become more redder after treatment in the case of unaged samples and less redder in the case of aged samples (and not green as the values are still positive, see table 5.6).

The Δa values of samples treated with $Ca(OH)_2$ NPs, $Mg(OH)_2$ NPs and Mixed NPs dispersion shows a similar trend of decreasing Δa value within one type of ink with increase in aging of the sample (Figure 5.31a, 5.32a and 5.33a). Δa values are positive for the unaged samples suggesting that the treatment with NPs in the three dispersions makes unaged samples (t0) more-redder and the negative value for the aged samples (4 and 5 weeks) suggests that the treatment makes the samples less-redder (and not green as the a* values are positive, see table: 5.6) as can be inferred from figure 5.34.

Batch 2: The samples after accelerated aging (Batch 2) have lower a* value in comparison to the respective sample in Batch 1 for the t4 and t5 samples from R1 and R2. However, in the case of R1_t0 (all kinds of NPs treatments) and R2_t0_Mg, the a*

value has increased more than that of Batch 1 while R2_t0_Ca and R2_t0_Mixed have decreased a* value after accelerated aging (Figure 5.34; Table 5.7).

The Δa values of samples after accelerated aging follows the same sequence as that of Δb values in the case of $Ca(OH)_2$ NPs treatment except for R2_t0_Ca where it is almost zero (Figure : 5.31b). In the case of treatment with $Mg(OH)_2$ NPs and Mixed NPs dispersion, the Δa values are very low and remain stable across the samples regardless of ink and aging time (Figure 5.32b and 5.33b). The highest Δa value in samples treated with $Mg(OH)_2$ NPs is for R1_t5 (-1.9) and in samples treated with Mixed dispersion is for R1_t0 (-2.77) which are very low values. The low Δa values suggest that the treatment and aging has not significantly affected the a* values of the samples.

Yellowness of sample (b* value)

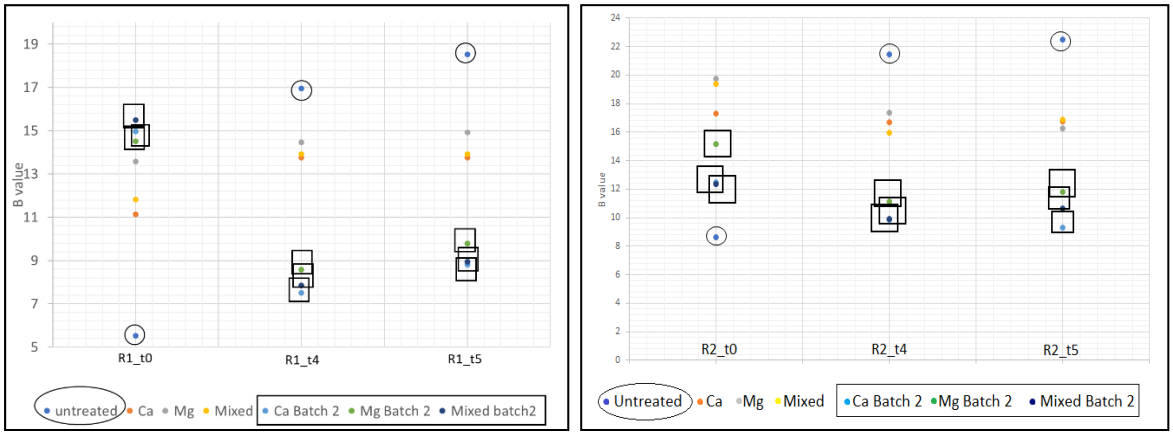

Figure 5.35 : b cordinates of samples (left): R1 (t0, 4 and 5 weeks); (Right): R2 (t0, 4 and 5 weeks) from before treatment (untreated- marked in black circle), Batch 1 and Batch 2 (Aged after treatment -values indicated by black square).*

Batch 1: The increase b* coordinates suggest yellowing of samples which is visible in the case for unaged samples (t0) of R1 and R2. The b* value has increased from the untreated sample for all the unaged papers whereas it has decreased from the untreated sample for all the aged samples (4 and 5 weeks) of R1 and R2 irrespective of the treatment (Figure 5.35). The yellowing of IGI papers after application of non-aqueous treatment has been reported (Wojciak, 2016; Malesic, 2019).

In the case of treatment with $Ca(OH)_2$ NPs, there is a gradual decrease in Δb values from positive values for unaged samples to negative values for aged samples within one type of ink and occurs in both R1 and R2 samples. This indicates that within one type of ink, the samples are becoming less yellow after treatment (and not blue as the b* values are positive, see table 5.6). The same behaviour is observed in treatment with $Mg(OH)_2$ NPs and Mixed NPs dispersion (figure 5.31a, 5.32a and 5.33a).

Batch 2: The samples after undergoing accelerated aging have lower b* value for aged samples (4 and 5 weeks) in comparison to untreated and Batch 1 b* values of the same samples (table: 5.7). The unaged samples (t0) have higher b* value in R1 sample in comparison to Batch 1 and untreated sample, indicating that the samples in R1_t0 irrespective of the type of treatment has become more yellow after accelerated aging. But the b* value of R2_t0 sample is lower than Batch 1 of the same indicating that the samples became less yellow after treatment and aging.

The Δb values of samples treated with $Ca(OH)_2$ NPs in Batch 2 are negative except for R1_t0 which has a positive Δb value. The Δb values of samples treated with $Mg(OH)_2$ NPs and Mixed NPs dispersion are similar to those of samples treated with $Ca(OH)_2$ NPs (figure 5.31b, 5.32b and 5.33b). Excluding R1_t0 sample, the Δb values of all the other paper samples after accelerated aging irrespective of the treatment is within the range of -4.5 and -7 suggesting a stability in the yellowing of the sample regardless of the ink type, aging time and kind of NP dispersion treatment.

Total Colour Difference (ΔE)

In terms of ΔE value of Batch 1, the aged samples (t4 and t5) have ΔE value with the minimum of 3.5 and 3.6 for R1_t4_Ca and R1_t4_Mixed respectively and maximum value of 7.2 for R2_t5_Mg. The unaged samples (t0) show the highest ΔE value with a maximum value of 12.8 for R2_t0_Mg and minimum value of 8 for R1_t0_Mixed. The ΔL and Δb values of the aged samples (t4 and t5) in Batch 1 are desirable as they increase the contrast between the ink and the paper thereby increasing legibility (Zervos & Moropoulou, 2006); however, it would also imply that the ΔL and Δb values of the unaged samples (t0) are not desirable.

The batch of samples that underwent accelerated aging (Batch 2) has an increased ΔE value which is caused by the large ΔL value and less influenced by Δa and Δb values suggesting that the colour has not changed significantly instead indicating the samples became darker due to oxidation of cellulose catalysed by the degradation of IGI as a result of the accelerated aging (Malesic, 2014) (figure 5.31b, 5.32b and 5.33b). Since there is not much variation in the Δa and Δb values after aging it is also suggestive that the treatment helps reduce colour change over time.

5.2.2.6. FTIR-ATR

Treatment with $Ca(OH)_2$ NPs: The FTIR spectra of all the samples treated with $Ca(OH)_2$ NPs (Figure 5.36a) do not show any significant change in the comparison to untreated spectra of the respective samples shown in Figure 5.15. However, the treated samples in Batch 1 show a small but sharp peak at 3635 cm^{-1} which represents the OH stretching of $Ca(OH)_2$ as can be seen in figure 5.7 (a and b) confirming the presence of NPs on the paper. The other bands that belong to the NPs appears to be overlapped

by the cellulose bands from the paper. however, this peak also disappears in Batch 2 as the sample undergoes artificial aging in the climate chamber and the water molecules disappear from the samples. This can be seen in R2_t4_Ca FTIR spectra in figure 5.36 (b) and the spectra of R1 samples are present in Appendix: A4.5.

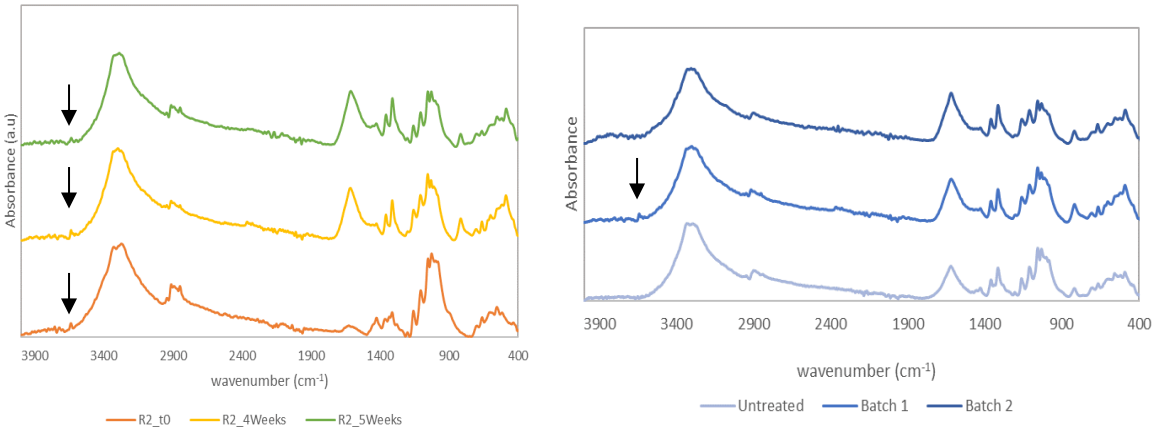

Figure 5.36: FTIR spectra (a)Samples treated with $Ca(OH)_2$ NPs with the black arrow marking the peak from NPs at 3635 cm^{-1} (b) Sample R2_t4_Ca before treatment, Batch1 and Batch 2(after aging).

Treatment with $Mg(OH)_2$ NPs: The FTIR spectra of all the samples treated with $Mg(OH)_2$ NPs (Figure 5.37a) do not show any significant change in the comparison to untreated spectra of the respective samples shown in Figure 5.15. Nevertheless, the treated samples in Batch 1 show a sharp peak at 3698 cm^{-1} which represents the OH stretching of $Mg(OH)_2$ as can be seen in figure 5.8 confirming the presence of NPs on the paper. The other bands that belong to the NPs appears to be overlapped by the cellulose bands from the paper. However, this peak also disappears in Batch 2 as the sample undergoes artificial aging in the climate chamber and the water molecules disappear from the samples. This can be seen in R2_t4_Ca FTIR spectra in figure 5.37 and the spectra of R1 samples are present in Appendix: A4.5.

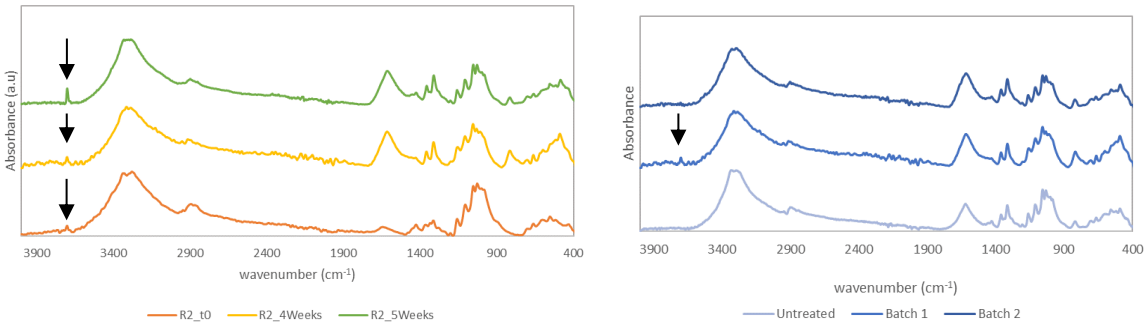

Figure 5.37: FTIR spectra (a) Samples treated with $Mg(OH)_2$ NPs with the black arrow marking the peak from NPs at 3698 cm^{-1} (b)Sample R2_t4_Mg before treatment, Batch1 and Batch 2(after aging).

Treated with Mixed dispersion: The FTIR spectra of all the samples treated with mixed dispersion (Figure 5.38 and Appendix: A4.5) do not show any significant change in the comparison to untreated spectra of the respective samples shown in Figure 5.15. Nevertheless, the treated samples in Batch 1 show a sharp peak at 3635 and 3698 cm^{-1} therefore confirming the presence of NPs on the paper (Figure 7 and 8). The other bands that belong to the NPs appear to be overlapped by the cellulose bands from the paper. However, these peaks disappear in Batch 2 as the samples undergo artificial aging in the climate chamber and the water molecules disappear from the samples. This can be seen in R1_t4_Mixed FTIR spectra in figure 5.38(b) and the spectra of R2 samples are present in Appendix: A4.5.

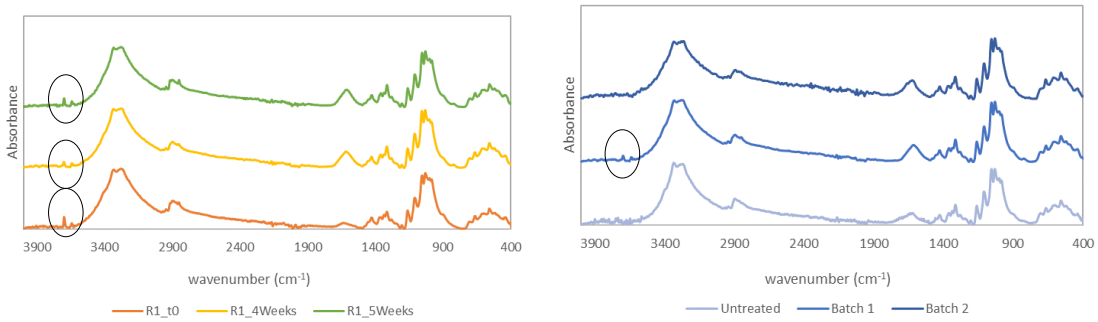

Figure 5.38: (a)FTIR spectra of samples treated with Mixed dispersion with the black circles marking the peak from NPs at 3635 and 3698 cm^{-1} (b) FTIR spectra of R1_t4_Mixed before treatment, Batch1 and Batch 2(after aging).

The FTIR-ATR analysis further confirms the presence of NPs in the paper samples. The analysis of Batch 2 shows that the treatment does not affect the composition of the paper samples in accelerated aging as there are no shifts in any of the bands in association with the treatment.

Chapter: 6

Conclusions

This study has shown the potential of laboratory-synthesized nanoparticle dispersions towards the conservation of iron gall ink-induced corrosion on paper as a deacidification treatment method.

Two types of nanoparticle were prepared, following precipitation methods which included Triton X-100 ($Ca(OH)_2$ NPs) and CTAB ($Mg(OH)_2$ NPs) as surfactants. SEM analysis showed that hexagonal plate-like shaped $Ca(OH)_2$ nanoparticles clustered together were formed with a mean diameter 483±204 nm and thickness 207±89 nm. As to $Mg(OH)_2$ NPs with the same morphological aspect were obtained but much smaller in size (mean particle diameter 142±27 nm and thickness 43±8 nm). Besides, the NPs are differently oriented, forming flower-like clusters. TGA and XRD showed low amounts of $CaCO_3$ (~7% (w/w) that may have formed during $Ca(OH)_2$ NPs drying or storage processes and the absence of surfactant was confirmed by TGA, XRD and FTIR. TGA also indicated that low amounts of $MgCO_3$ (~2% w/w) were observed in $Mg(OH)_2$ NPs but not found in XRD analysis. FTIR spectra corroborated these observations and confirmed together with TGA and XRD the absence of surfactant on the NPs.

To establish the most effective parameters of concentration and number of applications of NPs dispersions in 2-propanol, different concentrations were prepared and applied multiple times on trial samples. This resulted in the selection of 2.5 g/L concentration and 4&4 number of applications (4 times on the front and 4 times on the reverse).

Three types of NPs dispersions in 2-propanol were prepared and applied on paper samples and their effectiveness was observed and compared using different analytical techniques. $Ca(OH)_2$ NPs dispersion, $Mg(OH)_2$ NPs dispersion and mixed $Ca(OH)_2/Mg(OH)_2$ dispersion were sprayed on samples with IGI prepared according to two recipes, here named R1 and R2, that were previously prepared in a context different from this thesis. Three aging times were selected for the study: unaged samples (t0) and aged samples in artificial aging chamber for 4 and 5 weeks (t4 and t5, respectively). The treated samples were divided into 2 sets: one set (Batch 1) was aged under ambient conditions in the laboratory and the other (Batch 2) underwent one week of accelerated aging in the same temperature and humidity conditions as the untreated samples were exposed before, to observe the immediate and the long-term effect of the treatments, respectively.

Photographic documentation of the treated samples did not show any significant changes in the colour or appearance of the samples from Batch 1 after treatment. However, the ink in samples from Batch 2 has darken, which is more likely attributed to the degradation of IGI due to the accelerated aging procedure.

The 3D-digital microscopic observations confirmed the observations of photographic imaging. Besides, the images acquired showed that no morphological alteration was occurring on the surface texture of the paper fibres and ink in regards to the treatments, indicating that the treatment with different NPs do not form any visible residues on the surface of the paper or alter it from a morphological point of view.

The high magnification (1.5k and 8.00k) used in SEM-EDS analysis allowed us to observe the NPs on the paper fibres: how they were arranged within the fibres and the empty spaces in between as small clusters of NPs that are widely (but in non-uniform manner) distributed. The shape of the NPs are in agreement with was found in the nanoparticle characterization.

The SEM images of Batch 2 showed that the fibres and the NPs morphologies of do not change after accelerated aging, suggesting that the NPs have not yet carbonatated. This is further corroborated by the FTIR-ATR analysis where the bands of the untreated samples to do not have any shifts after treatment, while the new peaks at 3635 and 3699 cm^{-1} confirm the presence of $Ca(OH)_2$ and $Mg(OH)_2$ NPs, respectively. The pH of all the treated samples increased abruptly to alkaline level regardless of which NPs dispersion was applied in Batch 1. In Batch 2, there is a general decrease in the pH values but none of the samples have approached the initial acidic values reflective of the effectiveness of the treatments. The achieved values after treatments with the three kinds of dispersions (between pH 6.5 and 9) suggest the effectiveness and suitability of the treatments, because the NPs provide necessary amount of OH^- for deacidification to occur and at the same time the pH is the range of the optimal values. The treatments with $Ca(OH)_2$ and $Mg(OH)_2$ are similarly very effective, while, mixed NPs dispersions provide slightly lower pH values).

Colorimetric studies revealed that the unaged samples (t0) become lighter and more yellow after treatment with the nanoparticle dispersions while the aged samples (t4 and t5) became darker and less yellow after treatment. There is a noticeable difference in the ΔL value of the samples from Batch 2 which was evident from photographic documentation and also from the 3D-digital microscope, is more likely attributed to IGI degradation. However, the Δb and Δa values of the samples after treatment have not varied significantly suggesting that the samples did not change much in colour but noticeably changed in the lightness/darkness after treatment and aging.

References

Afsharpour, M., Rad, F. T., & Malekian, H. (2011). New cellulosic titanium dioxide nanocomposite as a protective coating for preserving paper-art-works. *Journal of Cultural Heritage*, *12*(4), 380–383. https://doi.org/10.1016/j.culher.2011.03.001

Ali, N. T., Abrahim, R. K., Saad, H. F., Jabr, N. K., Hindal, S. S., Hussain, D. R., & Sekp, A. M. (2019). Synthesis of calcium hydroxide for heritage conservation. *Journal of Physics: Conference Series*, *1234*(1). https://doi.org/10.1088/1742-6596/1234/1/012021

Artioli, G. (2010). *Scientific Methods and Cultural Heritage An introduction to the application of materials science to archaeometry and conservation science.* New York: Oxford University Press.

Artioli, G. (2013). Science for the Cultural Heritage: The contribution of X-ray diffraction. Rend. Fis. Acc. Lincei (2013) 24 (Suppl 1): S55–S62.

Asgari-Vadeghani, T., Ghanbari, D., Mozdianfar, M. R., Salavati-Niasari, M., Bagheri, S., & Saberyan, K. (2016). Sugar and Surfactant-Assisted Synthesis of Mg(OH)2 Nano-flower and PVA Nanocomposites. *Journal of Cluster Science*, *27*(1), 299–314. https://doi.org/10.1007/s10876-015-0930-6

Baglioni P., Chelazzi, D & Giorgi R. (2015). *Nanotechnologies in the Conservation of Cultural Heritage*. Springer. 117-141. https://doi.org/10.1007/978-94-017-9303-2

Baglioni, P & Giorgi R. (2006). Soft and hard nanomaterials for restoration and conservation of cultural Heritage. *Soft Matter*, 2, 293–303

Baglioni, P., Giorgi, R., & Chelazzi, D. (2012). Nano-Materials for the Conservation and Preservation of Movable and Immovable Artworks. *International Journal of Heritage in the Digital Era*. 1. 313-318. http://doi.org/10.1260/2047-4970.1.0.313

Baiza, B., Gil, M., Galacho, C., Candeias, A., & Girginova, P. I. (2021). Preliminary Studies of the Effects of Nanoconsolidants on Mural Paint Layers with a Lack of Cohesion. *Heritage*, *4*(4), 3288–3306. https://doi.org/10.3390/heritage4040183

Bastone, S., Chillura Martino, D. F., Renda, V., Saladino, M. L., Poggi, G., & Caponetti, E. (2017). Alcoholic nanolime dispersion obtained by the insolubilisation-precipitation method and its application for the deacidification of ancient paper. *Colloids and Surfaces A: Physicochemical and Engineering Aspects*, *513*, 241–249. https://doi.org/10.1016/J.COLSURFA.2016.10.049

Baudot, C., Tan, C. & Kong, J. (2010). FTIR spectroscopy as a tool for nano-material characterization. *Infrared Physics & Technology*. 53. 434-438. https://doi.org/10.1016/j.infrared.2010.09.002

Bicchieri, M., Valentini, F., Calcaterra, A., & Talamo, M. (2017). Newly Developed Nano-Calcium Carbonate and Nano-Calcium Propanoate for the Deacidification of Library and Archival Materials. *Journal of Analytical Methods in Chemistry*. https://doi.org/10.1155/2017/2372789

Caggiani, M. & Colomban, P. (2020). 7. Raman Microspectroscopy for Cultural Heritage studies. *Chemical Analysis in cultural Heritage,* ed. by L. Sabbatini and I. D. van der Werf, Berlin, Boston: De Gruyter, 151-180. https://doi.org/10.1515/9783110457537-007

Camera, D. la. (2007). Crystal Formations Within Iron Gall Ink: Observations and Analysis Crystal Formations Within Iron Gall Ink: Observations and Analysis. *Journal of the American Institute of Conservation.* Summer (Vol 46), 153-174.

Claro A., Nunes M., & Ferreira T. (2019). O que esconde a tinta ferrogálica usada em manuscritos portugueses dos séculos XVI e XVII (oral presentation). Contributed Talks for Universidade Nova.

Claro A., Nunes M., & Ferreira T. (21 July 2021). Conservation practices of document heritage (Oral presentation). *Frontiers of Humanity and beyond*.

Clayton, E. (n.d.). A brief history of writing materials and technologies. *A history of writing*. Retrieved on 13 November 2022 from https://www.bl.uk/history-of-writing/articles/a-brief-history-of-writing-materials-and-technologies.

Corregidor, V., Viegas, R.,Ferreira, L., & Alves, L. (2019). Study of Iron Gall Inks, Ingredients and Paper Composition Using Non-Destructive Techniques. *Heritage*, 2(4). 2691-2703. https://doi.org/10.3390/heritage2040166

Da Costa A.C.A , Corrêa F., Sant'anna G, Hannesch O, Gisele B. Tonietto, Godoy J., Gonçalves R., & Lutterbach M. (2018). Iron-Gall Ink Studies on Acid and Alkaline Papers and their relation to Cellulose Microbiological Degradation. *International Journal of Conservation Science, 9*(3), 413-428.

Daniele, V., & Taglieri, G. (2012). Synthesis of $Ca(OH)_2$ nanoparticles with the addition of Triton X-100. Protective treatments on natural stones: Preliminary results. *Journal of Cultural Heritage*, *13*(1), 40–46. https://doi.org/10.1016/j.culher.2011.05.007

David, M. E., Ion, R. M., Grigorescu, R. M., Iancu, L., & Andrei, E. R. (2020). Nanomaterials used in conservation and restoration of cultural heritage: An up-to-date overview. *Materials*, *13*(9). 2064-2088. https://doi.org/10.3390/ma13092064

Dhaouadi, H., Chaabane, H., & Touati, F. (2011). $Mg(OH)_2$ nanorods synthesized by a facile hydrothermal method in the presence of CTAB. *Nano-Micro Letters*, *3*(3), 153–159. https://doi.org/10.3786/nml.v3i3.p153-159

Eusman, E. (1998). Iron Gall Ink – Chemistry IGI. *The Iron Gall ink Website*. https://irongallink.org/iron-gall-ink-chemistry.html

Feller, R. J. (2002). *Colour Science in the Examination of Museum Objects Non-destructive Procedures*. Los Angeles: The Getty Conservation Institute.

Ferreira, P. J., Gamelas, J. A., Moutinho, I. M., Ferreira, A. G., Go´mez, N., Molleda, C., & Figueiredo M. M. (2009). "Application of FT-IR-ATR Spectroscopy to Evaluate the Penetration of Surface Sizing Agents into the Paper Structure." *Industrial & Engineering Chemistry Research, 48,* 3867–3872.

Ferrer, N., & Carme Sistach, M. (2013). Analysis of sediments on iron gall inks in manuscripts. *Restaurator*, *34*(3), 175–193. https://doi.org/10.1515/res-2013-0010

Fouda, A., Abdel-Maksoud, G., Abdel-Rahman, M. A., Salem, S. S., Hassan, S. E. D., & El-Sadany, M. A. H. (2019). Eco-friendly approach utilizing green synthesized nanoparticles for paper conservation against microbes involved in biodeterioration of archaeological manuscript.

International Biodeterioration and Biodegradation, *142*, 160–169. https://doi.org/10.1016/j.ibiod.2019.05.012

Garside, P. & Miller, Z. (2021 June 03). Iron gall ink on paper: Saving the words that eat themselves. *Blogs.bl.uk*. Retrieved 23 july 2022 from https://blogs.bl.uk/collectioncare/2021/06/iron-gall- ink-on-paper-saving-the-words-that-eat-themselves.html

Gascoigne, B. "History of writing materials" History World. From 2001, ongoing. http://www.historyworld.net/wrldhis/plaintexthistories.asp?historyid=aa92

Giorgi, R., Bozzi, C., Dei, L., Gabbiani, C., Ninham, B. W., & Baglioni, P. (2005). Nanoparticles of Mg(OH)2: synthesis and application to paper conservation. *Langmuir: the ACS journal of surfaces and colloids*, *21*(18), 8495–8501. https://doi.org/10.1021/la050564m

Girginova, P. I., Galacho, C., Veiga, R., Silva, A. S., & Candeias, A. (2020). Study of mechanical properties of alkaline earth hydroxide nanoconsolidants for lime mortars. *Construction And Building Materials*, *236*, Art. N° 117520. https://doi.org/10.1016/j.conbuildmat.2019.117520

Green, L.R., & Leese, M. (1991) "Non aqueous Deacidification of Paper with methyl Magnesium Carbonate. *Restaurator*. Vol. 12, N. 3, p. 149-162.

Gulik, R.V. (1997). Conservation - Current methods 1890-1960. *The Iron Gall ink Website*. https://irongallink.org/conservation-current-methods.html

Hanna, A. A., Abdelmoaty, A. S., & Sherief, M. A. (2019). Synthesis, Characterization, and Thermal Behavior of Nanoparticles of $Mg(OH)_2$ to Be Used as Flame Retardants. *Journal of Chemistry, Art. ID 1805280*. https://doi.org/10.1155/2019/1805280

Harris, C. 1983. Preservation of Paper Based Materials: Mass Deacidification Methods and Projects. Conserving and preserving library materials. www.ideals.illinois.edu:2142/453

Henniges, U., Reibke, R., Banik, G., Huhsmann, E., Hähner, U., Prohaska, T., & Potthast, A. (2008). Iron gall ink-induced corrosion of cellulose: Aging, degradation and stabilization. Part 2: Application on historic sample material. *Cellulose*, *15*(6), 861–870. https://doi.org/10.1007/s10570-008-9238-0

Hoffman, J. (n.d). The Spread of Papermaking Technology into Europe. *Science and Its Times: Understanding the Social Significance of Scientific Discovery*. Retrieved June 21, 2022 from Encyclopedia.com: http://www/encyclopedia.com/science/encyclopedias-almanacs-transcripts-and-maps/spread-papermaking-technology-europe

Hunter, D. (1947). *Papermaking: The History and Technique of an Ancient Craft*. New York: Dover Publications, Inc.

Ion, R.-M., Doncea, S.-M., & Țurcanu-Caruțiu, D. (2017). Nanotechnologies in Cultural Heritage - Materials and Instruments for Diagnosis and Treatment. In *Novel Nanomaterials - Synthesis and Applications*. InTech. https://doi.org/10.5772/intechopen.71950

Jia, Z., Yang, C., Zhao, F., Chao, X., Li, Y., & Xing, H. (2020). One-step reinforcement and deacidification of paper documents: Application of lewis base—chitosan nanoparticle coatings and analytical characterisation. *Coatings*, *10*(12), 1–15. https://doi.org/10.3390/coatings10121226

Kaminari, A. A., Boyatzis, S. C., & Alexopoulou, A. (2018). Linking Infrared Spectra of Laboratory Iron Gall Inks Based on Traditional Recipes with their Material Components. *Applied Spectroscopy*, *72*(10), 1511–1527. https://doi.org/10.1177/0003702818778319

Kolar J., Mozir A., Strlič M., de Bruin G., Pihlar B., & Steemers T. (2007) Stabilisation of iron gall Ink: aqueous stabilisation with magnesium phytate. *e-Preserv Sci* 4, 19–24. https://doi.org/10.1515/rest.2005.26.3.181

Kolar, J., Šala, M., Strlič, M. & Šelih, V. (2005). Stabilisation of Paper Containing Iron-Gall Ink with Current Aqueous Processes. *Restaurator* *26*(3), 181-189. https://doi.org/10.1515/rest.2005.26.3.181

Kwiatkowska, A., Wojech, R. & Wójciak, A. (2014). Paper deacidification with the use of magnesium oxide nanoparticles. *Forestry and Wood Technology*, *85*, 144-148.

Liu, G. and Kazarian, S. G. (2022). Recent advances and applications to cultural heritage using ATR-FTIR spectroscopy and ATR-FTIR spectroscopic imaging**.** *Analyst*. 147, 1777-1797. https://doi.org/10.1039/D2AN00005A

Malešič, J. & Šala, M., Šelih, V., Kocar, D. (2014). Evaluation of a method for treatment of iron gall ink corrosion on paper. Cellulose, 21, 2925–2936. https://doi.org/10.1007/s10570-014-0311-6

Manso, M., & Carvalho, M. L. (2009). Application of spectroscopic techniques for the study of paper documents: A survey. *Spectrochimica Acta - Part B Atomic Spectroscopy*, *64*(6), 482–490). https://doi.org/10.1016/j.sab.2009.01.009

Marieflemay. (2013 March 03). Iron Gall Ink posted by marieflemay in Inks and Pigments. Traveling Scriptorium*: ~ A Teaching Kit by the Yale University Library.* Retrieved on 24 July 2022 from https://travelingscriptorium.com/2013/03/21/iron-gall-ink/

Melo, M. J., Otero, V., Nabais, P., Teixeira, N., Pina, F., Casanova, C., Fragoso, S., & Sequeira, S. O. (2022). Iron-gall inks: a review of their degradation mechanisms and conservation treatments. *Heritage Science, 10*(1). https://doi.org/10.1186/s40494-022-00779-2

Mohamed, W. A., Abdel-Rahman, A. M., Hassan, R. R. A., & Hegazy, A. K. (2018). A new approach to the treatment of iron gall ink corrosion using plant biomass. *Mediterranean Archaeology and Archaeometry*, *18*(2), 35–47. https://doi.org/10.5281/zenodo.1297144

Mourdikoudis, S., Pallares, R. & Thanh, N. (2018). Characterization Techniques for Nanoparticles: Comparison and Complementarity upon Studying Nanoparticle Properties. *Nanoscale*. 10, 12871-12934. https://doi.org/10.1039/C8NR02278J

Neevel, J. G., & Reissland, B. (2005). Bathophenanthroline indicator paper. *Papier Restaurierung*, *6*, 28–36.

Nehring, G., Bonnerot, O., Gerhardt, M., Krutzsch, M., & Rabin, I. (2021). *Looking for the missing link in the evolution of black inks, 13*, Art. N° 71. https://doi.org/10.1007/s12520-021-01320-5

Nunes, M., Wanzeller, G., Correira, D., Mitchell, S., Olival, F., Claro, A., & Ferreira, T. (2022). A preliminary study on iron gall inks in historical documents of the Portuguese Inquisition (Poster). *Analytica 2020*.

Ohta N, & Robertson, A. R. (2005). Colorimetry: Fundamentals and Applications. John Wiley & Sons Ltd,: West Sussex PO19 8SQ, England.

Oliveira, E. F., & Hase, Y. (2001). Infrared study and isotopic effect of magnesium hydroxide. *Vibrational spectroscopy*, (25), 53-56.

Pires, J. & Cruz, A.J. (2007). Techniques of Thermal Analysis applied to the Study of Cultural Heritage. *Journal of Thermal Analysis and Calorimetry*, *87*, 2, 411–415. http://doi.org/10.1007/s10973-004-6775-0

Plutino, A. & Simone, G. (2021). The limits of Colorimetry in Cultural Heritage Applications. *Coloration Technology*, 137: 56–63. https://doi.org/10.1111/cote.12500

Poggi, G., Baglioni, P., & Giorgi, R. (2011). Alkaline earth hydroxide nanoparticles for the inhibition of metal gall ink corrosion. *Restaurator*, *32*(3), 247–273. https://doi.org/10.1515/rest.2011.012

Poggi, G., Giorgi, R., Toccafondi, N., Katzur, V., & Baglioni, P. (2010). Hydroxide nanoparticles for deacidification and concomitant inhibition of iron-gall ink corrosion of paper. *Langmuir*, *26*(24), 19084–19090. https://doi.org/10.1021/la1030944

Poggi, G., Sistach, M. C., Marin, E., Garcia, J. F., Giorgi, R., & Baglioni, P. (2016). Calcium hydroxide nanoparticles in hydroalcoholic gelatin solutions (GeolNan) for the deacidification and strengthening of papers containing iron gall ink. *Journal of Cultural Heritage*, *18*, 250–257. https://doi.org/10.1016/j.culher.2015.10.005

Poggi, G., Toccafondi, N., Melita, L., Knowles, J., Bozec, L., Giorgi, R & Baglioni, P. (2014). Calcium hydroxide nanoparticles for the conservation of cultural heritage: New formulations for the deacidification of cellulose-based artifacts. *Applied Physics A-Materials Science & Processing*, 114. 685-693. https://doi.org/10.1007/s00339-013-8172-7

Porck, H. J. (2000). Rate of Paper Degradation. The Predictive Value of Artificial Aging Tests. In *European Commission on Preservation and Access*.

Potthast A, Henniges U, & Banik G (2008) Iron gall ink-induced corrosion of cellulose: aging, degradation and stabilization. Part 1: model paper studies. *Cellulose* 15, 849–859. https://doi.org/10.1007/s10570-008-9237-1

Price, D. & Burton, J. (2011). *An Introduction to Archaeological Chemistry*. ISBN: 978-1-4419-6376-5. https://link.springer.com/book/10.1007/978-1-4419-6376-5

Proniewicz, L. M., Paluszkiewicz, C., Weseøucha-Birczyn Âska, A., Majcherczyk, H., Âski, A. B., & Konieczna, A. (2001). FT-IR and FT-Raman study of hydrothermally degradated cellulose. *Journal of Molecular structure*. (596), 163-169. www.elsevier.com/locate/molstruc

Rami, J.M., Patel, C.D., Patel, C.M. & Patel, M.V. (2021). Thermogravimetric analysis (TGA) of some synthesized metal oxide nanoparticles. *Materials Today: Proceedings*. 43. 655-659. https://doi.org/10.1016/j.matpr.2020.12.554

Reissland, B. (1997). Conservation - Early methods 1890-1960. *The Iron Gall ink Website*. https://irongallink.org/conservation-early-methods-1890-1960.html

Reissland, B., & Graaff, J. (2001). Conditioning Rating for Paper Objects with Iron-Gall Ink. *ICN-Information*, *1*, 1–4.

Rizzutto, M., Curado, J. F., Bernarde, S., Campos, P., Kajiya, E., Silva, T., Rodrigues L., Cleber, Moro, M., Tabacniks, Manfredo & Added, N. (2015). Analytical Techniques Applied to Study Cultural Heritage Objects. 5 *International Nuclear Atlantic Conference* - INAC 2015.

Rojas, J. A., Ardila-Rodríguez, L. A., Diniz, M. F., Gonçalves, M., Ribeiro, B., & Rezende, M. C. (2019). Optimization of Triton X-100 removal and ultrasound probe parameters in the preparation of multiwalled carbon nanotube buckypaper. *Materials and Design*, *166*. https://doi.org/10.1016/j.matdes.2019.107612

Rota, E., Bozzi, C., Cremonesi P., & Lucchini, A. (2021) Study of the Best Methodology for Measuring Surface pH of Linen Canvas, *Studies in Conservation*, *66*(6), 313-320. https://doi.org/10.1080/00393630.2020.1838711

Rouchon, V., Duranton, M., Belhadj, O., Bastier-Deroches, M., Duplat, V., Walbert, C., & Hansen, B. V. (2013). The use of halide charged interleaves for treatment of iron gall ink damaged papers. *Polymer Degradation and Stability*, *98*(7), 1339–1347. https://doi.org/10.1016/J.POLYMDEGRADSTAB.2013.03.028

Sequeira, S., Casanova, C., & Cabrita, E. J. (2006). Deacidification of paper using dispersions of Ca(OH)2 nanoparticles in isopropanol. Study of efficiency. *Journal of Cultural Heritage*, *7*(4), 264–272. https://doi.org/10.1016/j.culher.2006.04.004

Smith, R. D. (1966). Paper Deacidification: A Preliminary Report. *The Library Quarterly: Information, Community, Policy*, *36*(4), 273–292. http://www.jstor.org/stable/4305691

Stauderman, S.D., Bruckle, I., & Bischoff, J.J. (1996). Observations on the Use of Bookkeeper® Deacidification Spray for the Treatment of Individual Objects. *The Book and Paper Group Annual*. Retrieved on 25 July 2022 from https://cool.culturalheritage.org/coolaic/sg/bpg/annual/v15/bp15-17.html

Strlič, M., Kolar, J., & Scholten, S. (2005). "Paper and durability." In *Ageing and stabilisation of paper*, by Jana Kolar Matija Strlič, 3-8. Ljubljana: National and University Library Ljubljana.

Strlič, M., Kolar, J., Šelih, V.-S., Kočar, D. & Pihlar., B. (2003). A comparative study of several transition metals in Fenton-like reaction systems at circum-neutral pH. *Acta Chimica Slovenica*, *50*, 619-632.

Stuart, B. (2007). *Analytical Techniques in Material conservation*. John Wiley & Sons Ltd: West Sussex PO19 8SQ, England.

Teixeira, N., Nabais, P., de Freitas, V., Lopes, J. A. & Melo, M. J. (2021) In-depth phenolic characterization of iron gall inks by deconstructing representative Iberian recipes. *Scientific Reports*, 11, Art. N° 8811. https://doi.org/10.1038/s41598-021-87969-3

UNESCO convention 1972: Recommendation concerning the Protection, at National Level, of the Cultural and Natural Heritage, Records of the General Conference, 17th session, Paris (France), 17 Oct - 21 Nov 1972, v. 1: Resolutions, recommendations. UNESCO. General Conference, 17th, 1972. Doc. code: 17 C/Resolutions + CORR. (Eng & Spa). ISBN: 92-3-101093-x. Publication year: 1973. URL: https://unesdoc.unesco.org/ark:/48223/pf0000114044.page=145

UNESCO convention 2003: 2003 Convention for the Safeguarding of the Intangible Cultural Heritage, Records of the General Conference, 32nd session, Paris (France), 29 Sep - 17 Oct 2003. URL: https://ich.unesco.org/en/convention

Ursescu, M., Măluţan, T., & Ciovică, S. (2009). Iron gall inks influence on papers' thermal degradation FTIR spectroscopy applications. *European Journal of Science and Theology*, *5*(3). https://www.researchgate.net/publication/282724424

Verhoeven, G., 2016. Basics of photography for cultural heritage imaging, in: Stylianidis, E., Remondino, F. (Eds.), *3D Recording, Documentation and Management of Cultural Heritage*. Whittles Publishing, Caithness, 127–251.

Weng, J. & Zhang, X. & Jia, M. & Zhang, J. (2018). Deacidification of aged papers using dispersion of Ca(OH)2 nanoparticles in subcritical 1,1,1,2-tetrafluoroethane (R134a). *Journal of Cultural Heritage*, 37, 137-147. https://doi.org/10.1016/j.culher.2018.12.001

Wójciak, A. (2015). Washing, Spraying and Brushing. A Comparison of Paper Deacidification by Magnesium Hydroxide Nanoparticles. *Restaurator, International Journal for the Preservation of Library and Archival Material*, *36*, 3–23. https://doi.org/10.1515/res-2014-0010

Xu, Q., Poggi, G., Resta, C., Baglioni, M., & Baglioni, P. (2020). Grafted nanocellulose and alkaline nanoparticles for the strengthening and deacidification of cellulosic artworks. *Journal of Colloid and Interface Science*, *576*, 147–157. https://doi.org/10.1016/j.jcis.2020.05.018

Zamorano, G. M. C. (2018). The presence of iron in inks used in Valencian manuscripts from the 13th to 17th century. *Microchemical Journal*, *143*, 484–492. https://doi.org/10.1016/J.MICROC.2018.07.043

Zervos, S., & Alexopoulou, I. (2015). Paper conservation methods: a literature review. *Cellulose* *22*(5), 2859–2897). https://doi.org/10.1007/s10570-015-0699-7

Zervos, S., & Moropoulou, A. (2006). Methodology and criteria for the evaluation of paper conservation interventions: A literature review. *Restaurator*, *27*(4), 219–274). https://doi.org/10.1515/REST.2006.219

Zhu, J., Zhang, P., Ding, J., Dong, Y., Cao, Y., Dong, W., Zhao, X., Li, X., & Camaiti, M. (2021). Nano $Ca(OH)_2$: A review on synthesis, properties and applications. *Journal of Cultural Heritage*, 50, 25–42). https://doi.org/10.1016/j.culher.2021.06.002

Zidan, Y., El-Shafei, A., Noshy, W., & Salim, E. (2017). A comparative study to evaluate conventional and nonconventional cleaning treatments of cellulosic paper supports. *Mediterranean Archaeology and Archaeometry*, *17*(3), 337–353. https://doi.org/10.5281/zenodo.1005538

Appendices

Appendix 1 - *Details of paper mock ups.*

A1.1. Paper samples and ink preparation

The paper mock-ups used in this study were previously prepared in HERCULES laboratory by Margarida Nunes in the frame of the PhD research of Ref: SFRH/BD/147528/2019 under the IronIC project (PTDC/ART-HIS/32327/2017).

Two types of IGI were reproduced following historic recipes designated as R1 and R2 for recipe 1 and recipe 2, respectively and then applied in paper and aged in the climate chamber prior to the start of this work. The details of which are given below.

Ink recipe R1: This ink was recreated based on the recipe mentioned by António Pessoa (1648), in the Codex 99 (Fundos da Manizola) which belongs to the Biblioteca Pública de Évora, Évora. A total of 36.87 g of galls were crushed in medium pieces and added to 300 mL of Millipore water and left to extract at room temperature and in direct sunlight for 2 days. After which, the extracted solution was transferred to a beaker and the gallnut was discarded. Afterwards, 24.58 g of iron (II) sulphate, $FeSO_4$, were added and stirred using a branch from the fig tree. It was left to settle for two days in direct sunlight and at room temperature. After this period, 12.29 g ground Gum Arabic was dissolved in Millipore water magnetic stirring and added to the solution. The solution was then stirred with a branch from the fig tree. It was left to settle for 1 day after which, the solution was heated until boiling point and pomegranate peels was added to it. It was stored away from direct light after it cooled down.

Ink recipe R2: This ink was reproduced based on the recipe mentioned in the Memorial of the Congregation of S. João Evangelista located at Arquivo Nacional da Torre do Tombo, Lisboa (Manuscripts da Livraria, nº 1083) that was discovered by Professor Fernanda Olival. A total of 99.6 mL of vinegar was added to 300 mL of Millipore water. 2.04 g of crushed galls were added to this mixture and left to settle for 8 to 10 days (until the colour turned black). After this period, 2.04 g of iron(II) sulphate $FeSO_4$ and 1.53 g of Gum Arabic water were added to the extracted solution.

A1.2. Ink application and accelerated aging

Whatman filter paper (Whatman no.1) of dimensions 6 cm x 2.5 cm is used to write on because it doesn't have any sizing or fillers, and therefore it is apt for the study. The two inks R1 and R2 were applied to the paper as written or painted (as can be seen

from the images in table 4.1). For each Whatman paper, 20 μL of ink was measured using a micropipette and then painted onto the paper using Da Vinci 374 Fit Synthetics Flat Painting Brush 0. In the case of written samples, the ink was applied using feather tips.

The paper samples are meticulously tied with the help of a thread and then hung inside a climate chamber where they would remain for artificial aging (Figure A1.1). The samples are divided into small batches, which are removed from the chamber after 4 and 5 weeks thereby forming the criteria of less aged and more aged samples.

A1.3.*: Samples inside climate chamber for accelerated aging.*

Appendix 2 – *Experimental details and synthesis yield*

Table A2.1*: Chemicals used for synthesis*

Chemical	Chemical Formula	Molecular weight (g/mol)	Producer	Purity / %
Calcium Chloride	$CaCl_2$	110.98	Panreac	95
Magnesium Chloride	$MgCl_2$	95.22	Alfa Aesar	99
Sodium Hydroxide	NaOH	40	Merck	98
Triton X-100	$(C_2H_4O)_nC_{14}H_{22}O$		Sigma-Aldrich	99.9
Hexadecyltrimethylammonium bromide (CTAB)	$C_{19}H_{42}BrN$	364.45	Alfa Aesar	98
Ethanol	C_2HO	46.069	Sigma-Aldrich	99.9
2-propanol	C_3H_8O	60.10	Merck	99.9
Iron (II) Sulphate 7-hydrate PA-ACS	$FeSO_4.7H_2O$	278.02	Panreac	99
Potassium Bromide (IR) PAI	KBr	119.01	Panreac	
Gum Arabic	$C_{12}H_{36}$	180.41	Kremer pigmente	
Chitosan from shrimp shells, low viscous			Sigma-Aldrich	

Table A2.2.*: Specification of nanomaterial synthesis*

Sample	*Solutions*	*Surfactant*	*Nanoparticles synthesised*	$w_{experimental}$ / g	$w_{theoretical}$ / g	Yield / %
S1	$CaCl_2$+NaOH	Triton X-100	$Ca(OH)_2$	1.3024	2.9570	44.04
S2	$MgCl_2$+NaOH	CTAB	$Mg(OH)_2$	0.9645	2.3275	41.41
S3	$MgCl_2$+NaOH	CTAB	$Mg(OH)_2$	0.4908	2.3275	21.07*
S4	$CaCl_2$+NaOH	Triton X-100	$Ca(OH)_2$	1.5443	2.9750	52.21

**Low yield of S3 is possibly due to loss of material during washing cycles*

Appendix 3 – *Additional data regarding paper characterization before treatment*

A3.1. 3D-*Digital microscope and SEM images of R1 samples (t0, 4 and 5 weeks) before treatment.*

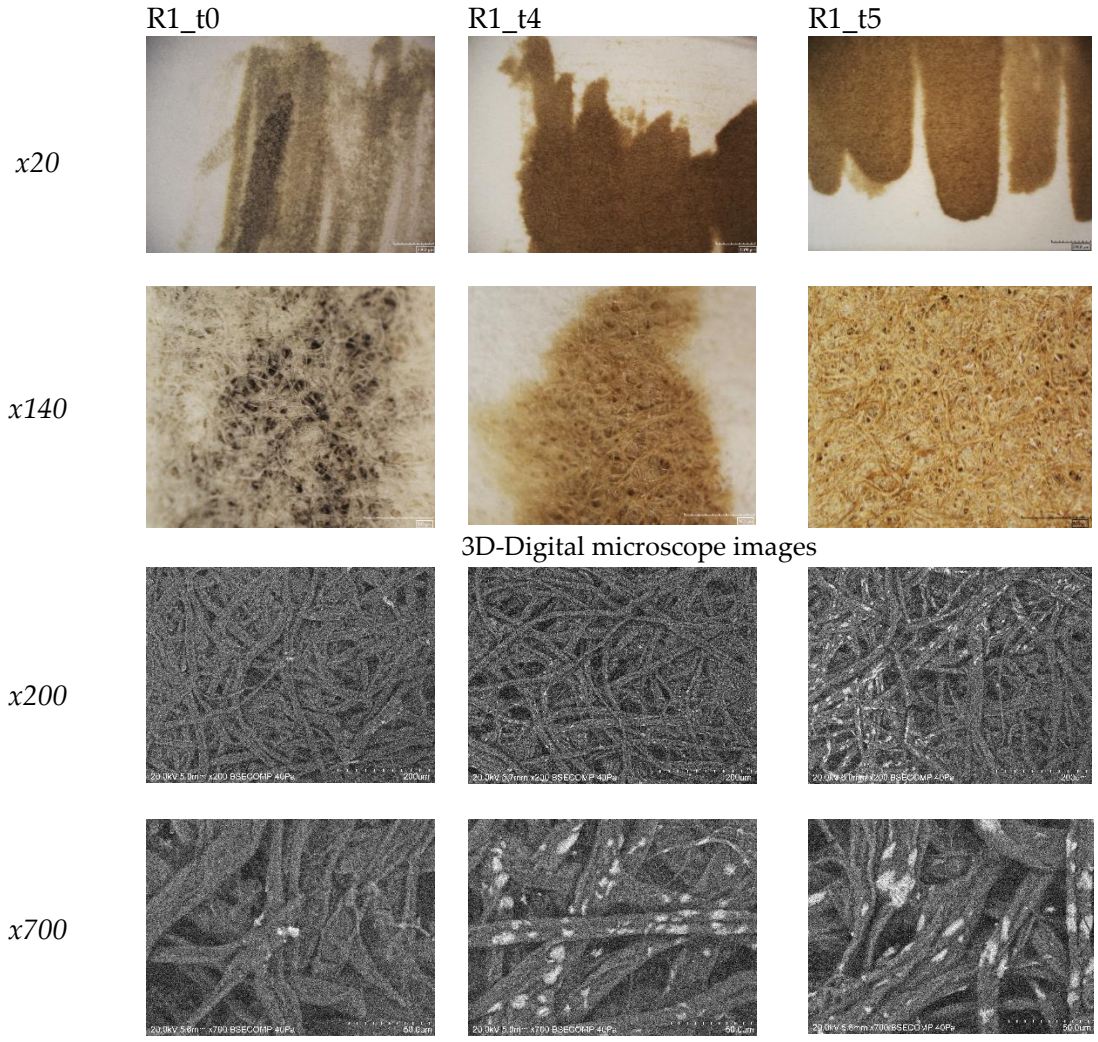

A3. 2. *FTIR spectra of R1 samples (t0, 4 and 5 weeks) before treatment.*

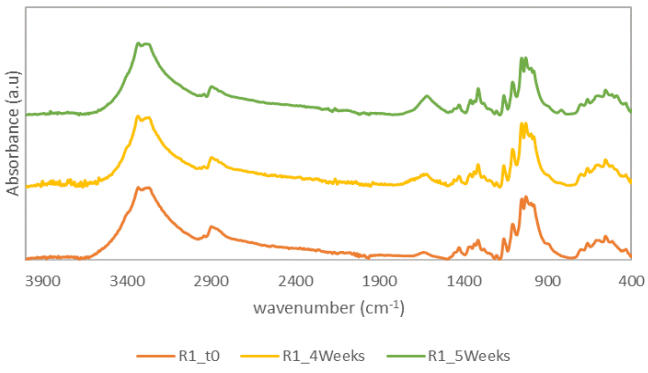

Appendix 4 – *Additional data regarding paper characterization after treatment*

A4.1. – *Images of treated samples from R1 and R2 (t0, 4 and 5 weeks) (Batch 1) and treated and aged (Batch 2).*

	Sample name	Batch 1 *(treated)*	Batch 2 *(treated and aged)*
1	R1_t0_Ca	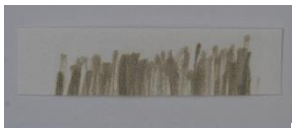	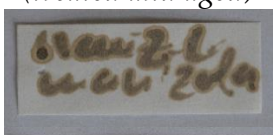
2	R1_t0_Mg	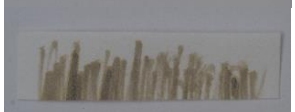	
3	R1_t0_Mixed		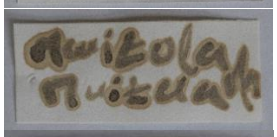
4	R1_t5_Ca		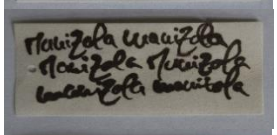
5	R1_t5_Mg		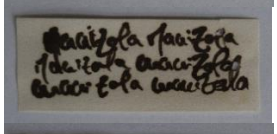
6	R1_t5_Mixed		
7	R2_t0_Ca		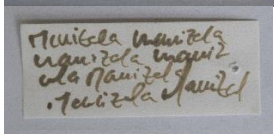
8	R2_t0_Mg		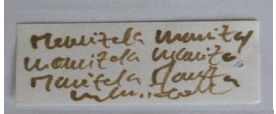
9	R2_t0_Mixed		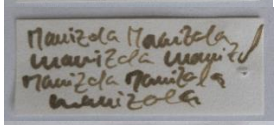
10	R2_t5_Ca	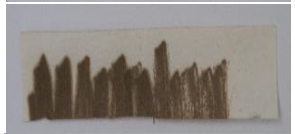	
11	R2_t5_Mg		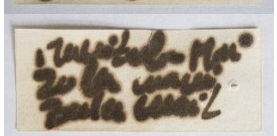
12	R2_t5_Mixed		

A4.2. *3D-digital microscope images of treated samples of R1 (t0 and t5, Batch 1). a) Sample R1 t0. b) Sample R1_t5.*

a) *Sample R1_t0.*

	R1_t0_Ca		R1_t0_Mg		R1_T0_Mixed	
	x20	x140	x20	x140	x20	x140
Batch1 (#1)	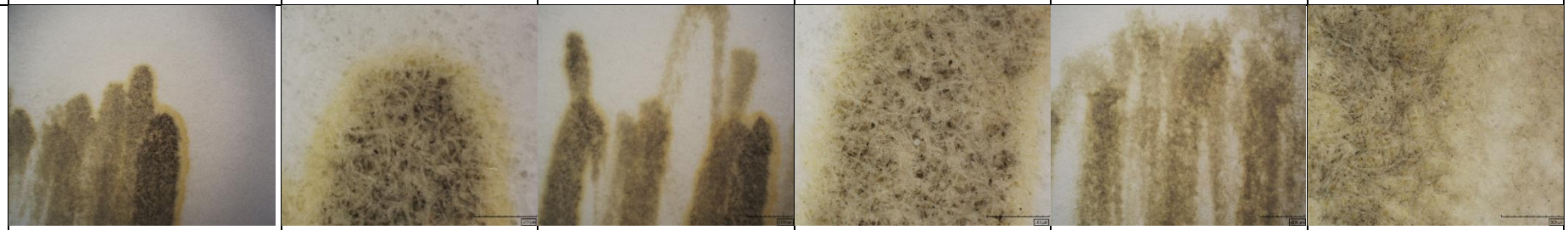					
Batch 1 (#2)	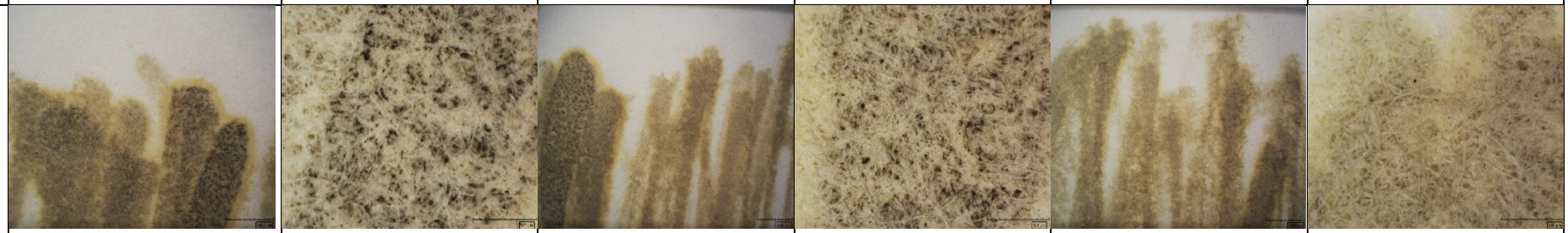					
Batch 1 (#3)	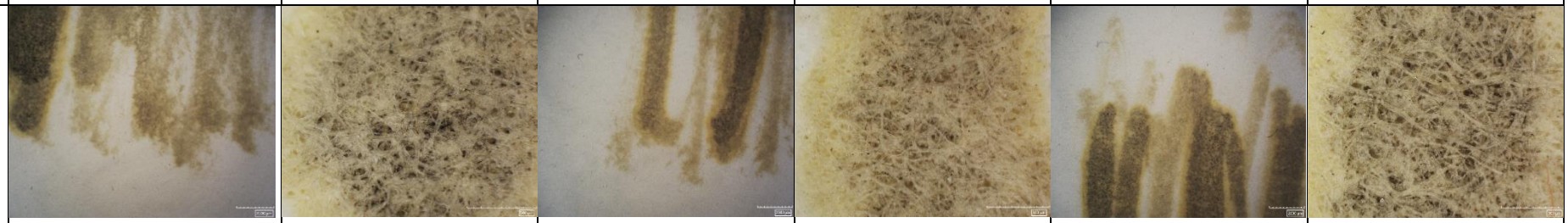					

b) R1_t5 after treatment

	R1_5Weeks_Ca		R1_5Weeks_Mg		R1_5Weeks_Mixed	
	x20	x140	x20	x140	x20	x140
Batch 1 (#1)		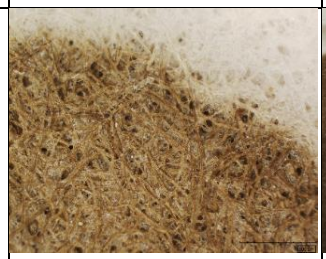		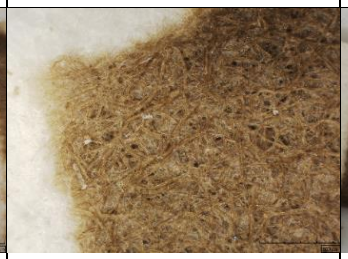		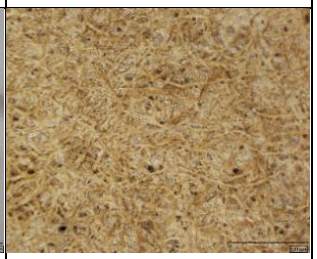
Batch 1 (#2)	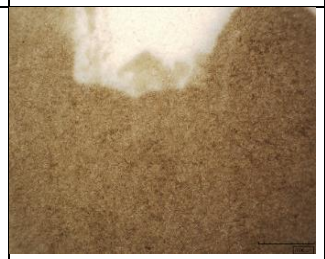	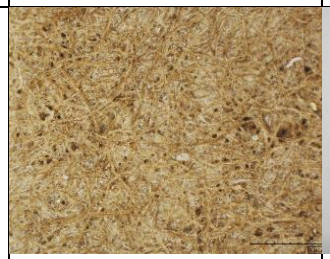		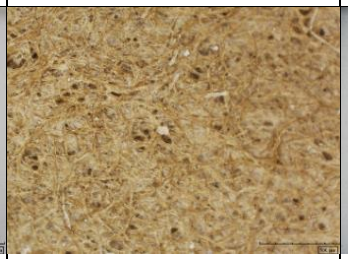	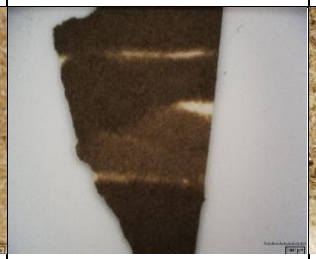	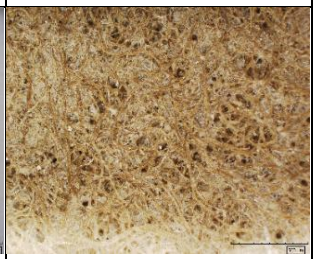
Batch 1 (#3)		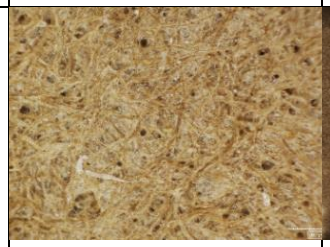		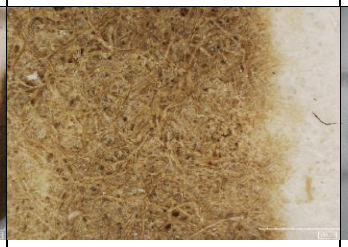		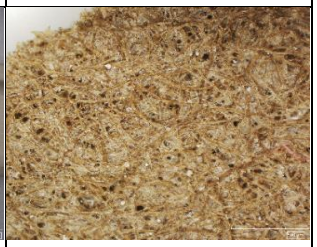

A4.3. *3D-digital microscope images of treated samples of R2 (t0 and t5, Batch 1). a) Sample R2_t0. b) Sample R2_t5.*

a) Sample R2_t0.

	R2_t0_Ca		R2_t0_Mg		R2_t0_Mixed	
	x20	x140	x20	x140	x20	x140
Batch 1(#1)		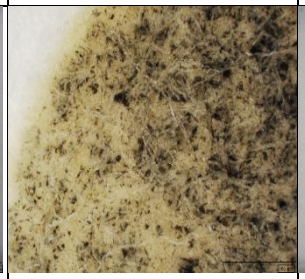	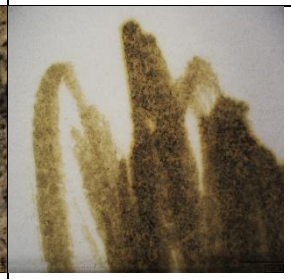	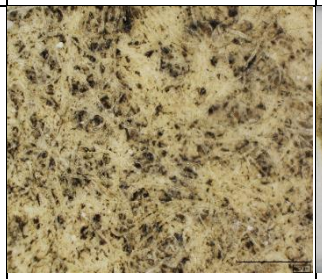	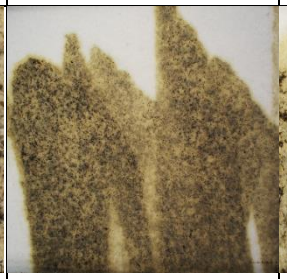	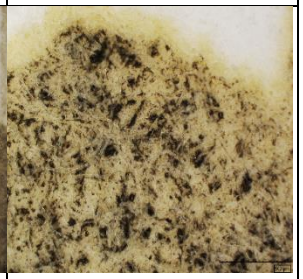
Batch 1 (#2)	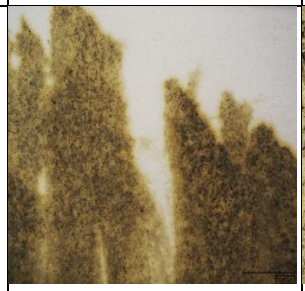	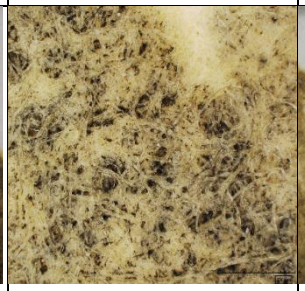	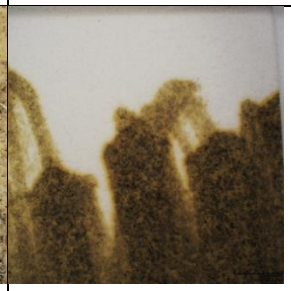	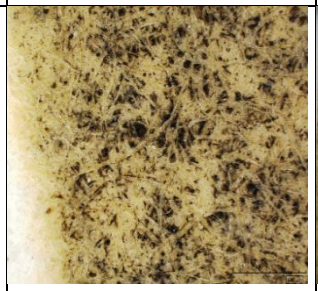	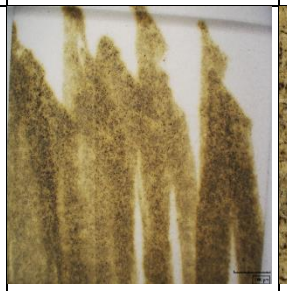	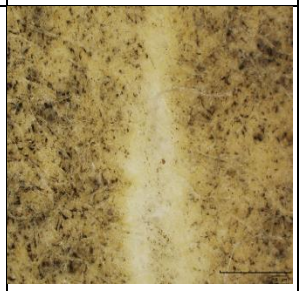
Batch 1(#3)	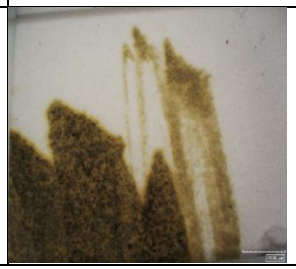	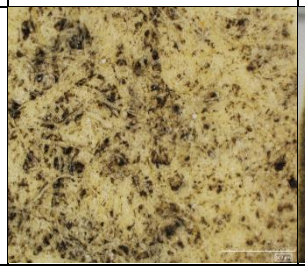		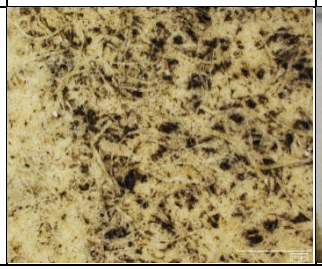	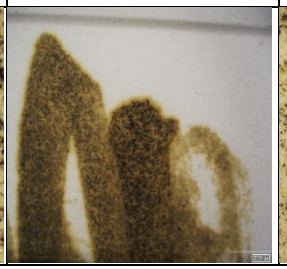	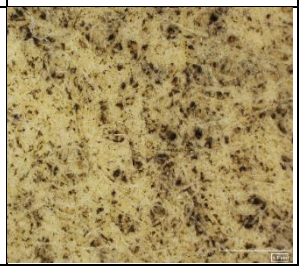

b) R2_t5

	R2_5Weeks_Ca		R2_5Weeks_Mg		R2_5Weeks_Mixed	
	x20	x140	x20	x140	x20	x140
Batch 1 (#1)				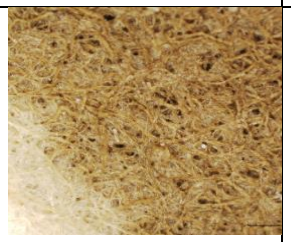		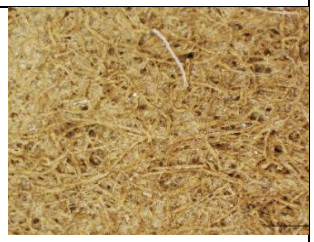
Batch 1 (#2)		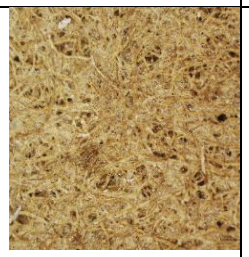		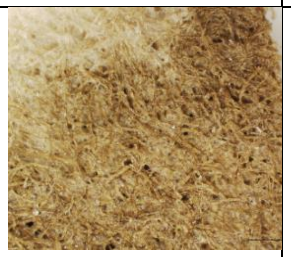	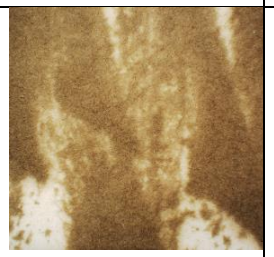	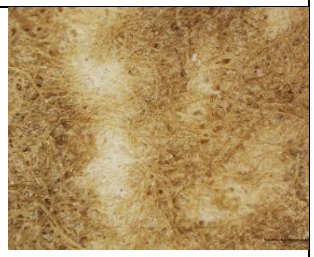
Batch 1 (#3)			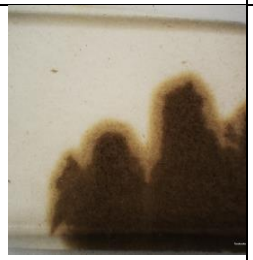			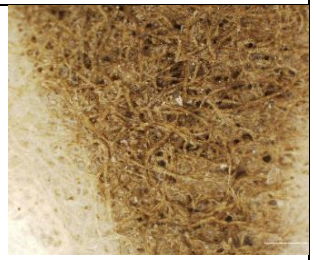

A4.4. *3D-digital microscope and SEM images of samples of R1_t4 after treatment. a) Sample R1_t4_Ca. b) Sample R1_t4_Mg. c) Sample R1_t4_Mixed.*

a) Sample R1_t4_Ca

R1_4Weeks_Ca	3D-digital Microscope		SEM		
	x20	x140	x200	x700	x8.00k
Batch 1 (#1)	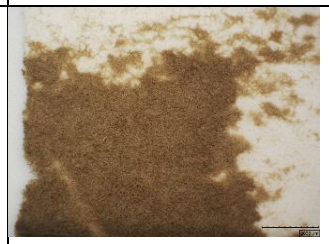		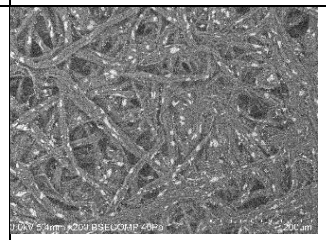	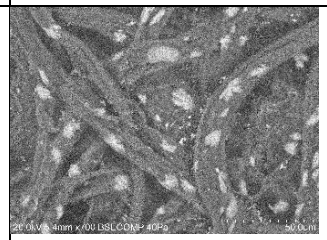	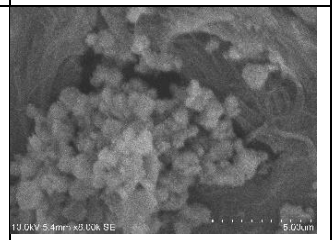
Batch 1 (#2)		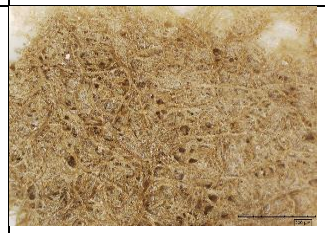	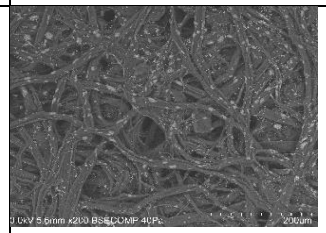	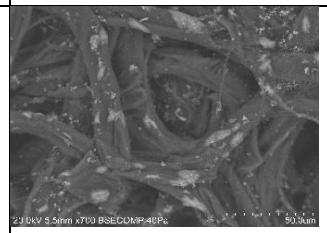	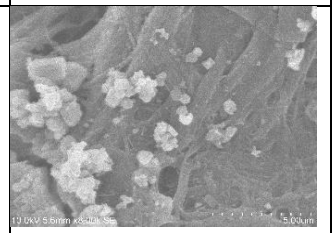
Batch 1 (#3)		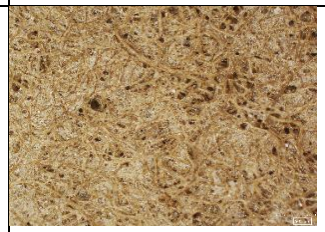	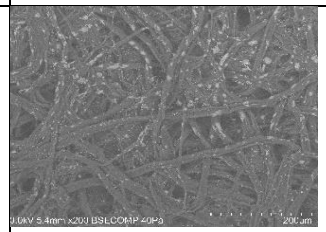	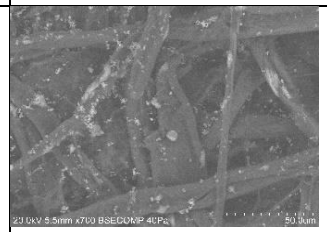	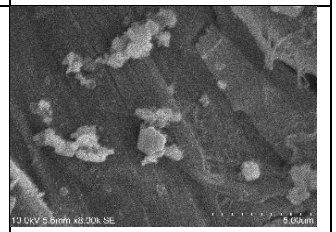
Batch 2			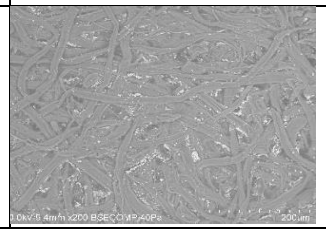	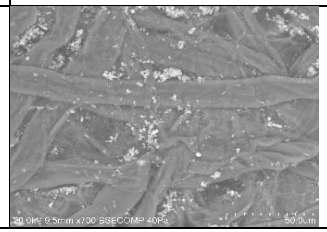	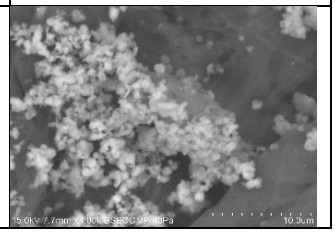

b) R1_t4_Mg

R1_4Weeks_Mg	3D-digital Microscope		SEM		
	x20	x140	x200	x700	x8.00k
Batch 1 (#1)		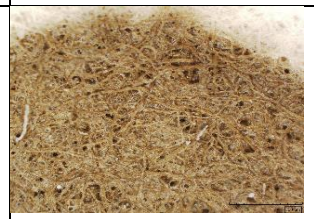	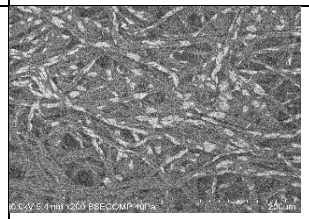		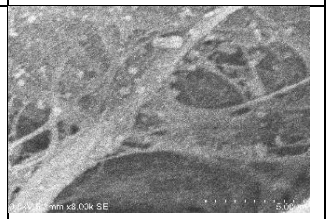
Batch 1 (#2)		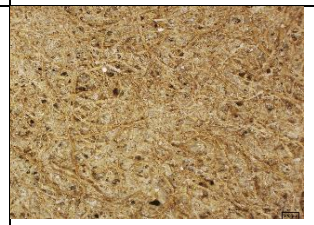	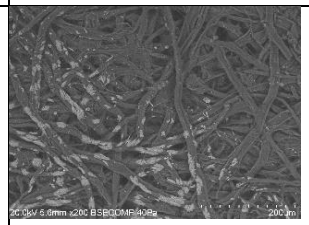	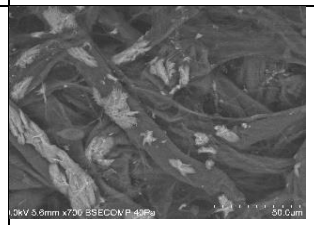	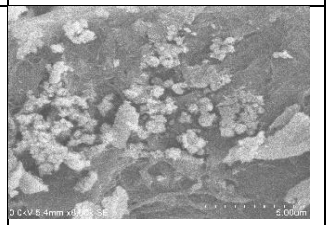
Batch 1 (#3)	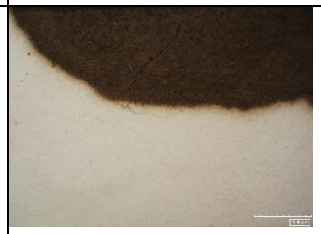	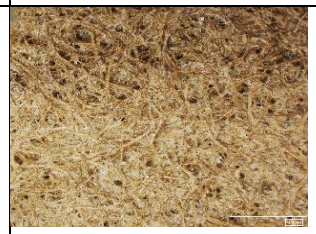	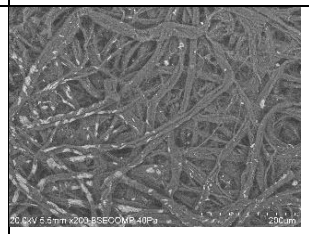	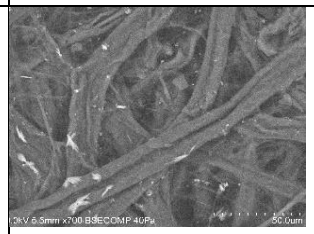	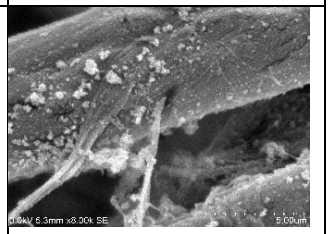
Batch 2			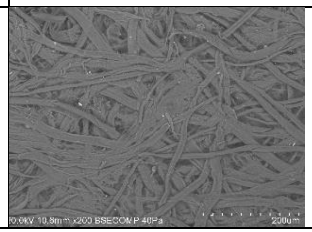		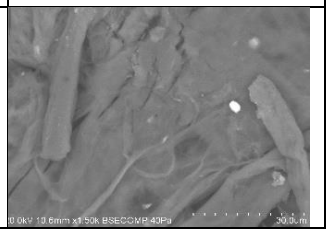

c) R1_t4_Mixed

R1_4Weeks_Mixed	3D-digital Microscope		SEM		
	x20	x140	x200	x700	x8.00k
Batch 1 (#1)		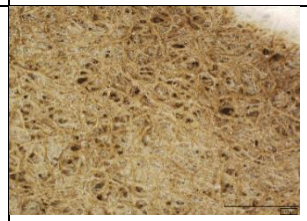	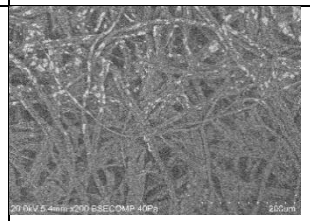	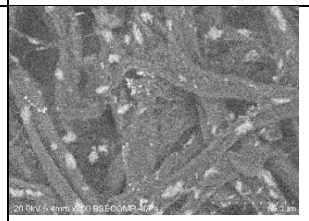	
Batch 1 (#2)			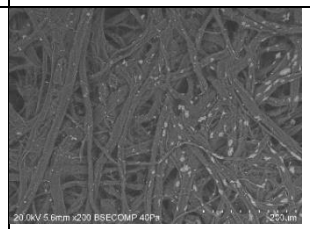	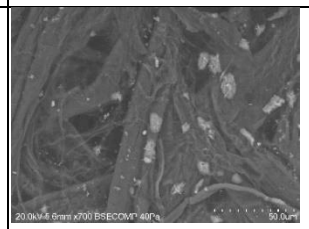	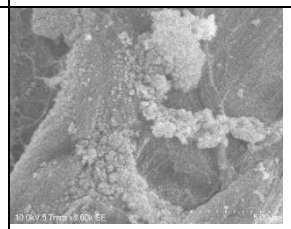
Batch 1 (#3)		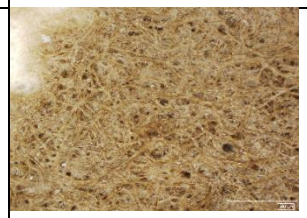	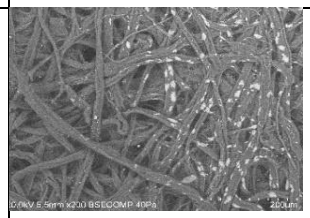	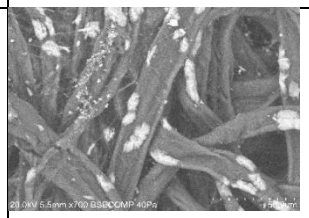	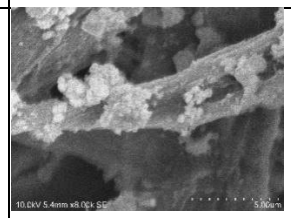
Batch 2		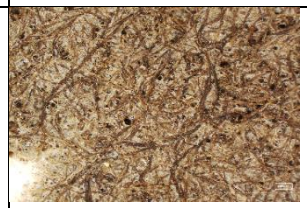	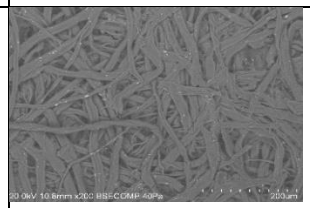	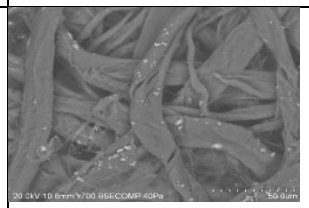	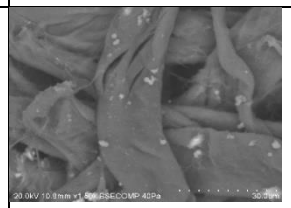

A4.5. *SEM images of treated samples of R1 and R2 (t0 and t5, Batch 1). a) Sample R1_t0. b) Sample R1_t5.*

a) Sample R1_t0.

	R1_t0_Ca		R1_t0_Mg		R1_t0_Mixed	
	x200	x700	x200	x700	x200	x700
Batch1 (#1)	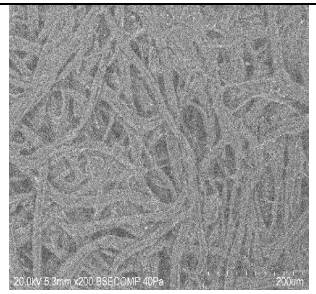	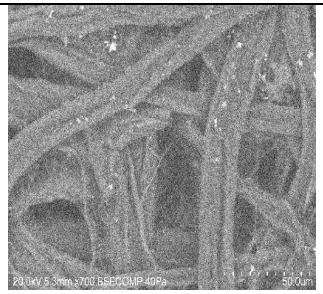	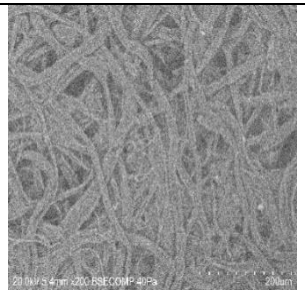	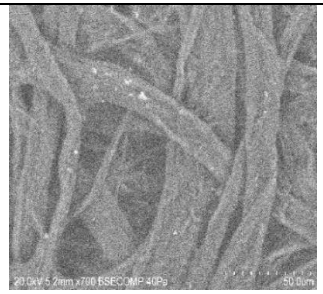	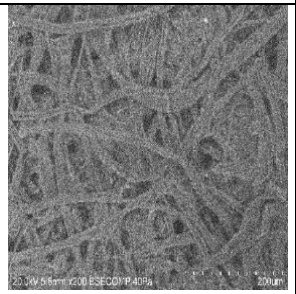	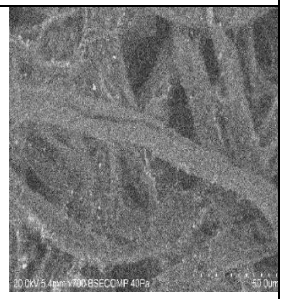
Batch 1 (#2)	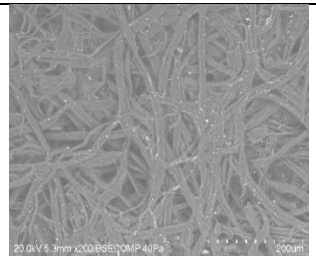	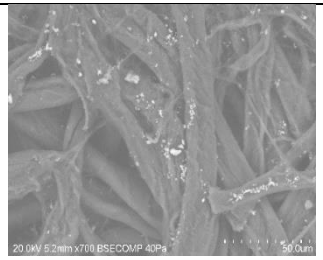	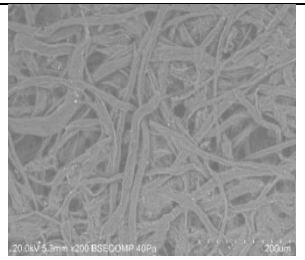	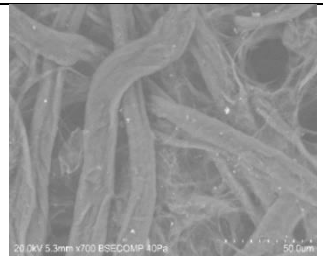	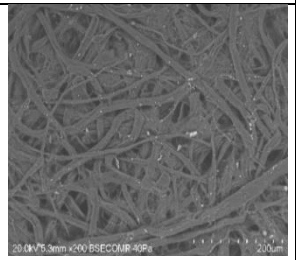	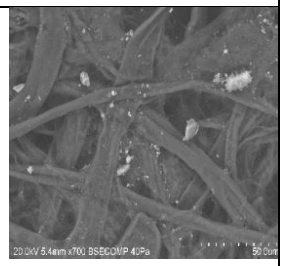
Batch 1 (#3)	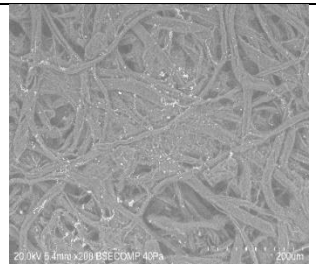	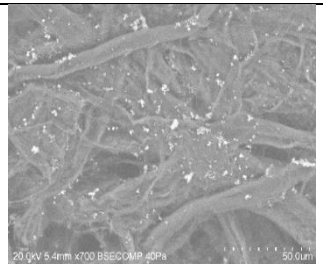	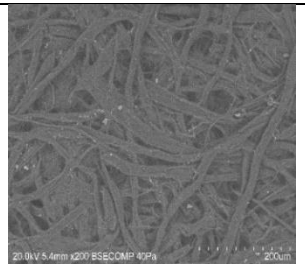	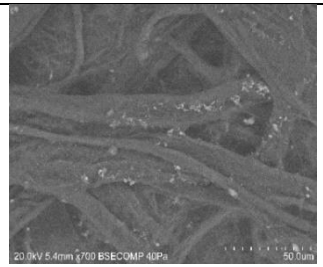	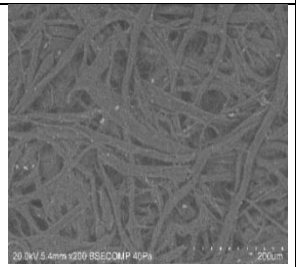	

b) Sample R1_t5.

	R1_5Weeks_Ca		R1_5Weeks_Mg		R1_5Weeks_Mixed	
	x200	x700	x200	x700	x200	x700
Batch 1(#1)	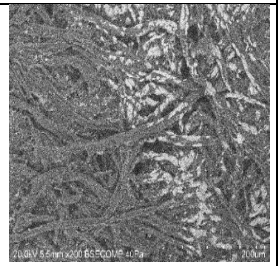	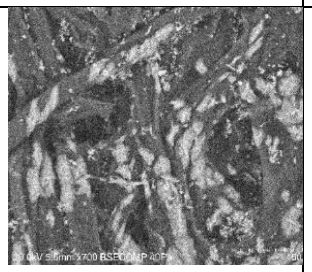	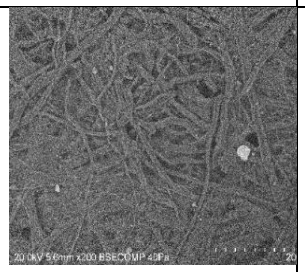	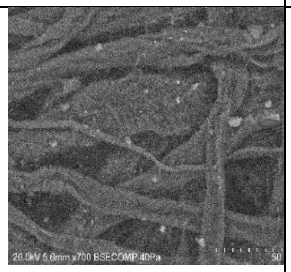	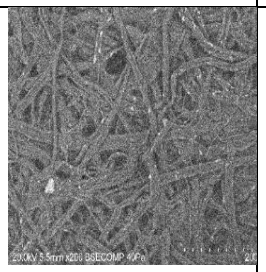	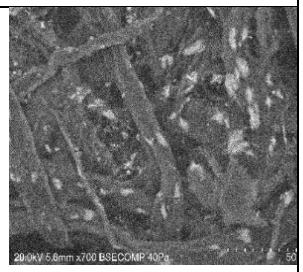
Batch 1 (#2)	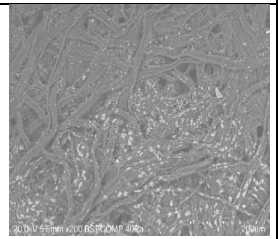	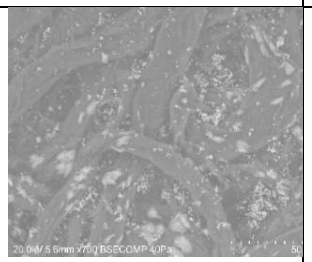	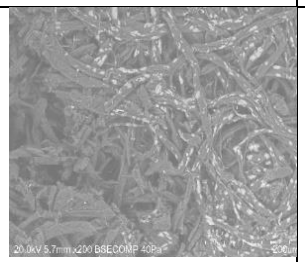	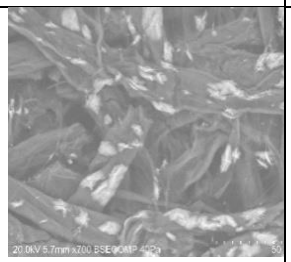	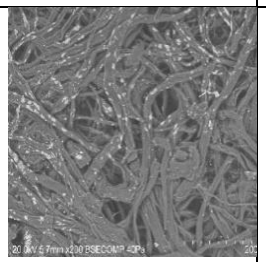	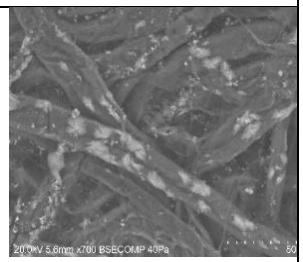
Batch 1(#3)	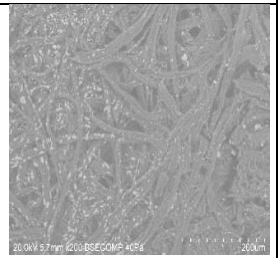	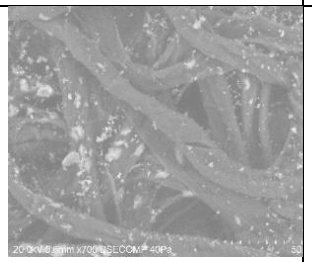	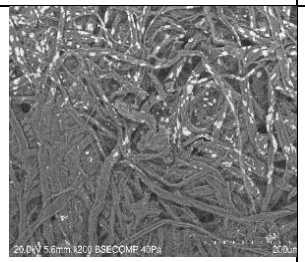	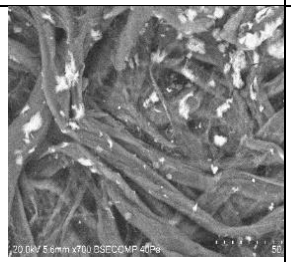	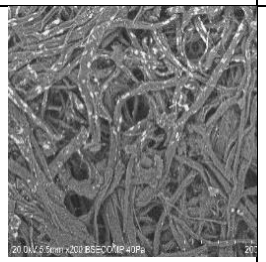	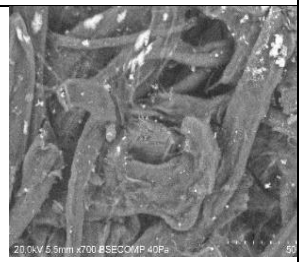

A4.6. *SEM images of treated samples of R2 (t0 and t5, Batch 1). a) Sample R2_t0. b) Sample R2_t5.*

a) Sample R2_t0.

	R2_t0_Ca		R2_t0_Mg		R2_t0_Mixed	
	x200	x700	x200	x700	x200	x700
Batch 1(#1)	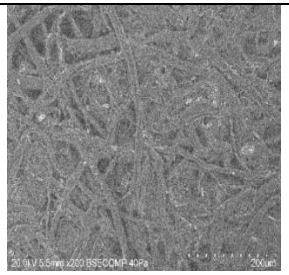	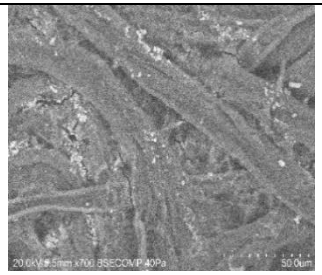	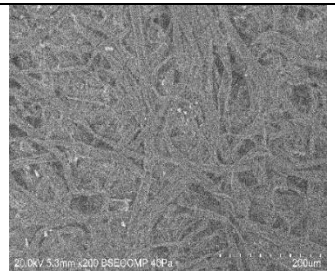	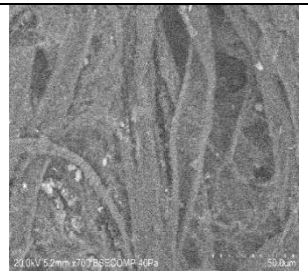	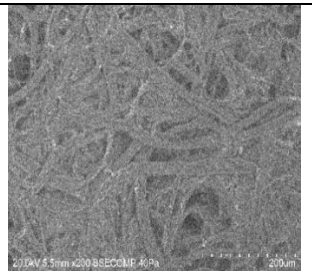	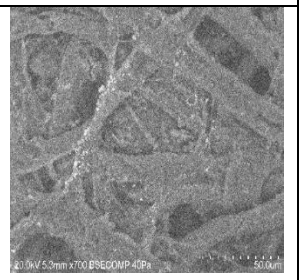
Batch 1 (#2)	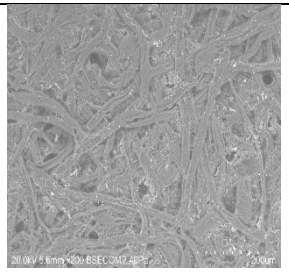	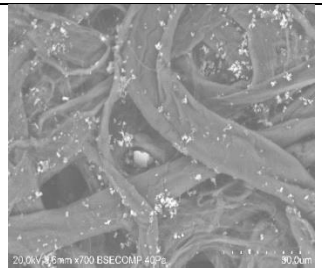	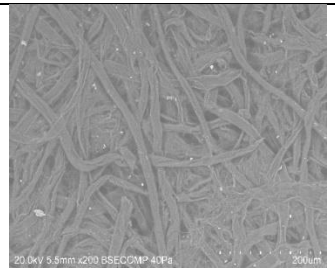	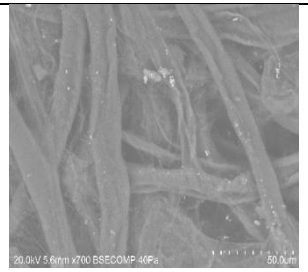	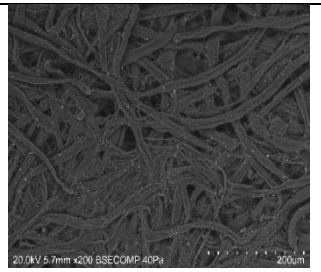	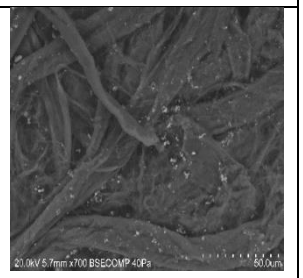
Batch 1(#3)	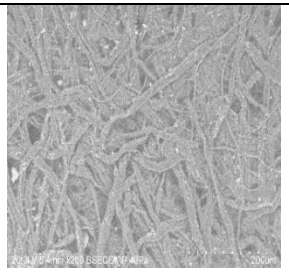	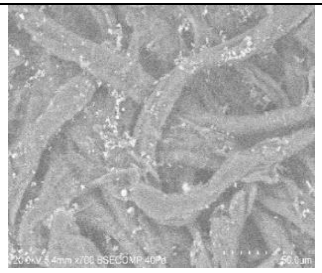	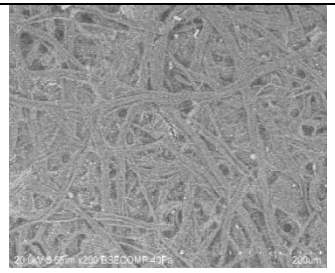	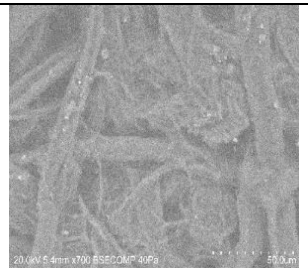	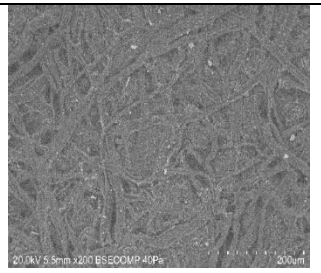	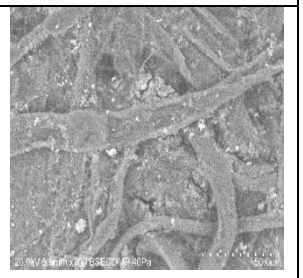

b) Sample R2_t5.

	R2_5Weeks_Ca		R2_5Weeks_Mg		R2_5Weeks_Mixed	
	x200	x700	x200	x700	x200	x700
Batch 1 (#1)	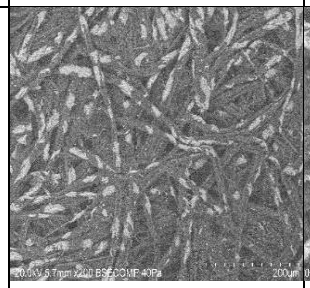	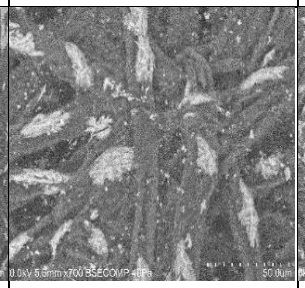	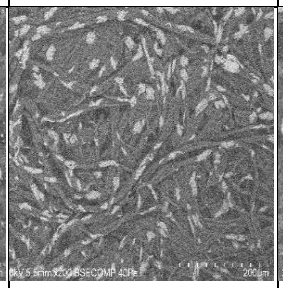	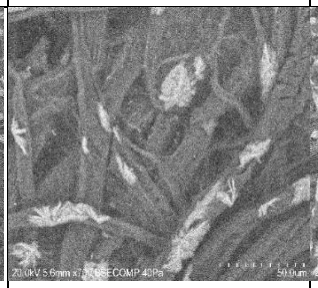	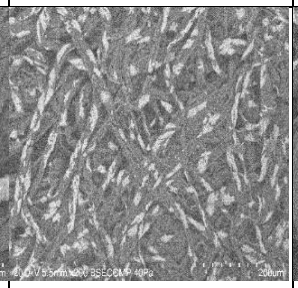	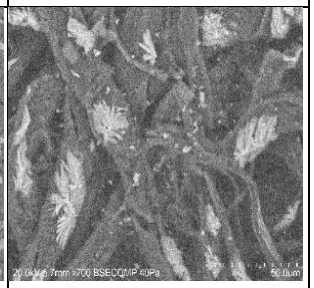
Batch 1 (#2)	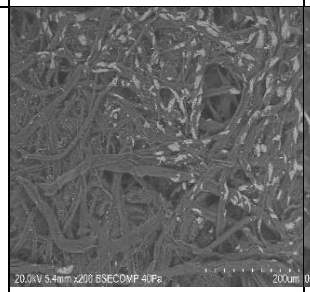	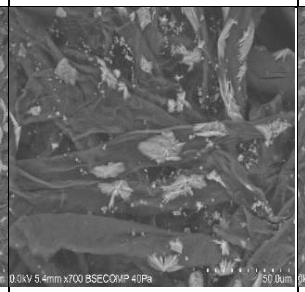	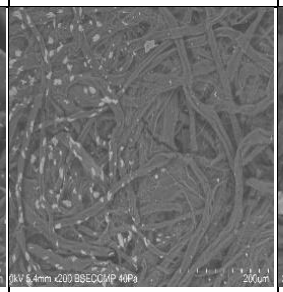	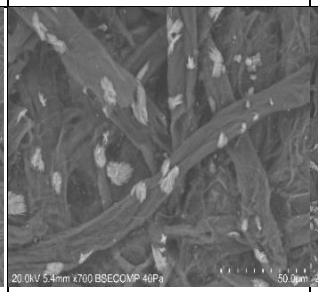	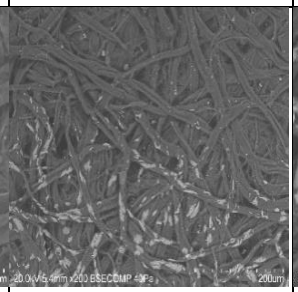	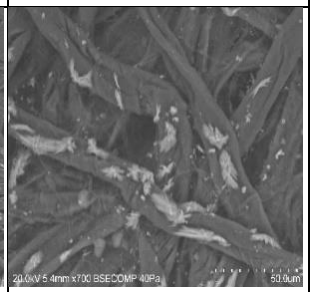
Batch 1 (#3)	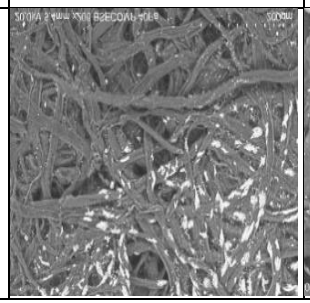	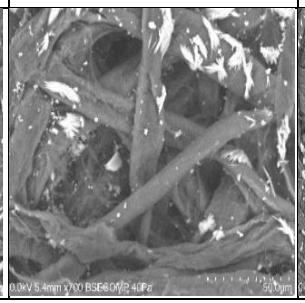	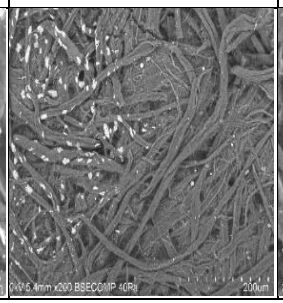	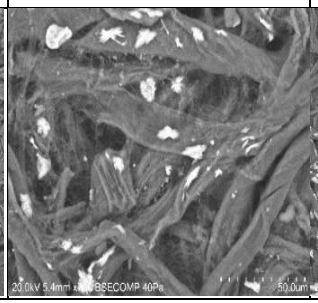	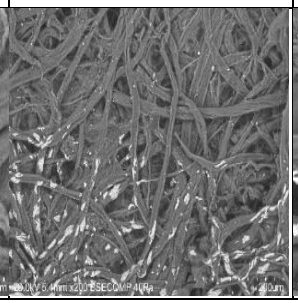	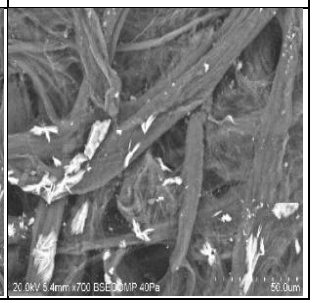

A4.7. *FTIR spectra of the treated paper samples*

g) *R1 samples from Batch 1 treated with $Ca(OH)_2$ NPs*

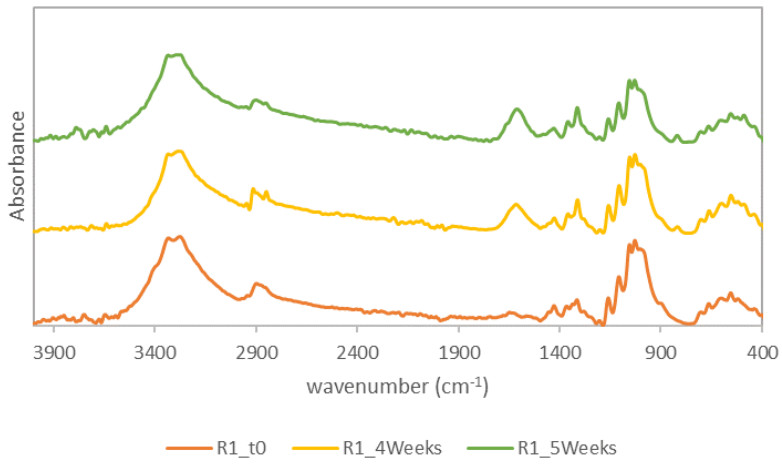

h) *R1_t4_Ca samples- Untreated, Batch 1 and Batch 2*

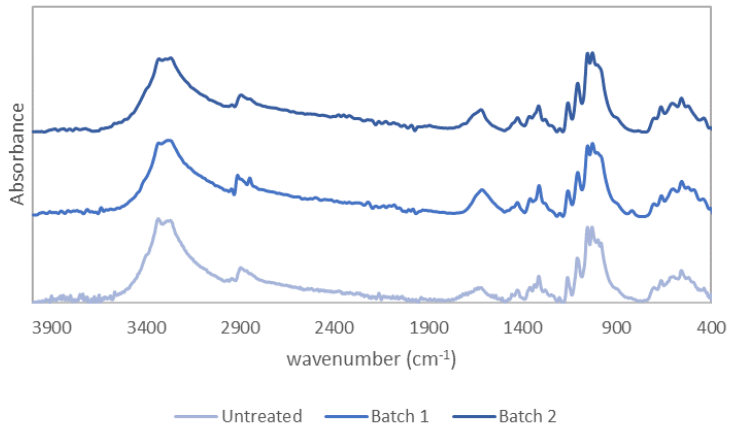

i) *R1 samples from Batch 1 treated with $Mg(OH)_2$ NPs*

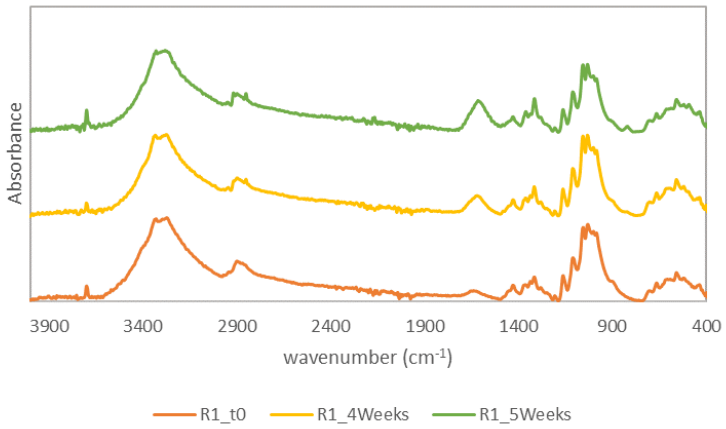

j) R1_t4_Mg samples- Untreated, Batch 1 and Batch 2

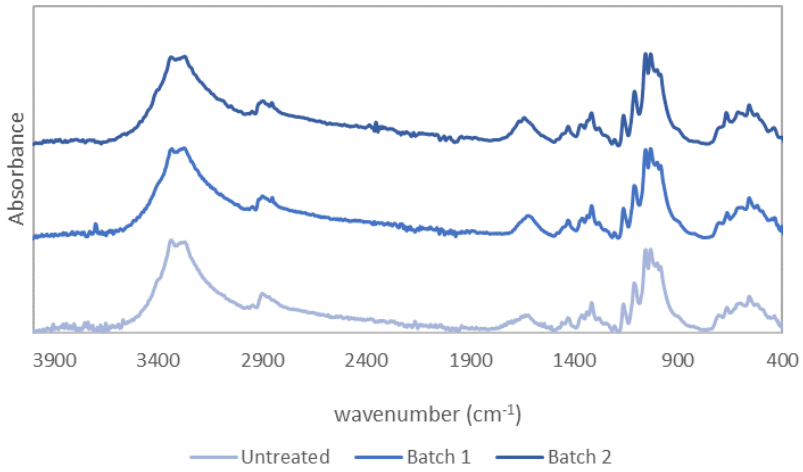

k) R2 samples from Batch 1 treated with Mixed NPs dispersion

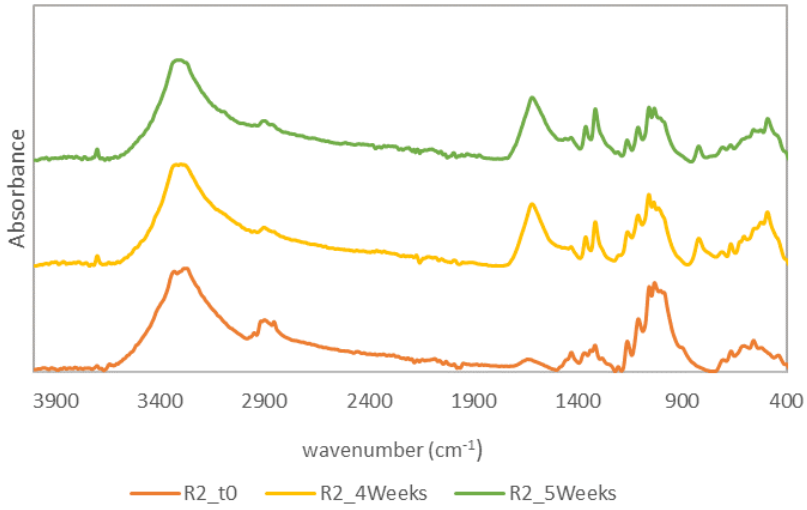

l) R2_t4_mixed samples- Untreated, Batch 1 and Batch 2